N.M.I.M.T.
LIBRARY
SOCORRO, N.M.
A68
N81
c.2

THE MINERALIZING FLUIDS RESPONSIBLE FOR SKARN AND ORE FORMATION AT THE CONTINENTAL MINE, FIERRO, NEW MEXICO, IN LIGHT OF REE ANALYSES AND FLUID INCLUSION STUDIES

Beth S. Abramson

N.M.I.M.T.
LIBRARY
SOCORRO, N.M.

Submitted in Partial Fulfillment
of the Requirements for the Degree of
Masters of Science in Geology

New Mexico Institute of Mining and Technology
Socorro, New Mexico

December 1981

Acknowledgements

Financial support for this study was provided by The Department of the Interior, Office of Surface Mining, Grant No. G5105040.

I would like to thank the members of my thesis committee Dr. David I. Norman, advisor; Kent Condie; and Clay T. Smith for their suggestions and critical review of this thesis. Special thanks to David I. Norman for suggesting this thesis, serving as my thesis advisor, for his advice, guidance, and very helpful criticism during the writing of this thesis.

I would also like to thank Phillip Allen for the numerous hours of teaching and discussions about the procedures involved with Instrumental Neutron Activation Analysis. Invaluable suggestions and discussions with other students primarily Mike Palin, Francois Nguene and Bob Smith are greatly appreciated. In addition, I want to thank all the computer science people that helped me get a copy of this thesis typed and put together.

I want to thank the Sharon Steel Corporation for allowing permission to do this thesis on their property. Roy Leigh and Bill Worthington are especially thanked for their extremely valuable assistance at the Continental mine.

TABLE OF CONTENTS

ABSTRACT..... i

INTRODUCTION.....1
Location.....1
Purpose of Investigation.....1
Previous Work 4
Geology.....4
REE Studies.....5
Fluid Inclusion Studies.....6
Method of Investigation.....7
General Geology.....14
Regional and Tectonic Setting.....14
General Structure of the Central Mining District.....16
Structural History of the Central Mining District....18
Stratigraphy of the Central Mining District.....20
Stratigraphic Nomenclature of the Central Mining District.....23
General Geology of the Continental Mine.....24
Hanover-Fierro Intrusive.....26
Regional Economic Geology.....27
RECRYSTALLIZED SEDIMENTARY ROCKS.....29
MINERAL ASSEMBLAGES AT THE CONTINENTAL MINE.....30
Dolomite and Siliceous Dolomite.....30
Shale Members.....34
Shaly Limestone Members.....35
Limestones.....38
Quartzite Formations.....41
Igneous Dikes and Sills.....41
Garnet Skarn.....44
Hydrothermal Alteration 47
Ore Mineralization.....48
Hanover-Fierro Intrusive.....52
Mineral Paragenesis.....53

FLUID INCLUSION ANALYSES.....54
General Observations of Fluid Inclusions in Garnet...54
Microthermometry of Fluid Inclusions in Garnet.....59
General Observations of Fluid Inclusions in Quartz Bearing Veins.....66
Microthermometry of Fluid Inclusions in Quartz-Bearing Veins.....73
Pressure Determinations From Fluid Inclusion Data....79
Temperature Correction for Fluid Inclusions.....79
Relationship Between Fluid Inclusions From Garnet And Fluid Inclusions From Quartz-Bearing Veins.....81

REE ANALYSES.....82
Introduction.....82
Sample Preparation and Chemical Analyses.....83

Results.....83
REE Geochemistry of the Limestones.....84
REE Geochemistry of the Shaly Limestones.....88
REE Geochemistry of the Garnet.....88
REE Geochemistry of the Dolomites.....88
REE Geochemistry of the Shales.....94
REE Geochemistry of the Bliss Quartzite and the Beartooth Quartzite.....99
REE Geochemistry of the Abo and Colorado Formations.....99
REE Geochemistry of Granodiorte Dikes, Felsite Dike, and Diorite Sill.....102
REE Geochemistry of the Granodioritic Hanover-Fierro Intrusive.....102

DISCUSSION.....105
Skarn Mineralization at the Continental Mine.....105
Origin of Skarn and Ore Mineralization in Light of Fluid Inclusion Evidence.....107
Possible Origins of the Fluids Responsible for Skarn Formation.....107
Possible Origins of the Fluids Responsible for Late Ore Mineralization.....108
Suggested Origin of the Fluid(s) Responsible for Skarn and Ore Mineralization.....109
REE Geochemistry.....111
REE Geochemistry of the Limestones and Shaly Limestones.....111
REE Geochemistry of the Garnet.....112
REE Geochemistry of the Dolomites.....113
REE Geochemistry of the Shales.....115
REE Geochemistry of the Bliss Quartzite and the Beartooth Quartzite.....117
REE Geochemistry of the Abo and Colorado Formations.....117
REE Geochemistry of the Altered Granodiorite Dikes, Felsite Dike and Diorite Sill.....118
REE Geochemistry of the Hanover-Fierro Intrusive.....119
REE Geochemistry at the Continental Mine.....121
Possible and Suggested Origins of the REE at the Continental Ore Deposit.....126

SUGGESTED GENETIC MODEL.....128

SUMMARY AND CONCLUSIONS.....133

REFERENCES.....136

APPENDICES

APPENDIX I: Thin section description of Rock Samples
APPENDIX II: Samples for Fluid Inclusion Study
APPENDIX III: Individual Fluid Inclusion Measurements
APPENDIX IV: REE Concentrations (ppm and chondrite) Normalized for Individual Samples
APPENDIX V: Concentrations of Selected Trace Elements For Individual Samples
APPENDIX VI: History of the Central Mining District
APPENDIX VII: Chondrite normalized REE plots for the Montoya Dolomite and Bliss Quartzite
APPENDIX VIII: Mass-Volume Calculation

FIGURES

1. Index map.....2
2. General geology of the Continental open pit and location of collected samples.....8
3. Geologic map of the southwest corner of the San Lorenzo quadrangle showing location of collected samples.....10
4. Geologic map of a portion of the Santa Rita quadrangle showing location of collected samples.....12
5. Generalized geologic map of the Southern Cordillera..15
6. Tectonic mapping showing the Farallon plate in relation to the North American plate.....17
7. Stuctural geologic setting of the Santa Rita quadrangle.....19
8. Major structural features in the Santa Rita quadrangle.....21
9. Stratigraphic column.....22
10. Skarn assemblages at the Continental oredeposit.....25
10a. Ore Deposits, mines, and towns in the Central Mining District.....28
11. Photomicrograph of Forsterite-Phlogopite-Talc-(Carbonate) Skarn.....30
12. a) Aleman Chert Member.....32
b) Photomicrograph of the Aleman Chert Member.....32
13. Photomicrograph of Forsterite-Magnetite.....33
14. a) Photomicrograph of Garnet-Diopside-Quartz-Feldspar hornfels.....36
b) Photomicrograph of Garnet-Diopside-Quartz-Feldspar hornfels; close up view of 14a.....36
15. Photomicrograph of Garnet Replacing Carbonate and Diopside and later Replaced by Carbonate.....37
16. Photomicrograph of Magnetite Replacing Garnet and Filling Open Spaces.....39
17. Photomicrograph of Magnetite Skarn.....40
18. Photomicragh of Metasomatized Granodiorite Dike...42
19. Photomicrograph of Altered Felsite Sill.....43
20. Garnet Skarn.....45
21. Garnet Skarn.....45
22. a) Photomicrograph of Garnet Skarn that Replaced Carbonate and Diopside.....47
b) Photomicrograph of Extremely Zoned Garnets with Diopside Inclusions.....47
23. Photomicrograph of Garnet partially replaced by Magnetite.....49
24. Garnet-Magnetite Skarn.....50
25. Garnet-Magnetite-Chalcopyrite Skarn.....50
26. a) Massive Magnetite Skarn with Chalcopyrite and Pyrite Veins.....51
b) Magnetite-Chalcopyrite-Pyrite Skarn.....51
c) Magnetite-Chalcopyrite-Pyrite Skarn with Boxwork Structure.....51
27. Photomicrograph of the Hanover-Fierro Intrusive.....52

28. Fluid Inclusion Photomicrographs from Garnet.....55
29. Fluid Inclusion Photomicrographs from Garnet.....57
30. Homogenization Temperatures of Primary and Secondary Fluid Inclusions in Garnet.....60
31. Summary of Homogenization Temperatures and Salinities for Primary and Secondary Fluid Inclusions in Garnet.61
32. Equivalent Wt. % NaCl for Fluid Inclusions in Garnet.62
33. Homogenization Temperature vs Eq. Wt. % NaCl.....65
34. Fluid Inclusion Photomicrographs from Quartz-Bearing Veins.....67
35. Fluid Inclusion Photomicrographs from Quartz-Bearing Veins.....69
36. Homogenization Temperatures for Fluid Inclusions in Quartz-Bearing Veins.....74
37. Equivalent Wt. % NaCl for Fluid Inclusions in Quartz-Bearing Veins.....75
38. Chondrite-Normalized REE Concentrations for the Oswaldo Limestone.....85
39. Chondrite Normalized REE Concentrations for the Lower Blue Limestone.....86
40. Chondrite Normalized REE Concentrations for the Hanover Limestone.....87
41. Chondrite Normalized REE Concentrations for the Syrena Shaly Limestone and Garnet Skarn Bands.....89
42. Chondrite Normalized REE Concentrations for Garnet Separates.....90
43. Chondrite Normalized REE Concentrations for the Montoya-Fusselman Dolomite.....91
44. Chondrite Normalized REE Concentrations for the El Paso Limestone.....93
45. Chondrite Normalized REE Concentrations for the Ready Pay Member of the Percha Shale.....95
46. Chondrite Normalized REE Concentrations for Selected Shales, Sandstones, Limstones and Quartzite.....96
47. Chondrite Normalized REE Concentrations for the Augen Member of the Percha Shale.....97
48. Chondrite Normalized REE Concentrations for the Parting Shale.....98
49. Chondrite Normalized REE Concentrations for the Bliss Quartzite and the Beartooth Quartzite.....100
50. Chondrite Normalized REE Concentrations for the Abo and Colorado Formations.....101
51. Chondrite Normalized REE Concentrations for the Dikes and Sills.....103
52. Chondrite Normalized REE Concentrations for the Hanover-Fierro Intrusive.....104
53. Relationship between the Porphyritic and Equi-granular facies of the Hanover-Fierro stock.....110
54. REE concentrations of Altered and Recrystallized Samples Compared to Unaltered Samples.....122
55. Suggested Genetic Model for Skarn Formation and Ore Mineralization.....131

TABLES

I. Relationship Between Unaltered, Thermally Altered and Metasomatically Altered Sediments
II. Mineral Paragenesis
III. Depth Estimates

THE MINERALIZING FLUIDS RESPONSIBLE FOR SKARN AND ORE FORMATION AT THE CONTINENTAL MINE, FIERRO, NEW MEXICO IN LIGHT OF REE ANALYSES AND FLUID INCLUSION STUDIES

Beth S. Abramson

Abstract

The Continental mine is a Fe-Cu-(Zn) skarn deposit located on the northern margin of the Hanover-Fierro stock. Mineralization occurs in a thermally zoned, contact metasomatic skarn and hornfels zone that surrounds the intrusive. Garnet skarn and garnet-clinopyroxene skarn replaced limestone. Hornfels comprised of clinopyroxene, biotite, feldspar and quartz replaced shales. Shaly limestones are replaced by diopside, quartz, feldspar, epidote, and lesser amounts of garnet. Dolomite is replaced by magnesian skarn comprised of forsterite, serpentine, magnetite and lesser amounts of phlogopite and tremolite.

Ore mineralization followed skarn formation and includes deposition of magnetite followed by deposition of pyrite, chalcopyrite and lesser amounts of sphalerite, bornite, chalcocite and pyrrhotite. Magnetite in large amounts is restricted to forsterite-serpentine skarn and garnet skarn. In garnet skarn, magnetite veined and replaced garnet and filled open spaces. Sulfides replaced and cemented brecciated garnet, replaced magnetite, and filled open spaces.

Fluid inclusion studies on garnet indicate skarn formation mostly in the range of 245°C to 345°C but extends from 215°C to 435°C by fluids with 4.5 to 19.0 eq. wt.% NaCl. A magmatic origin with dilution from metoric and/or

connate waters is suggested for these fluids.

Quartz veins associated with ore mineralization indicate deposition in the range of 200°C to >600°C by low to high salinity fluids ranging from 2.0 to 47.0 eq. wt.% NaCl. The presence of both liquid-rich and vapor-rich fluid inclusions in these veins suggests that the fluids were boiling. CO2-rich fluid inclusions occurred in the quartz-bearing veins but were not present in earlier garnet. A magmatic origin is postulated for the quartz-bearing veins with possible late contributions from a meteoric and/or connate source. Pressures during mineralization were on the order of 315 to 325 bars.

Fluid inclusions in garnet and from later quartz-bearing veins are filled with fluids that differ in composition, temperature and salinity. This suggests different fluids were responsible for earlier skarn formation and later ore mineralization.

Limestones, shaly limestones and quartzites showed increases in absolute REE concentrations with an enrichment in the lREE from the least altered to the most altered (metasomatized) samples. Dolomites and shales showed no or only a very small change in absolute REE concentrations and fractionation from the least altered to the most altered samples and indicate that metasomatism and recrystallization has not greatly affected the REE concentrations of these sediments. Garnet that replaced limestone show lREE (light REE) enrichment, hREE (heavy REE) depletion, and positive Eu

anomolies. The garnet have REE fractionation patterns similar to the limestone they replaced but show increases in absolute concentrations of the REE.

The metasomatized, and to a lesser extent, the recrystallized limestones, shaly limestones, and quartzites show increases in absolute REE concentrations with lREE enrichment. This requires an available source for the REE. This source was probably not the carbonate rocks since they have relatively low REE concentrations. The shales have high enough REE concentrations but metasomatism did not cause significant changes in the REE concentrations of the shales, suggesting they did not donate or accept REE. The most likely source of the REE is the Hanover-Fierro intrusive. However, the REE concentrations and fractionation of the altered and recrystallized sediments probably also reflects a) the original composition of the sedimentary rock, and, b) the mineral assemblages that replaced sediments and their partion coefficients for REE, and c) remobilization of the REE in the presence of CO_2 or by introduction of other later fluids.

INTRODUCTION

The Continental mine is a Fe-Cu-(Zn) skarn deposit located in the Central mining district, in Grant County, southwest New Mexico. The mine is located northeast of Silver City and one mile north of the town of Fierro (Fig. 1). The deposit occurs at the northern margin of the Hanover-Fierro intrusive stock in the skarn that has replaced Paleozoic and Mesozoic carbonate sediments.

Purpose Of Investigation

Most skarn deposits are usually structurally associated with and considered to be genetically related to an intrusion suggesting a magmatic origin for these deposits. However, the effects of other sources such as meteoric and/or connate fluids may be important during skarn formation and are not usually considered. It is suggested that the REE because of their coherent and somewhat predictable behavior can serve as tracers of the mineralizing fluids responsible for skarn formation at the Continental mine.

The object of this study is to determine the source of the fluids that were responsible for the formation of the skarn and ore mineralization at the Continental mine in light of REE analyses and fluid inclusion studies. This study is designed to answer the following questions:

1. Can the REE be used as geochemical tracers?
2. What are the source(s) of the mineralizing fluids responsible for skarn mineralization at the Continental mine? Can any changes in REE be attributed to a magmatic and/or meteoric source?

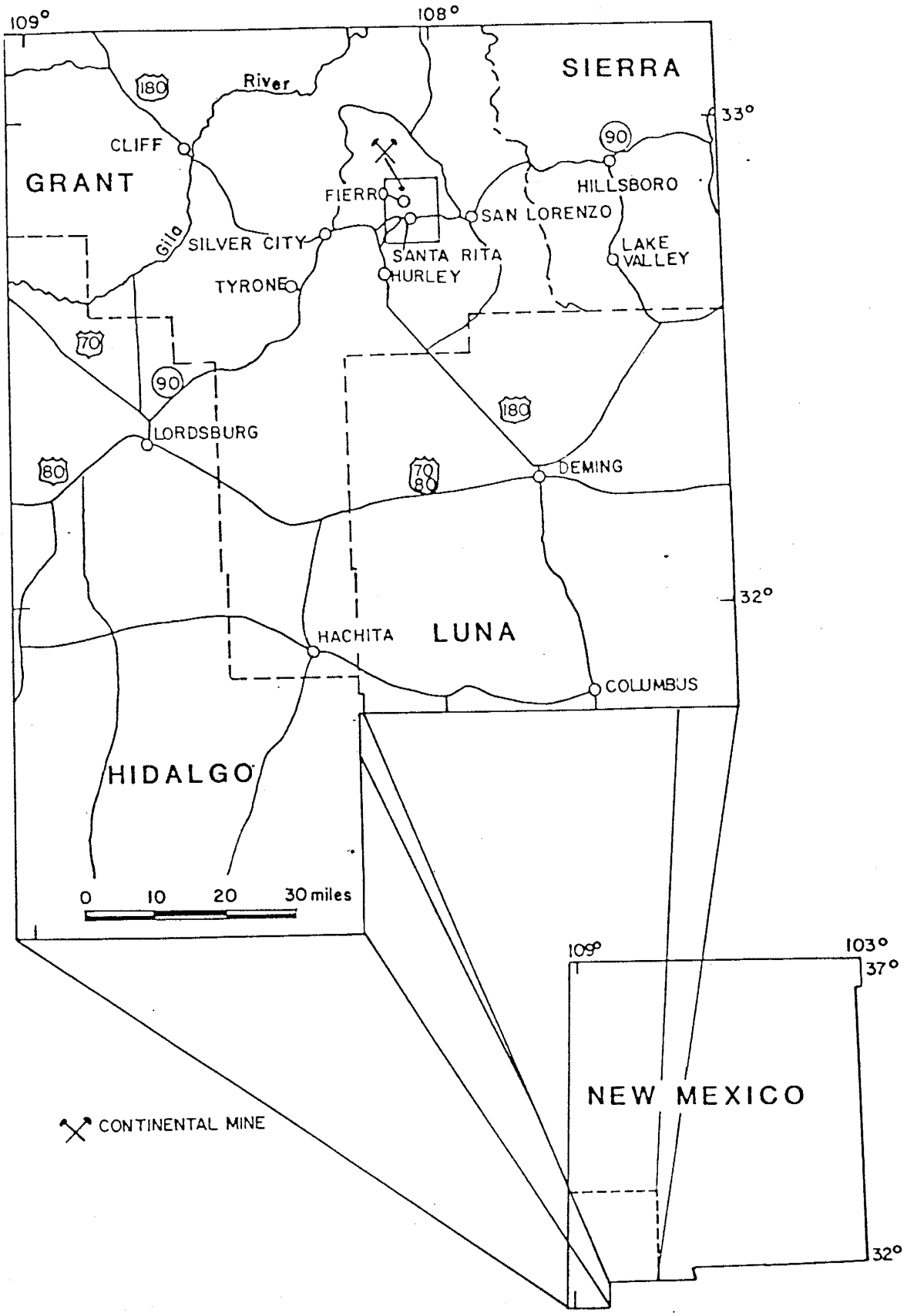

Figure 1. Index map of the Continental mine, Grant County, New Mexico Modified after Jones and others, 1967.

3. Are the REE in sediments altered during recrystallization, during skarn and hornfels formation or during ore mineralization?
4. What was the temperature, pressure, and composition (salinity) of the mineralizing fluids?

This study also includes an investigation of mineralogical changes, petrological relationships, and paragenesis related to the formation of the Continental skarn deposit.

Previous Work

Geology

An excellent summary of previous work can be found in Jones and others (1967) which includes most of the information contained in the earlier papers. The ore deposits in the Central Mining District are best summarized in Hernon and Jones (1968).

There are few studies on the Continental mine. Tonnage, general geology, and production at the Hanover mine located in the hanging wall of the Barringer fault southeast of the present day Continental No. 4 shaft is described by Lindgren, (1910) and Spencer and Paige, (1935). Kelley, (1949) described the occurrence of the magnetite ores associated with the Hanover-Fierro intrusive. The metasomatic ore deposits surrounding the Hanover-Fierro stock were described by Landon, (1929). Schmitt, (1933b, 1939a, and 1949) described the occurrence of zinc-iron mineralization at the Pewabic mine located at the southern margin of the Hanover-Fierro stock.

The structure in the Hanover-Santa Rita area was studied by Aldrich (1972). Skarn assemblages were mapped, described, and mineral zonation was determined at the Continental mine as a M.S. thesis (Forrester, 1972). Yousefpour (1977) described skarn assemblages and mineral zonation surrounding the Hanover-Fierro intrusion. Yousefpour (1979) described the igneous rocks and ore mineralization at the Continental mine as a PhD thesis. Forrester (1972) and Yousefpour (1977, 1979) concluded that

skarn formation was genetically related to the Hanover Fierro intrusion.

REE

REE studies related to ore deposits are limited. Beus (1958), Kosterin (1959), Bandurkin (1961), Mineyev (1963) and Choppin and others (1963) determined that REE are transported as F, CO3, and SO4 complexes in hydrothermal solutions. Graf (1972) used REE to monitor the alteration reactions that occur in hydrothermal systems that are responsible for the formation of massive sulfide deposits. Schneider and others, (1975, 1977) and Moller and others, (1976) sucessfully used REE fractionation patterns of fluorites to determine the genesis of the fluorites and the origin of the related Pb-Zn mineralization. Ganzeyev, (1976) used REE patterns of fluorites to identify fluorites of different origins. Martin and others (1978) determined that REE were mobile and added during fenitization of quartzites. Moller and others, (1979) used REE and C and O isotope patterns in calcite to determine the origin of the ore bearing fluids in Pb-Zn veins. Calcites of hydrothermal origin showed REE patterns distinctive from calcites of other origins. Moller and others (1981) used REE concentrations in Ca minerals, sphalerite, and cassiterite to determine the conditions under which the minerals formed. The REE distribution in these minerals showed distinct patterns and could be interpreted as having a sedimentary, hydrothermal or pegmatitic origin.

Fluid Inclusion Studies

Only fluid inclusion studies on skarn assemblages and ore mineralization that are similar to this study will be discussed. Ohmoto and others (1968) conducted a study on massive lead-zinc ore bodies associated with earlier formed skarn and fluid inclusion measurements made on quartz, calcite, and sphalerite indicate that major sulfide deposition occurred between 450°C and 370°C. De-Grout-Pommart (1975) studied a skarn deposit in Greece and determined that garnet-hedenbergite-magnetite skarn formed at between 550°C to 600°C. Huang and others (1975) studied a contact metasomatic replacement deposit and fluid inclusions from garnet, pyroxene, and quartz homogenized to a liquid at 450°C to >500°C. Sigurdson and Lawrence (1976) determined garnets associated with a tungsten-tactite skarn deposit filled at 350°C. Grabezhev (1977) determined that pyroxene-garnet-vesuvianite skarn formed at 500°C to 450°C in a skarn deposit from Russia. Ahmad and Rose (1980) conducted a fluid inclusion study on porphyry and skarn ore at Santa Rita, New Mexico and determined that skarn formation occurred between 250°C to 450°C. Tan and Kwak (1979) and Kwak and Tan (1981) studied the geology and genesis of a skarn deposit at Moina, Tasmania. Their work also included a fluid inclusion study on garnet and diopside skarn and they concluded that the composition and homogenization temperatures of fluid inclusions was strongly dependent upon and varied systematically with distance from, the intrusion.

Method Of Investigation

A total of eighty-four samples were collected. These samples included each mineralized formation from the Continental mine (Fig. 2) and the equivalent unaltered formations were sampled (Fig. 3). Samples of the same formations thermally altered (recrystallized) but not metasomatized or mineralized were also studied (Fig. 4). The samples collected from the Continental open pit mine (Fig. 2) do not always match the geologic formations shown on the open pit map because of changes in the surface geology of the mine between when the mine was last mapped (1977) and when samples were collected for this study (1981).

Fifty-seven thin sections and eighteen polished sections were examined petrographically.

X-ray diffraction analyses were done for determining mineral composition of garnets, for mineral identification and for verification that garnet samples used for Instrumental Neutron Activation Analysis (INAA) were pure.

REE concentrations were determined on forty-eight samples by INAA. Other trace element data was also collected.

Forty-five doubly polished sections of garnet from skarn and quartz-magnetite and quartz-magnetite-sulfide veins that cut skarn were used to obtain fluid inclusion measurements (Fig. 2).

EXPLANATION

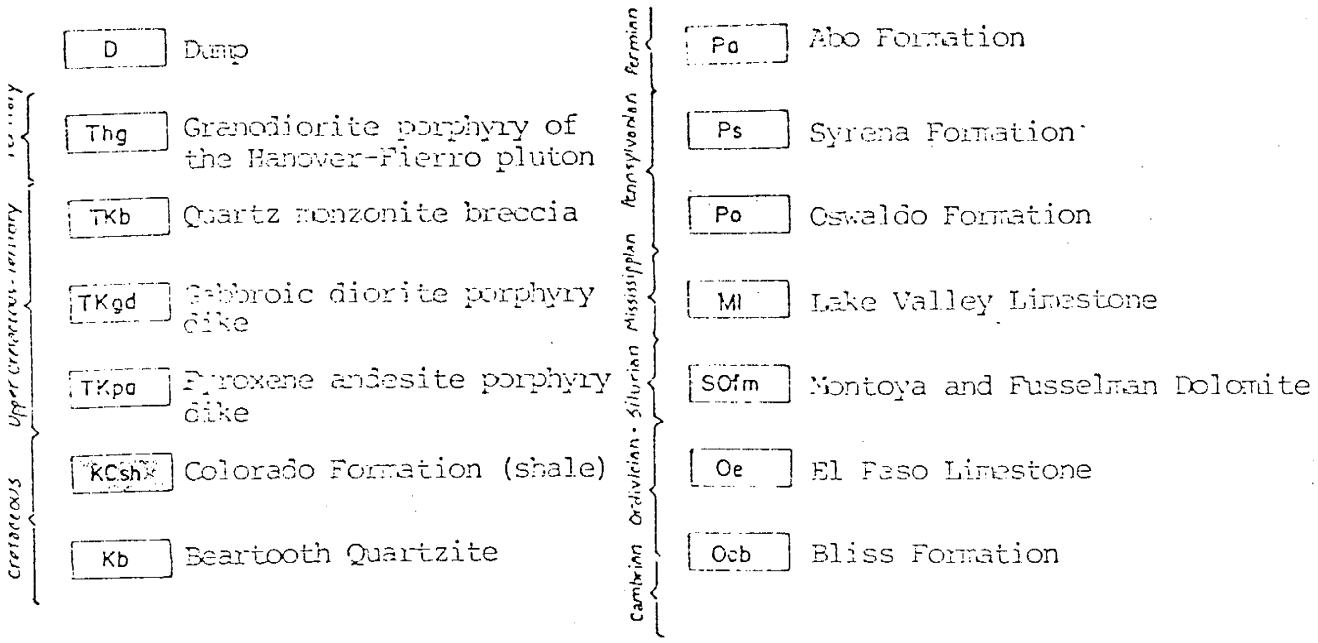

------ Contact dashed line indicates approximate location

------ Fault dashed line indicates approximate location

● Location of samples from the Continental mine, note: some of the samples are located in a formation that does not match lithology of the sample because the sample was either collected underground and differs from surface geology, and because of changes in surface geology from 1977 when this map was completed and 1980, when samples were collected.

CBQ-1 Bliss Quartzite
CG-2 Hanover-Fierro granodiorite
CEP-3 El Paso Limestone
CM-4 Montoya Dolomite
CMA-5 Aleman Chert
CGD-6 Granodiorite dike garnetized
CC-7 Chert
CBR-8 Breccia
CGD-9 Granodiorite dike garnetized
CM-10 Montoya Dolomite
CDM-11 Montoya Dolomite magnetite skarn
COS-H-12 Hanover Formation
CPS-13 Parting Shale dike
CPS-H-14 Parting Shale
COS-15 Oswaldo Formation
CAG-16 Augen Percha Shale
CLV-17 Lower Blue Lake Valley Limestone
CPS-18 Percha Shale
COS-19 Oswaldo Formation
CBQ-20 Beartooth Quartzite
CABO-21 Abo Formation
CCF-22 Colorado Formation
CCV-23 Chalcocite vein Colorado Form.
CAMP-24 Amphibolite dike Colorado Form.
CDS-25 Diorite sill Colorado Formation
CDS-26 Diorite sill Colorado Formation
CSY-1-27 Syrena Formation
CSY-2-27 Syrena Formation
CSY-28 Syrena Formation (garnet band)
GTl-1 Garnet skarn Lake Valley Limestor
GT-1 Garnet skarn Oswaldo Formation
GT-2 Garnet skarn Lake Valley Limestone
GT-3 Garnet skarn Lake Valley Limestone
GT-4 Garnet skarn Lake Valley Limestone
GT-5 Garnet skarn Oswaldo Formation
GTH Garnet skarn Oswlado Formation

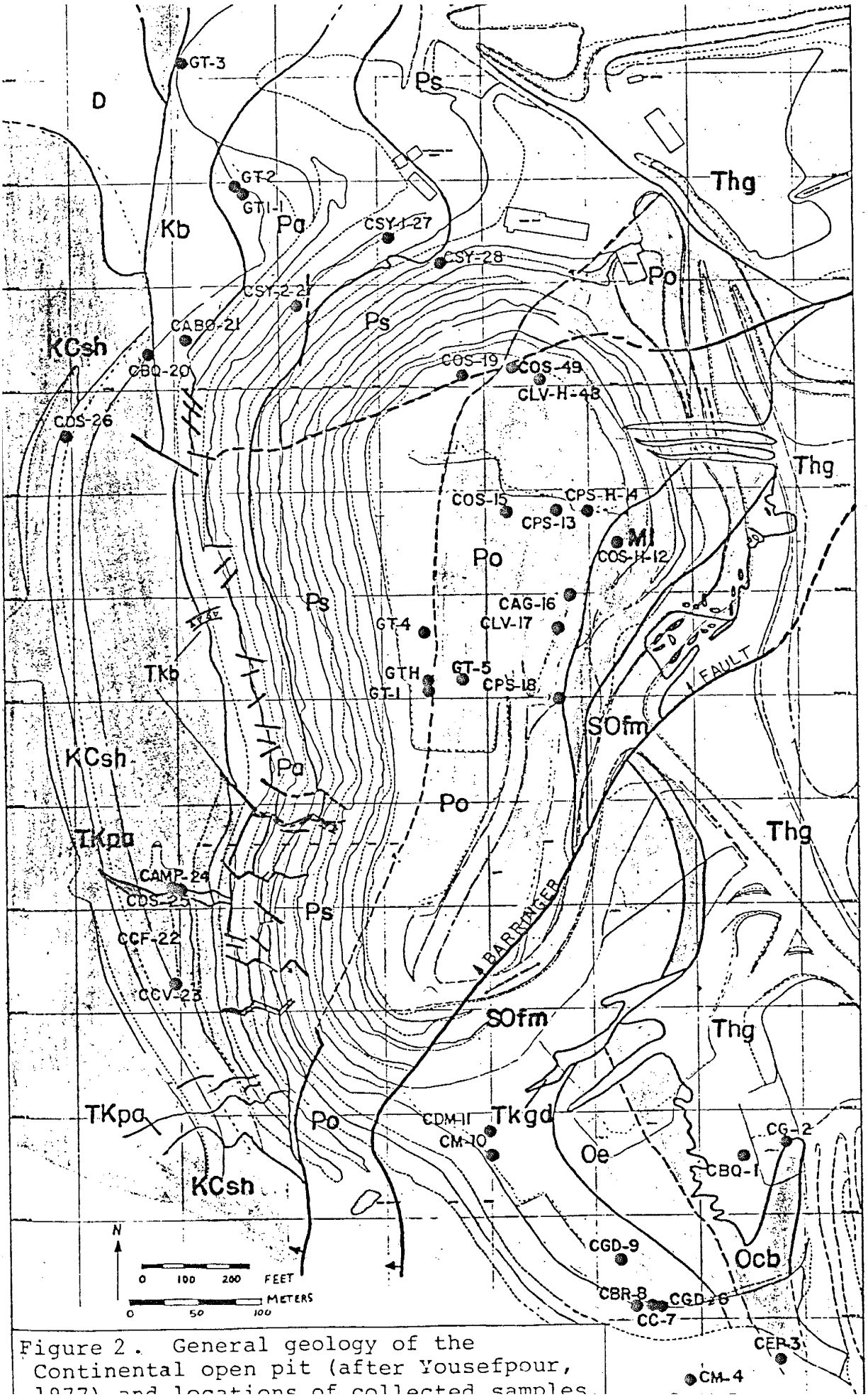

Figure 2. General geology of the Continental open pit (after Yousefpour, 1977) and locations of collected samples

Kql:quartz latite porphyry dike.

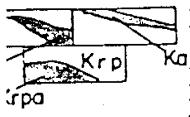

Krp: andesite; andesite breccia, latite.
Krpa: andesite.
Ka: andesite dikes, sills.

Kb Beartooth Quartzite

Pa Abo Formation

Pm Magdalena Group

Ml Lake Valley Limestone

Dp Percha Shale

SOfm Fusselman-Montoya Dolomite

Oep El Paso Limestone

OCb Bliss Sandstone

Pch Hornblende-chlorite schist

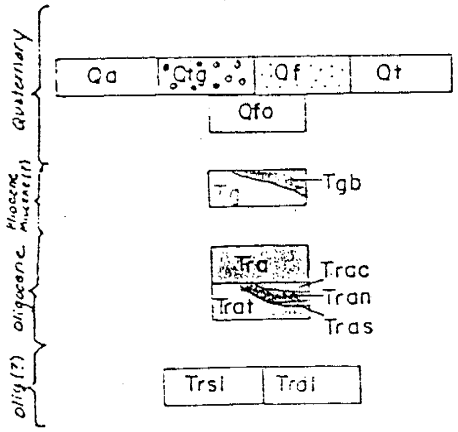

Qa: Alluvium
Qtg: Terrace gravel
Qf: Fan deposits
Qt: Talus deposits

Tg: Gila Conglomerate
Tgb: Olivine basalt

Tra: Razorback Formati
Trac: Sandstone-pebble
Tran: Air-fall tuff
Tras: Tuffaceous sands
Trat: Ash-flow tuff

Trsl: Rhyolite sill of lampbright draw
Trdl: Rhyolite dome of lampbright draw

——— Contact, dashed where approximated

——— Fault, dashed where approximated

- Sample locations

-41 Augen Percha Shale
42 Percha Shale
3 Bliss Formation
44 PreCambrian greenstone
45 Bliss Formation
-46 El Paso Limestone
7 Montoya Dolomite

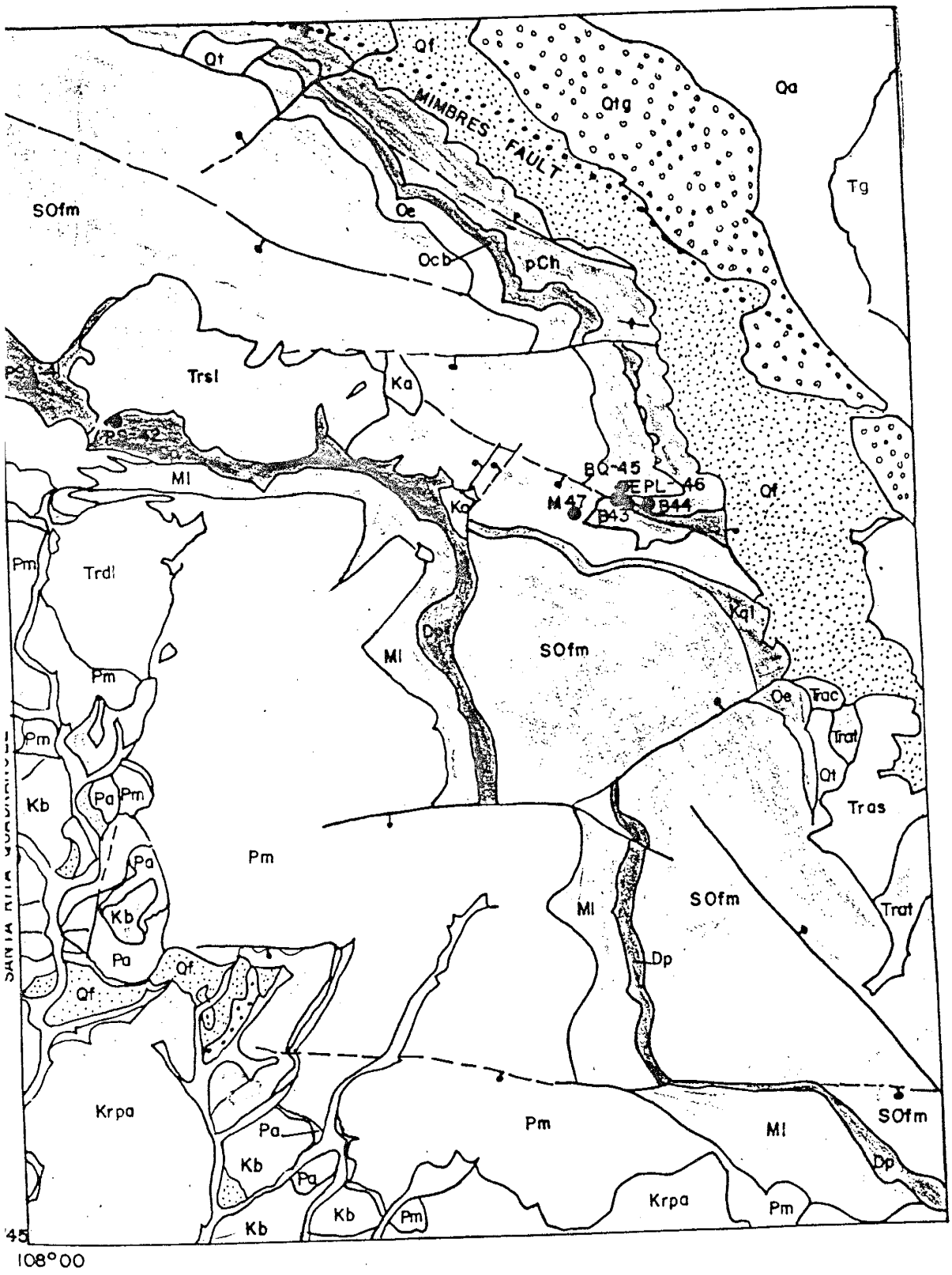

Figure 3. Geologic map of the southwest corner of the San Lorenzo quadrangle modified from Hedlund, 1975 showing the location of collected samples.

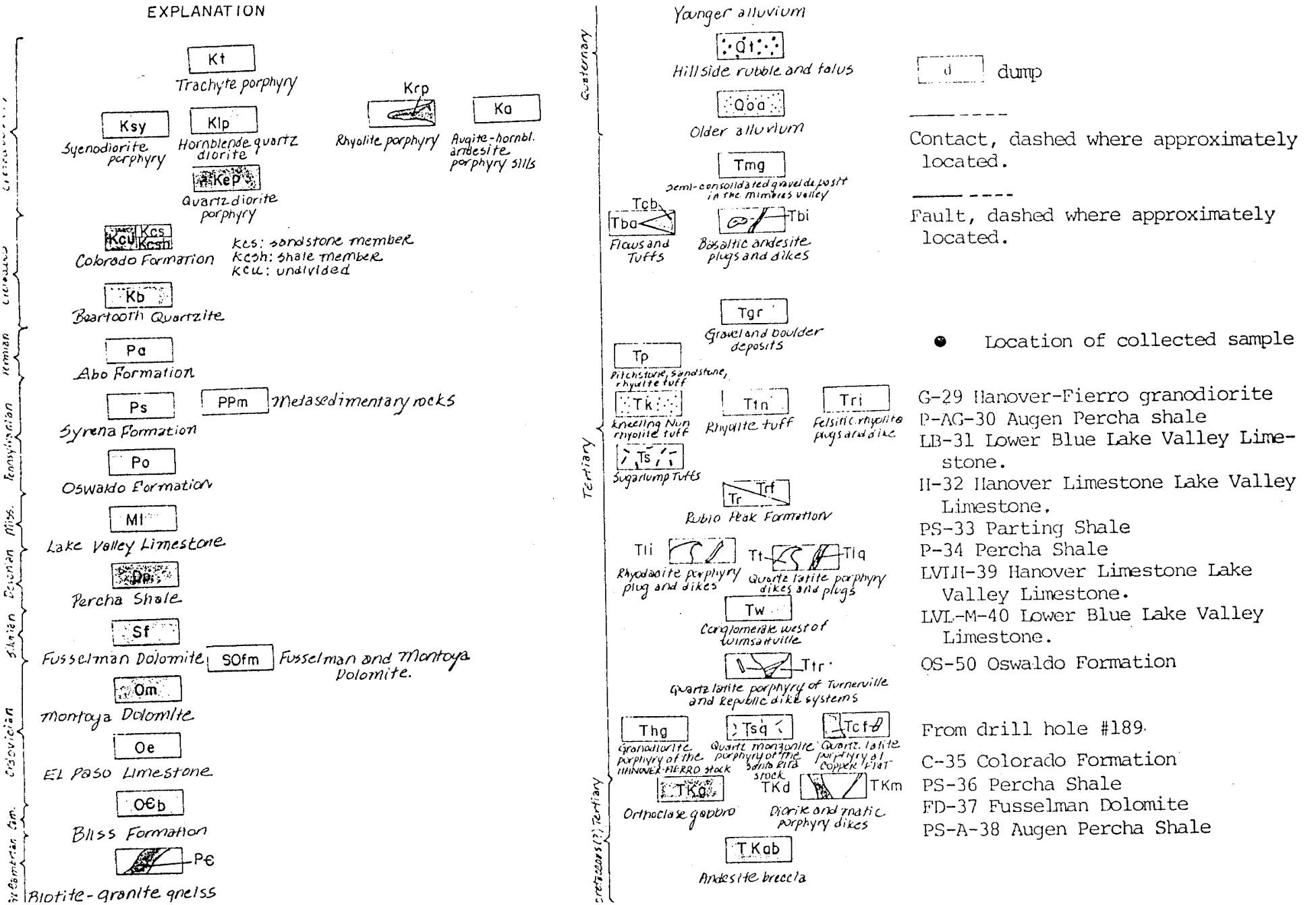
EXPLANATION
Cretaceous
Kt
Trachyte porphyry
Krp
Rhyolite porphyry
Ka
Augite-hornbl. andesite porphyry sills
Ksy
Syenodiorite porphyry
Klp
Hornblende quartz diorite
KeP
Quartz diorite porphyry
Kcu Kcs Kcsh
Colorado Formation
Kcs: sandstone member
Kcsh: Shale member
Kcu: undivided
Cretaceous
Kb
Beartooth Quartzite
Permian
Pa
Abo Formation
Pennsylvanian
Ps
PPm
Metasedimentary rocks
Syrena Formation
Po
Oswaldo Formation
Miss.
Ml
Lake Valley Limestone
Devonian
Dp
Percha Shale
Silurian
Sf
Fusselman Dolomite
SOfm
Fusselman and Montoya Dolomite.
Ordovician
Om
Montoya Dolomite
Oe
EL Paso Limestone
Oeb
Bliss Formation
Camb.
Pe
Biotite-granite gneiss
Quaternary
Younger alluvium
Qt
Hillside rubble and talus
Qoa
Older alluvium
Tmg
Semi-consolidated gravel deposit in the Mimbres valley
Tcb
Tba
Flows and Tuffs
Tbi
Basaltic andesite plugs and dikes
Tgr
Gravel and boulder deposits
Tp
Pitchstone, sandstone, rhyolite tuff
Tk
kneeling Nun rhyolite tuff
Ttn
Rhyolite tuff
Tri
Felsitic rhyolite plugs and dike
Ts
Sugarlump Tuffs
Tr
Trf
Rubio Peak Formation
Tertiary
Tli
Rhyodacite porphyry plug and dikes
Tt
Tlq
Quartz latite porphyry dikes and plugs
Tw
Conglomerate west of Winsantville
Ttr
Quartz latite porphyry of Turnerville and Republic dike systems
Thg
Granodiorite porphyry of the HANOVER-FIERRO stock
Tsq
Quartz monzonite porphyry of the Santa Rita stock
Tcf
Quartz latite porphyry at COPPER FLAT
TKg
Orthoclase gabbro
TKd
TKm
Diorite and matic porphyry dikes
Cretaceous(?) Tertiary
TKab
Andesite breccia
d
dump
Contact, dashed where approximately located.
Fault, dashed where approximately located.
Location of collected sample
G-29 Hanover-Fierro granodiorite
P-AG-30 Augen Percha shale
LB-31 Lower Blue Lake Valley Limestone.
H-32 Hanover Limestone Lake Valley Limestone,
PS-33 Parting Shale
P-34 Percha Shale
LVLH-39 Hanover Limestone Lake Valley Limestone.
LVL-M-40 Lower Blue Lake Valley Limestone.
OS-50 Oswaldo Formation
From drill hole #189.
C-35 Colorado Formation
PS-36 Percha Shale
FD-37 Fusselman Dolomite
PS-A-38 Augen Percha Shale

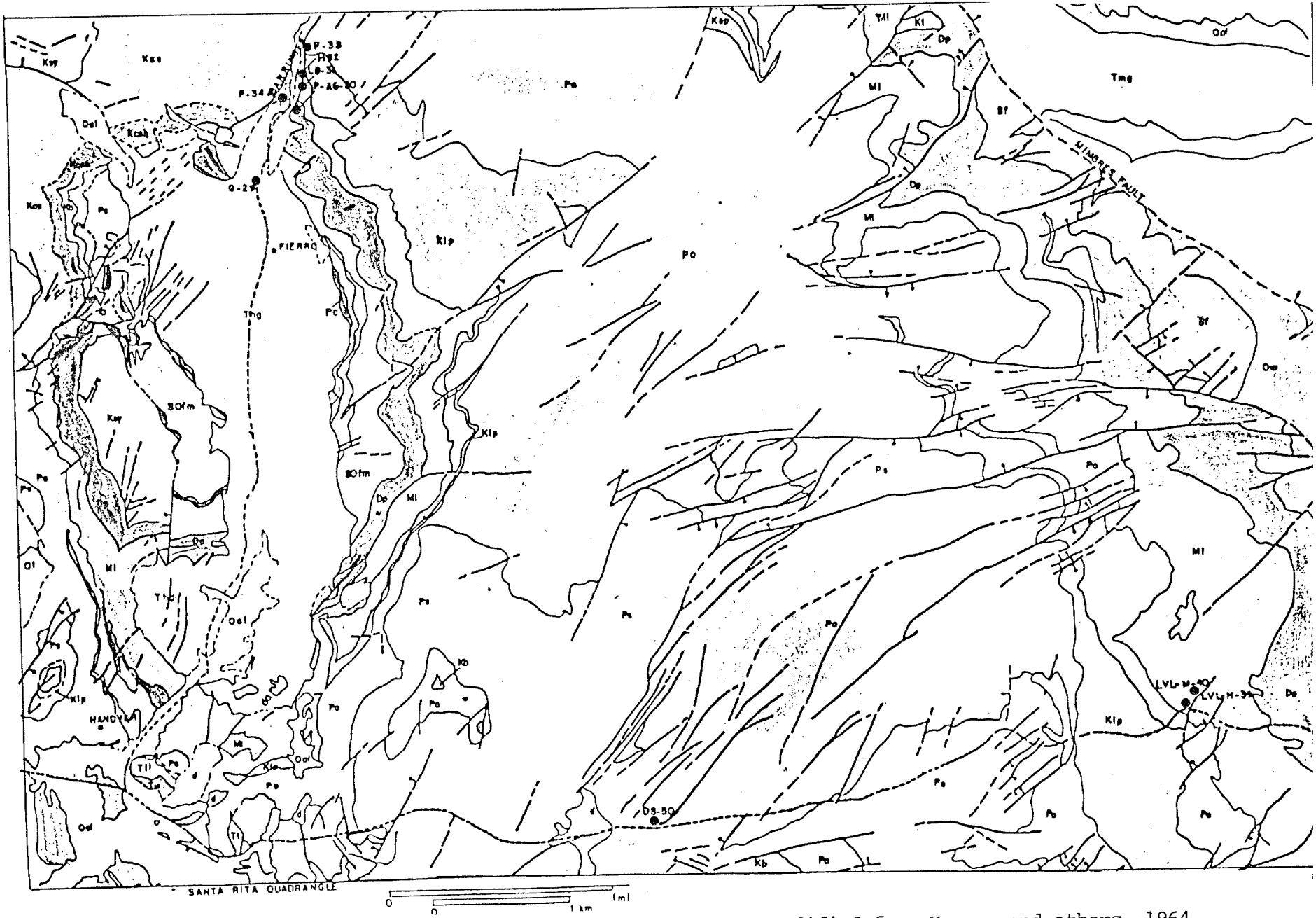

4. Geologic map of a portion of the Santa Rita quadrangle modified from Hernon and others, 1964

General Geology

Regional and Tectonic Setting

The Hanover-Fierro intusive and nearby Pinos Altos, Santa Rita, Copper Flat, and Tyrone intrusives are part of the Laramide porphyry copper belt (80-45 myBP) of the southern Cordillera. Most deposits lie within the Basin and Range province of southeastern Arizona, New Mexico, and Sonora. The Cordillera occurs in a deformed belt of Paleozoic and Mesozoic rocks and occupies a position between coastal batholiths and uplifted or widely exposed basement rocks of PreCambrian or lower Proterozoic age (Fig. 5).

Paleozoic strata were deposited in a cratonic environment that lay east of the Cordillera Miogeocline. Carbonate rocks dominate the Paleozoic stratigraphy in most regions. Substantial evidence (Kottlowski, 1963; Butler, 1971) indicate a northwest trending tectonic grain that affected deposition, although no great magnitude of structural movement is indicated. Volcanism and intrusive activity was widespread in a northwest trending belt in Triassic and Jurassic; however, these rocks are not present in the Central mining district. During early Cretaceous the southern Cordillera was the site of deposition of great thicknesses of clastic rocks and lesser amounts of marine carbonates. Northwest-trending tectonics was active in the pre-Laramide Mesozoic.

During the Laramide (80-45 myBP) extensive calc-alkaline volcanism and igneous activity gave rise to

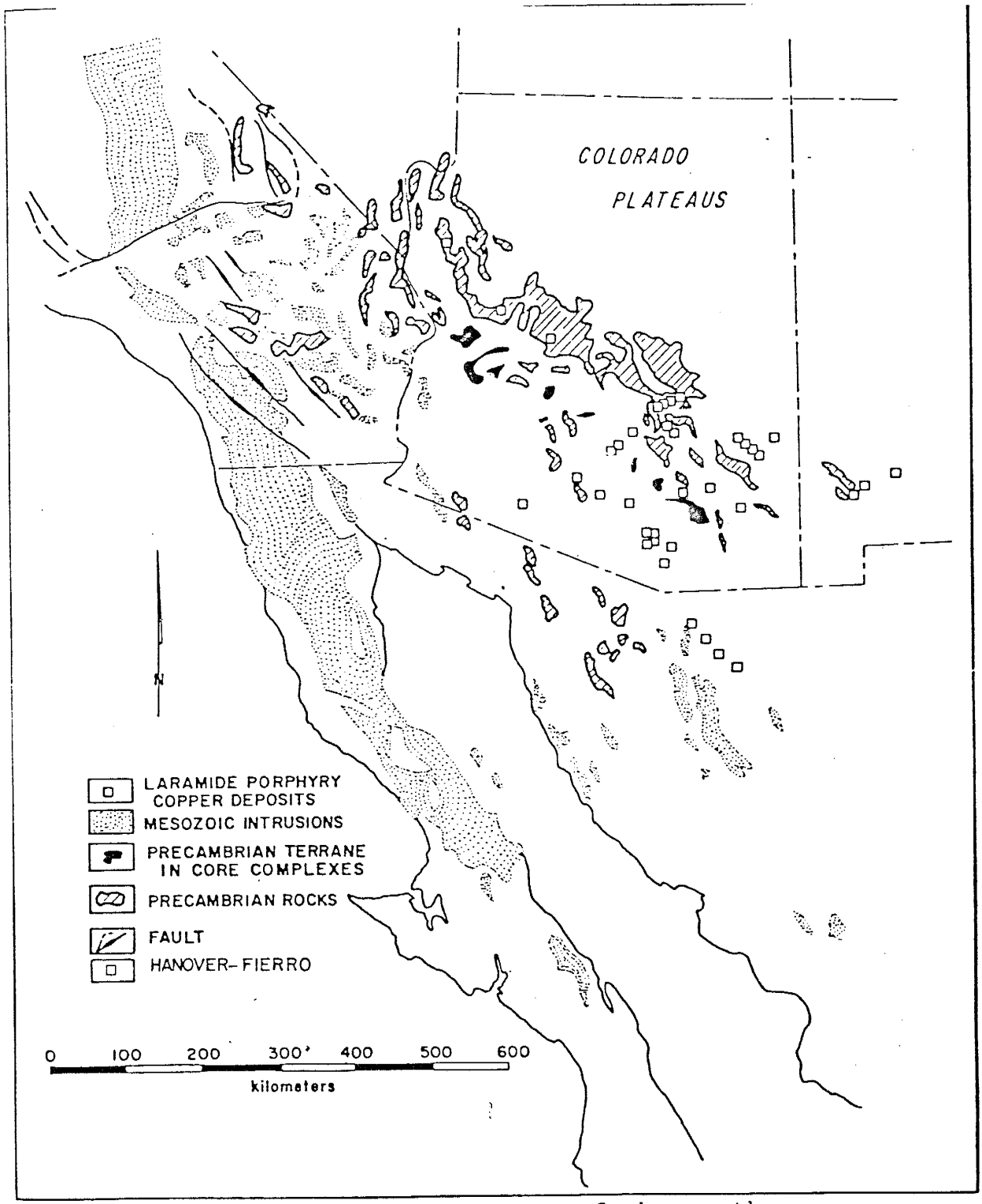

Figure 5. Generalized geologic map of the southern Cordillera showing the location of most porphyry copper deposits of the region, PreCambrian exposures and the Coastal Batholiths (after Titley, 1981).

many porphyry copper and related ore deposits. The Laramide event is believed to be related to times of high convergence rates produced by movement of the oceanic Farallon plate and the continental North American plate (Fig. 6). Flattening of the subduction zone (Lipman and others, 1972; Coney and Reynolds, 1977) is considered to have resulted in the broad areal extent of subduction related, calc-alkaline intrusive and volcanic activity in the southern Cordillera. The eastward sweep of arc magmatism and associated tectonism during Laramide time was followed by a westward sweep accompaned by complex extensional tectonics during mid Cenozoic times. Ridge subduction of the Farallon plate initiated the formation of the San Andreas transform fault in Late Cenozoic, extinguished arc magmatism and opened the Gulf of California. After a gap in time (40-15 myBP) calc-alkaline volcanism changed to bimodal tholeiitic volcanism and tectonic style changed from dominantly compressional to dominantly extensional.

Extensional deformation within Basin and Range tectonics (15-0 myBP) was characterized by the formation of horsts, grabens, tilted blocks bounded by steeply dipping normal faults, valley-filled sediments, and bimodal volcanism. Basin and Range tectonics is not associated with the formation of the porphyry copper deposits.

General Structure of the Central Mining District

The Continental deposit occurs in the crudely triangular, fault bounded, uplifted Santa Rita Horst in an

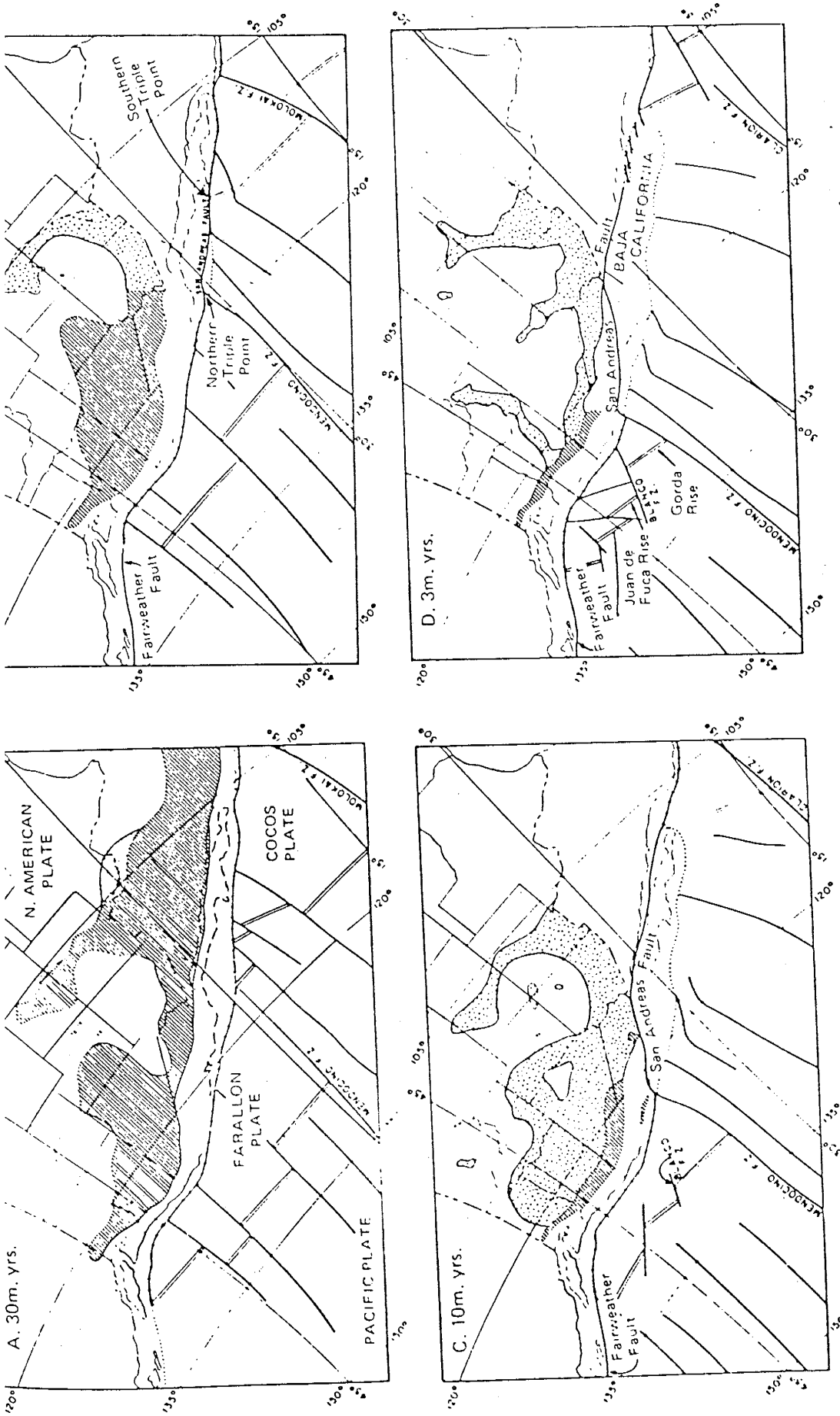

Figure 6. Map showing the Farallon Plate in Relation to the North American Plate and the evolution of the San Andreas Fault, showing the Cordilleran Belt (modified from Atwater, 1970, Christiansen and Lipman, 1972 in Plate Tectonics and Crustal Evolution, K.C. Condie, 1976).

area of erosion of Miocene(?) volcanics and younger sediments. Exposures of the older Paleozoic formations and their associated ore deposits occur in the Santa Rita horst. The Mimbres fault to the east, the Barringer fault to the northwest, and to the south a zone of primarily discontinuous normal faults which trend N.75E. bound the Santa Rita horst (Fig. 7).

Structural History of the Central Mining District

Little is known concerning the deformation of PreCambrian rocks because of the small amount of exposed rocks in the area. No folds or faults are known to have formed during the entire Paleozoic era.

Major structural features in the Central mining district are related to Laramide intrusive and volcanic activity and to later Basin and Range tectonics. Most of this structural deformation is directly related to intrusion of igneous rocks. The emplacement of intrusives occurred in definite chronological order and includes: 1) sills, laccoliths and generally concordant plutons, 2) mafic plugs and dike swarms related to the andestic volcanic complex, 3) disconcordant plutons (Hanover-Fierro stock), and, 4) dike swarms and plugs. The major intrusive stocks such as the Hanover-Fierro and Santa Rita stocks have locally domed the overlying sedimentary rocks forming small anticlinal structures.

Complete development of fault and fracture patterns and deposition of massive iron-oxide ore bodies followed the

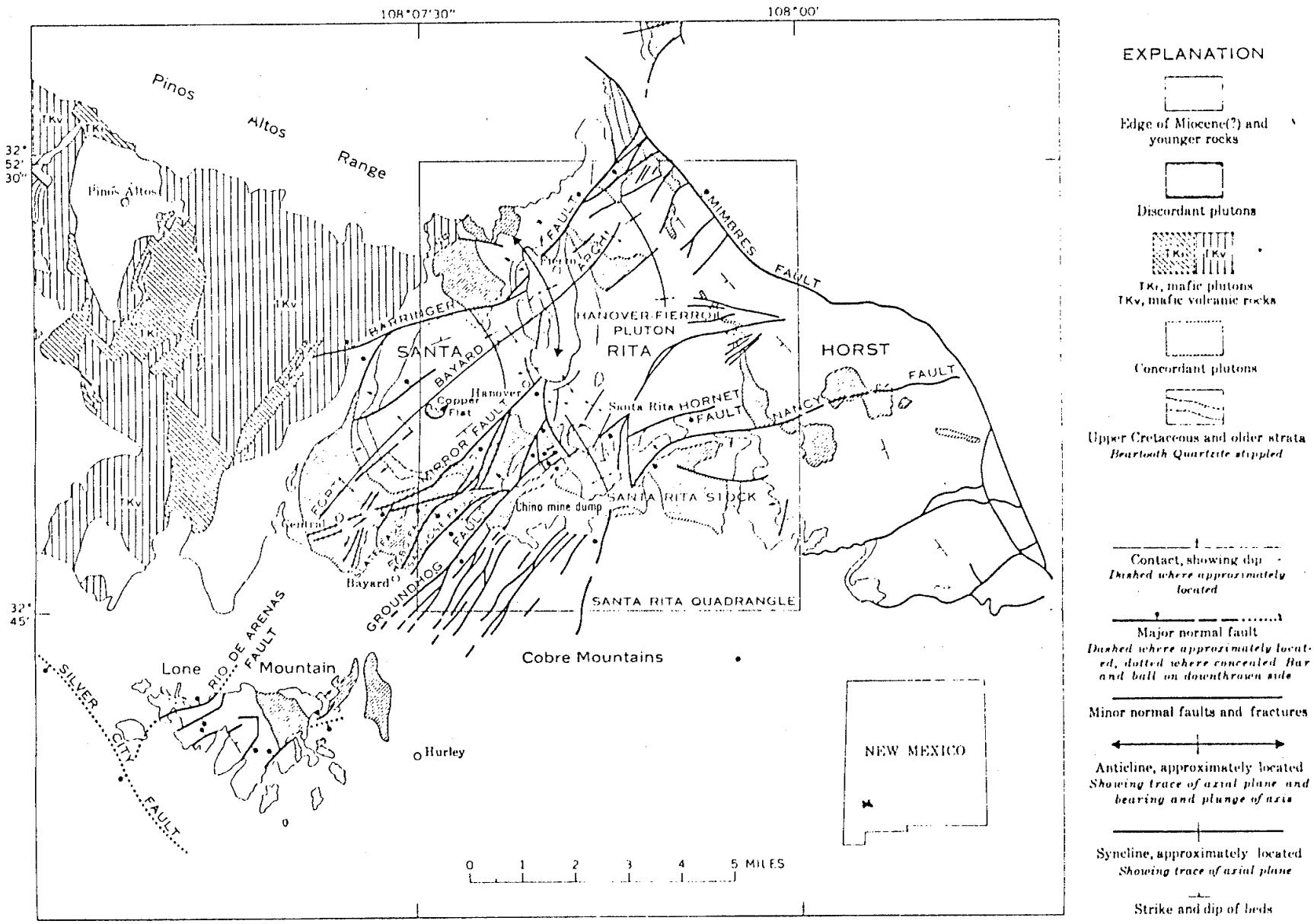

Figure 7. Structural geologic setting of the Santa Rita quadrangle (from Kuellmer, 1

intrusion of the major stocks. Some faults such as the Barringer, Modoc and Zuniga faults were in existence prior to the intrusion of the sills and the major stocks and many faults were reactivated during the period of intrusion of major stocks to after deposition of the Miocene volcanics.

Northeast-trending and northwest-trending Basin and Range faults formed (15-0 myBP) and sometimes reactivated faults. The northeast-trending faults predominate in size, amount of displacement and number (Figs. 7 and 8).

According to Jones and others, (1967) six breccia pipes occur in the Central mining district (Fig. 8). One of the breccias occurs in the southern lobe of the Hanover-Fierro pluton. The age of the breccia pipes in each area is based on the type of rocks included in the breccia or by alteration and ore mineralization. The ages of the breccia pipes range from pre-intrustion to post-intrustion.

The Hanover Hole located just south of Hanover is a circular cavity that has been filled with sedimentary rocks (Fig. 8). An origin of subsidence or explosion has been postulated (Jones and others, 1967).

Stratigraphy of the Central Mining District

The PreCambrian rocks in the Central mining district are grantite, micaceous schists, gneisses, greenstones, and quartzites (Figs. 4 and 9).

According to Jones and others (1967) the PreCambrian basement is covered by approximately 1000 meters of Paleozoic rocks which are predominately limestone, dolomite, and lesser amounts of shale (Fig. 9). Ordovician and Silurian

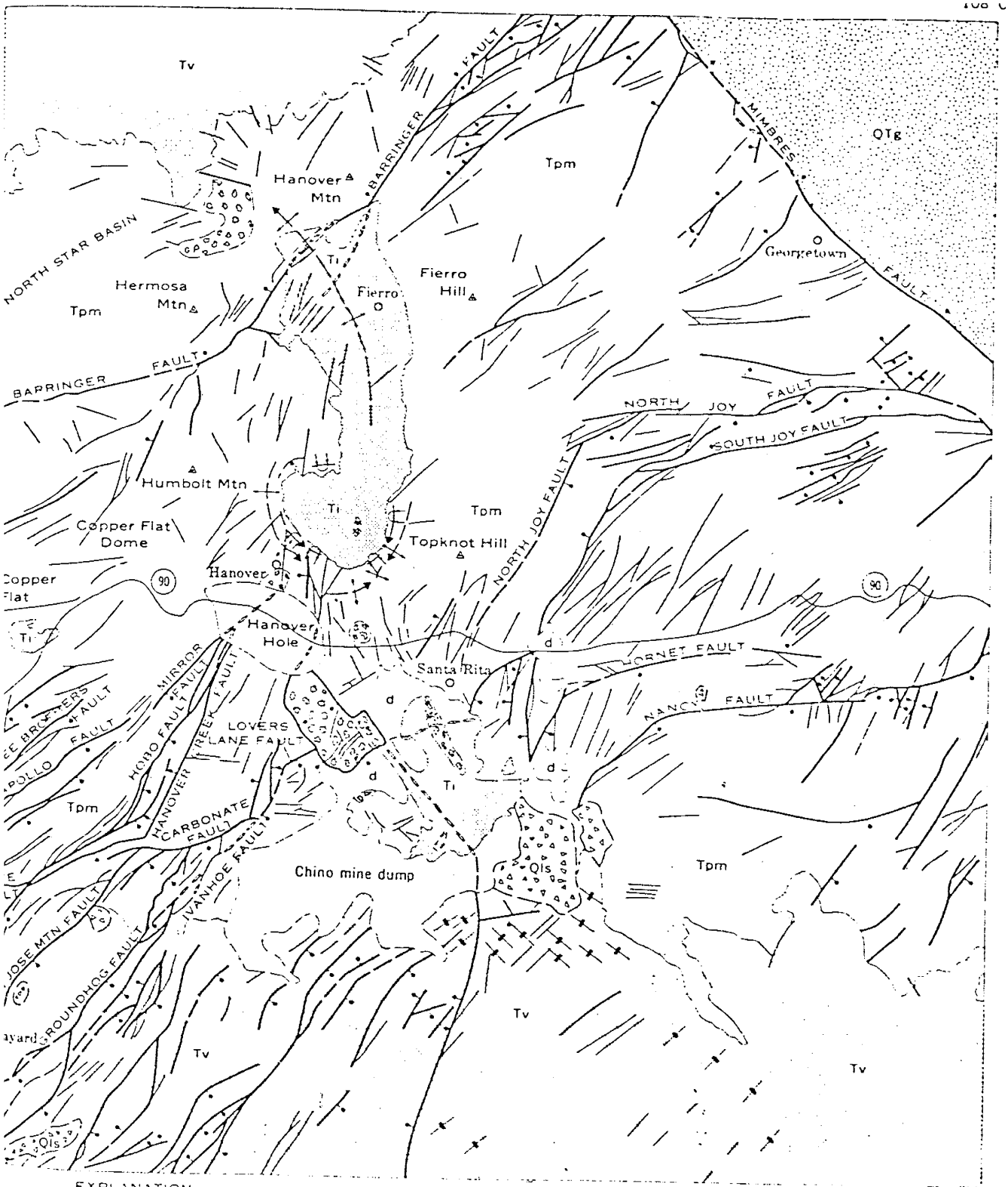
Tv
Hanover Mtn
BARRINGER FAULT
MIMBRES FAULT
QTg
Tpm
NORTH STAR BASIN
Hermosa Mtn
Fierro
Fierro Hill
Georgetown
FAULT
BARRINGER FAULT
NORTH JOY FAULT
SOUTH JOY FAULT
Humbolt Mtn
Tpm
Copper Flat Dome
Topknot Hill
NORTH JOY FAULT
Copper Flat
Hanover
90
Hanover Hole
HORNET FAULT
Santa Rita
NANCY FAULT
MIRROR FAULT
HOBO FAULT
LOVERS LANE FAULT
APOLLO FAULT
HANOVER CREEK FAULT
CARBONATE FAULT
IVANHOE FAULT
Chino mine dump
Qls
JOSE MTN FAULT
ROUNDHOG FAULT
0 1 2 3 MILES
EXPLANATION
Landslide deposits
Upper Miocene or younger gravel deposits
Miocene(?) volcanic and detrital rocks
Lower Tertiary
Contact
Normal fault
Pre-Miocene rocks
Fractures or minor faults
Area of brecciated rock
Anticline
Overturned syncline
Folds
Strong vertical joint set

System	Formation	Approx. thick. meters	Lithology
Recent and Pliestocene	Younger alluvium Older alluvium		Unconsolidated alluvium and colluvium in valley floors, flat uplands and slopes. Includes sand silt, gravel.
Pliocene and Miocene	Gravel deposits in Mimbres River System	0-250	Somewhat consolidated poorly sorted bolson deposits ranging from silt to boulder deposits.
Miocene(?)	Basaltic andesite flows and underlying gravel and boulder deposits	0-260	Dark-gray finely crystalline porphyritic flows; weather reddish brown contain phenocrysts of pyroxene, magnetite, and olivine in matrix of labradorite
	Pitchstone, sandstone, and indurated rhyolite tuff underlain by Kneeling Nunn Tuff	0-185	Crystal fragments of quartz, sanidine, biotite, and oligoclase, and rock fragments imbedded in compacted glass shards, in part devitrified and in part replaced by chalcedony. Black pitchstone contains rock fragments and and is locally vesicular.
	Sugarlump Tuff	0-185	Puniceous tuff, gravel, and sandstone locally replaced by clinoptlolite Generally well stratified.
			Andesite breccia (see below)
	Rubio Peak Formation	0-185	Conglomeratic containing intercalated indurated tuffs and rhyodacite and andesite flows. (Rubio Peak Form.)
Lower Tertiary and Upper Cret.	Andesite breccia	0-150	Andesite breccia and fine-grained crystal tuff, volcanic sandstone, and some nonvolcanic sandstone and mudstone.
Upper Cret.	Colorado Formation	0-300	Upper 250 m. consists of tan, green-brown, and white sandstone interbedded with dark-green, brown, and black shale. Lower 70 m. is black limy shale except for 6.5 m. of quartzite about 25 m. above base. Thin beds of fossiliferous impure limestone conspicuous in lower part above the lower beds of black shale
Upper(?) Cret.	Beartooth Quartzite	20-45	Fine-grained quartzite containing thin black-shale partings locally. Conglomerate beds near top.
Lower Permian	Abo Formation	0-80	Red shale, mudstone, and limy mudstone containing lenses of algal conglomerate locally.
Upper Pennsylvanian	Syrena Formation	50-120	Impure limestone and limestone interbedded with irregular lenses of red calcareous shale and with shale beds particularly in the lower 45 m.
Upper and Middle Penn.	Oswaldo Formation (Upper Blue Limestone) (Middle Blue Limestone) (Parting Shale): basal	100-125	Blue-gray limestone, fairly pure except in upper part, interbedded with thin shale beds; gray to red siliceous shale or grit about 6.5 m. thick occurs at the base.
Lower Miss.	Lake Valley Limestone (Lower Blue Limestone) (Hanover Limestone)	90-125	Limestone, pure crinoidal and massive in upper part, argillaceous and thin bedded in central part. Much nodular chert throughout.
Upper Devonian	Percha Shale (Augen) Box Member (Ready Pay Member)	70-95	Upper member (Box Member) is gray calcareous shale containing abundant limestone nodules; lower member (Ready Pay Member) is black fissile shale, calcareous base.
Silurian	Fusselman Dolomite	30-90	Gray cherty finely crystalline vuggy massive dolomite
Upper and Middle Ordovician	Montoya Dolomite	90-105	Light gray to gray very finely crystalline massive dolomite containing interbedded dolomite and dark chert in central part and concentrarions of opalescent quartz sandstone at the base.
Lower Ordovician	El Paso Limestones	150-160	Thin to thickbedded light-gray limestone and dolomite. Chert nodules in upper part; abundant fucoidal markings in lower part.
Upper Cambrian	Bliss Formation	40-60	Predominantly dark-brown massive quartzite, locally hematitic and glauconitic. Grayish-brown shaly dolomite and basal course conglomerate locally
PreCambrian			Granite, granite gneiss, and greenstone

Figure 9 Description of layered rocks in the Central Mining District, Grant County, New Mexico modified after Jones and others, 1967. Names occurring in parantheses refer to local terminology employed by miners and appear in the order in which they occur stratigraphically.

sediments are dolomites with the exception of the El Paso Limestone which is in part dolomite. Above the Devonian shale all Paleozoic sediments are limestones. Cretaceous basal quartzite and overlying shales and sandstones approximately 550 m thick unconformably rest on Upper Paleozoic formations.

The nine Paleozoic formations range from Cambrian to Permian and are important hosts of skarn and ore mineralization at the Continental mine. These nine formations and the two Upper Cretaceous formations are the complete stratigraphic section at the Continental mine (Fig. 9).

Overlying the eroded surface of the Lower Cretaceous sedimentary rocks is up to 185 m of andesitic breccia and conglomerate of Upper Cretaceous to Lower Tertiary age. Numerous mafic dikes of probable Tertiary age intruded the volcanic rocks before mineralization (Jones and others, 1967).

After extensive erosion, Basin and Range Miocene (?) latitic and rhyolitic volcanic rocks followed by basaltic andesite flows associated with caldera complexes formed the Datil-Mogollon volcanic field.

Stratigraphic Nomenclature of the Central Mining District

Two sets of stratigraphic nomenclature are used for the Central mining district and Figure 9 relates these two terminologies. One is that of the United States Geological Survey used to describe the unaltered sediments. The other terminology is used by the mine geologists and refers to

alteration rather than lithology. The terminology employed by the United States Geological Survey will be used when referring to the unaltered section of rocks and the mine terminology will be used when referring to altered rocks in the Continental mine.

General Geology of the Continental Mine

The Continental mine is an Fe-Cu-(Zn) skarn deposit that occurs on the northern margin of the Hanover-Fierro stock. The skarn and hornfels replace Paleozoic and Upper Cretaceous limestones, argillaceous limestones, limy shales, and dolomites. The most pure limestones such as the Hanover, Lower, Middle and Upper Blue Limestones have been replaced by garnet skarn and are the most important hosts of sulfide and magnetite mineralization. The argillaceous limestones are replaced by garnet-clinopyroxene skarn and are less important hosts of sulfide and magnetite mineralization. The limy shales are altered to fine-grained garnet-clinopyroxene-feldspar-quartz hornfels with minor sulfide and magnetite mineralization that is usually disseminated or restricted to veins. Dolomite is replaced by forsterite-serpentine+magnetite skarn, forsterite-serpentine-clinopyroxene+magnetite skarn and massive magnetite skarn (Fig. 10).

Numerous fractures and faulting of the overlying sediments is directly related to the Hanover-Fierro intrusive. However, the Barringer Fault (Fig. 2) and the Zuniga and Modoc Faults that occur parallel and to the west

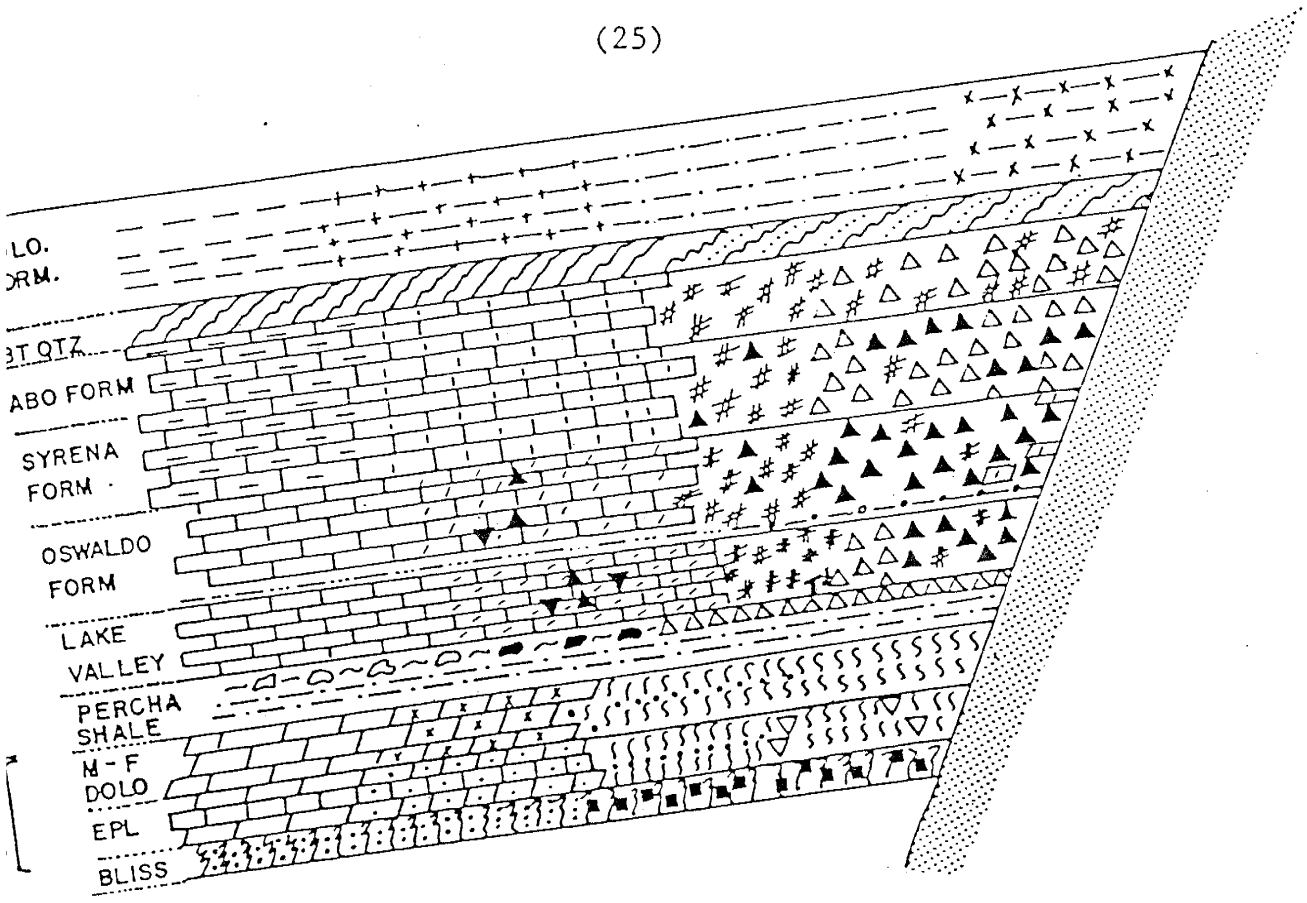

Shale
Clinopyroxene hornfels (quartz-feldspar)
Biotite hornfels
Recrystallized shale (slate)
Chlorite hornfels
Biotite-epidote hornfels
Limestone nodules in shale
Marble/recrystallized shale
Quartzite
Orthoquartzite
Recrystallized limestone-shale
Limestone-shale
Marble
Brucite-marble
Limestone

Dolomite
Limestone-dolomite
Recrystallized dolomite and mar
Serpentine-fosterie-phlogopite tremolite-hum
Serpentine-fosterite-carbonat
Massive quartzite (locally hema glauconitic dolom
Massive quartzite (epidote-hornblende-actino
Garnet skarn
Garnet bands
Garnet-diopside skarn
Isolated clinopyxrone skarn
Clinopyxroxene skarn
Wollastonite
Hanover-Fierro granodiorite

Continental Mine

and northwest respectively of the Barringer fault are pre-intrusive. The Barringer fault passes through the north end of the Hanover-Fierro stock where it has been mapped (Jones and others, 1967) as a series of parallel shear zones (Fig. 4). The Barringer, Zuniga, and Modoc Faults all served as important channelways for mineralizing fluids. Intensity of skarn mineralization decreases away from the faults. Skarn formation extends outward up to 1400 m from the contact with the intrusive along major faults. Thermal effects of the Hanover-Fierro intrusive extend approximately 600 to 800 m outward from the contact (Yousefpour, 1979).

Hanover-Fierro Intrusive

The Hanover-Fierro intrusive has an approximate north-south length of 4.0 kms and is approximately 0.8 to 1.6 kms wide (Fig. 4). The intrusive has two distinct parts (Schmitt, 1939a). The main mass comprises approximately eighty percent of the stock and is referred to as the porphyritic facies. The Hanover lobe which contains the remaining twenty percent of the stock is commonly referred to as the equigranular facies and forms the bulbous southern extremity of the pluton (Jones and others, 1967).

The two distinct facies occurred in two stages and it is suggested that the stock has a compound origin (Spencer and Paige, 1935; Jones and others, 1967). Structural evidence suggests that the main mass (porphyritic facies) of the Hanover-Fierro stock was intruded after the intrusion of the southern lobe (equigranular facies) or simply continued

to rise after the south lobe was emplaced. The structures around the northeast half of the southern lobe have been tilted southward as the main mass rose.

Regional Economic Geology

Most of the ore deposits in the Central mining district are genetically related to Laramide calc-alkaline intrusions and volcanism. Eight Fe, Fe-Zn, or Fe-Zn-Cu open pit mines surround the Hanover Fierro intrusive. Copper porphry deposits are spatially and genetically associated with the nearby Santa Rita, Copper Flat and Tyrone Laramide intrusives. Silver mineralization occurs at Georgetown and Chloride Flat (Fig. 10a).

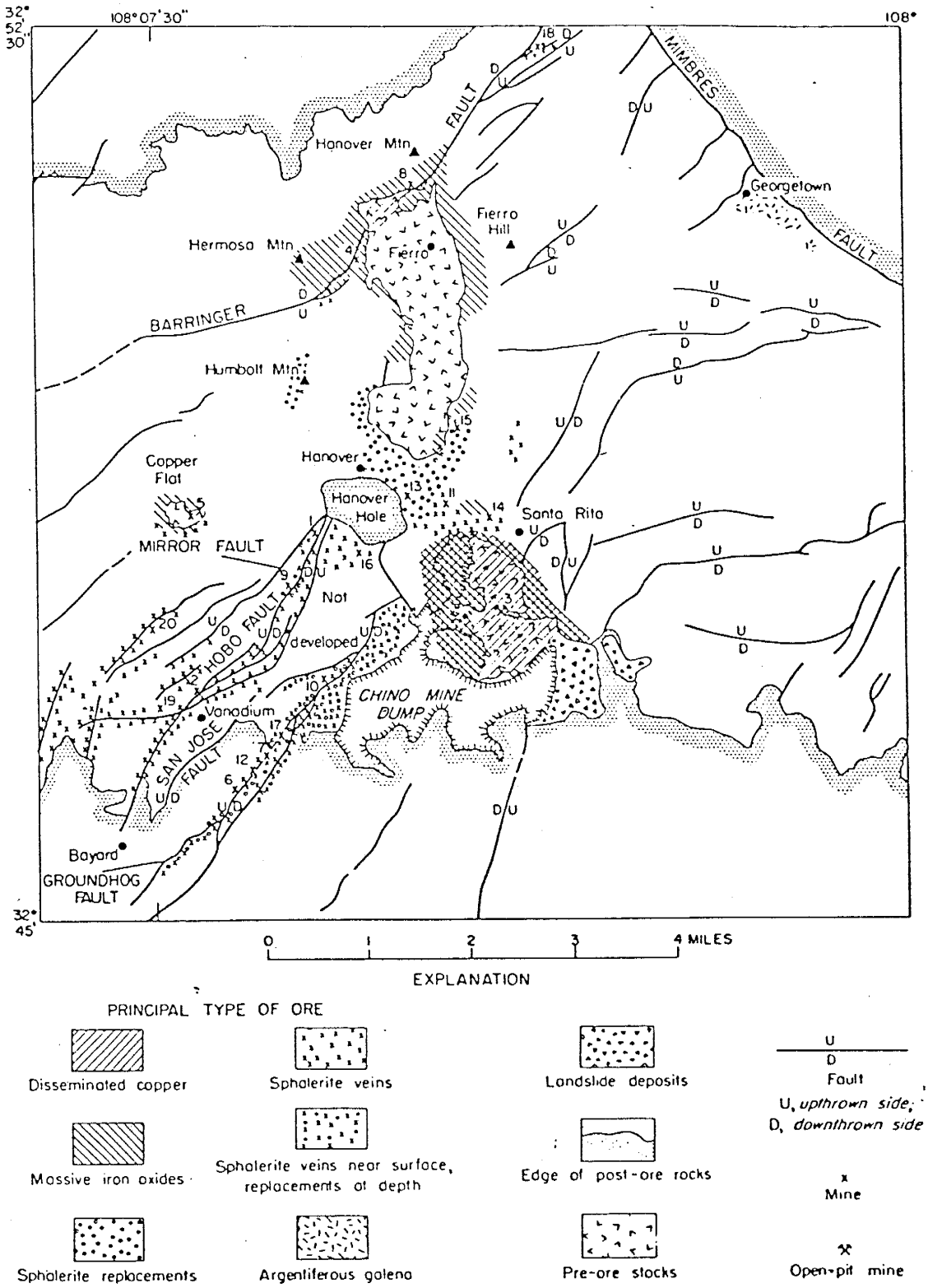

Figure 1Ca. Index map of ore deposits, mines, and towns in the Central Mining District, Grant County, New Mexico. From Hernon and Jones, 1968.

RECRYSTALLIZED (THERMALLY ALTERED) SEDIMENTARY ROCKS

The recrystallized sedimentary rocks have been thermally altered by the Hanover-Fierro intrusive (Fig. 4). Thin section and hand sample examination indicate that these rocks have been recrystallized without significant introduction of elements by metasomatizing fluids. The carbonate sediments are themally altered to impure to pure marbles. Shaly carbonates are altered to impure marble associated with hornfels. Shales are recrystallized to biotite and/or chloritic hornfels or slate. One sample had garnet associated with the limestone. Only minor sulfides occur, either disseminated or associated with quartz in veins.

Mineralized, metasomatized sediments from the Continental orebody, the equivalent thermally altered sedimentary rocks and the equivalent unaltered sedimentary rocks are compared (Table 1). Detailed mineralogy of individual samples can be found in Appendix I.

Form.	Unaltered	Thermally Altered	Recrystallized
Lake Valley Limestone	Green, glauconitic, ferruginous orthoquartzite; dolomitic limestone; shale partings.	Sample not available	Green-blue to black actinolite, hornblende-magnetite hornfels. Chlorite-epidote-magnetite hornfels.
Percha Shale	Light-gray, thick to thin bedded limestone and dolomite with siliceous crenulations.	Sample not available	Fosterite-diopside skarn, fosterite-serpentine skarn, diopside skarn; local accumulations of magnetite, serpentine, sulfides
Fusselman Dolomite	Upham Dolomite: light to dark gray dolomite; locally chert nodules, crinoid plates. Aleman Chert Member: thin layers of alternating black chert and gray dolomite. Cutler Dolomite: gray, apanitic, dolomite, basal fossil zone.	Montoya and Fusselman Dolomites are not divisible at the Continental Mine and other localities. Fusselman Dolomite: dolomite-marble, minor silicification, rare tremolite.	Upham Dolomite: marble, brucite marble, fosterite-serpentine skarn, fosterite-diopside skarn, tremolite skarn, magnetite skarn, disseminated sulfides. Aleman Chert Member: banded serpentine, fosterite, carbonate, chert, magnetite. Cutler Dolomite: marble, brucite marble, fosterite-serpentine skarn, Fosterite-diopside hornfels, tremolite hornfels, magnetite skarn, sulfides.
Lime.	Basal Ready Pay Member: calcareous shale; black fissile shale. Upper Box Member (Augen): abundant limestone nodules in gray shale.	Basal Ready Pay Member: light-gray to green calcareous chlorite-muscovite slate/hornfels. Disseminated pyrite and chalcopyrite. Augen: white to light-gray marble with calcareous shale/hornfels.	Basal Ready Pay Member: fine-grained, biotite hornfels. Augen: green-black diopside-epidote-garnet skarn. Magnetite and sulfides.
Form.	Andrecito Member: limestone, shaly-limestone; abundant bryozoan, crinoidal fragments; black chert nodules. Alamagordo Member (Lower Blue Limestone): dark, gray-black, thick-bedded limestone; abundant chert nodules. Tierra Blanca Member (Hanover Limestone): almost pure carbonate, chert nodules.	Andrecito Member: not recognizable as a divisible unit. Lower Blue Limestone: micritic carbonate, dolomite, marble, chert grains. Hanover Limestone: marble	Andrecito Member: not recognizable at the Continental mine. Lower Blue Limestone: dark-gray green to black diopside-garnet skarn, garnet skarn, marble-biotite hornfels, local mineralization. Hanover Limestone: garnet skarn, diopside-garnet skarn, marble skarn, magnetite skarn. Principal host rock to the magnetite, chalcopyrite, pyrite, and sphalerite ores.

Table 1. Stratigraphic Section Comparing Unaltered, Recrystallized and Metasomatically Altered Rocks.

	Group 1. Unaltered sediments	Group 2. Recrystallized Thermally Altered	Group 3. Metasomatized/Altered
Magdalena Group	Parting shale: grey-brown shale, locally silicified. Oswaldo Formation (Middle and Upper Blue) basal: grey, silty limestone; numerous thin shale beds. Syrena Formation upper: thick, black fissile, limey shale; silty limestone; limestone nodules.	Parting shale: recrystallized silicified, epidotized slate/hornfels. Samples not available for the Oswaldo and Syrena Formations.	Parting shale: blue-grey-green pyroxene hronfels; disseminated pyrite and chalcopyrite. Oswaldo Formation: garnet skarn; More shaly units are diopside-garnet skarn or diopside-quartz-feldspar hornfels. Syrena Formation: diopside-quartz feldspar hornfels; diopside-garnet quartz-feldspar hornfels with layers of garnet skarn.
Colorado Form. Quartzite Form.	Silty, calcareous mudstone; silty argillaceous mudstone; conglomeratic limestone lenses.	No sample available	Very fine-grained dark green-grey diopside hornfels with diopside commonly altering to form epidote amphibole carbonate mineralogy.
	Light-grey, buff, fine-grained quartzite; interbedded shale partings.	Quartzite with clays	Primarily quartzite; minor muscovite chlorite and clay.
	Basal shale: black, fissile, interbedded shale; minor snady and calcareous beds. Upper sandstone: tan, yellow-brown shaly sandstone; mudstone beds, locally fossiliferous limestone.	Basal shale: chloritic hornflels Upper sandstone: extremely fine-grained, blue-grey slaty-shale.	Basal shale: diopside hornfels, biotite hornfels. Upper sandstone: green-gray, tan diopside hornfels; biotite hornfels; chalcocite+pyrite+chalcopyrite veins

MINERAL ASSEMBLAGES AT THE CONTINENTAL MINE

The principal mineral assemblages at the Continental deposit are garnet+magnetite skarn, garnet-diopside+magnetite skarn, forsterite-serpentine+magnetite skarn, magnetite skarn, garnet-diopside-quartz-feldspar hornfels, brucite-marble skarn and locally occurring wollastonite skarn and tremolite skarn.

Dolomite And Siliceous Dolomite

The Lower Paleozoic cherty dolomites include the Montoya and Fusselman Dolomites and the predominately dolomitic rocks of the El Paso Limestone. These formations are altered to a magnesian skarn or a brucite-marble skarn. Mineralogy of the magnesian skarn include forsterite, calcite, dolomite, marble, phlogopite, tremolite, serpentine, talc, brucite, chlorite, magnesite, and humite group minerals (Fig. 11).

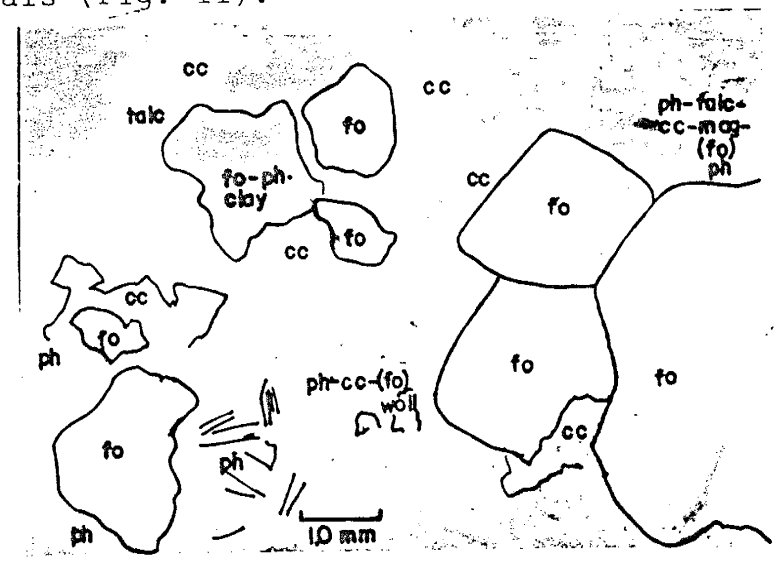

Figure 11. Forsterite-phlogopite-wollastonite-actinolite-talc skarn with highly fractured forsterite (ol), altering to phlogopite (ph), serpentine, and magnetite (mag) and surrounded by talc (talc), calcite (cc), biotite (bt), actinolite (act) and wollastonite (woll). Granular diopside occurs in isolated areas. Sample from the Montoya Dolomite (CDM-11)

Clinopyroxene occurs in isolated areas within the magnesian skarn.

Magnesian skarn close to the intrusive contact is predominantly forsterite-serpentine+magnetite skarn, clinopyroxene-forsterite-serpentine+magnetite skarn or forsterite-dolomite-calcite skarn. Further away from the intrusive, the dolomite has been altered to periclase-brucite-marble skarn.

Hand samples and petrographic examination of these lower dolomitic units indicates that recrystallized brucite marble grades into a forsterite-serpentine skarn over a relatively short distance. Nearing the intrusive, highly altered forsterite first occurs as relatively isolated grains then increases until it becomes the predominant mineral. This general zonation pattern is interrupted by the Barringer Fault, in which mineralization extends to greater distances away from the intrusive along the fault.

Magnesian skarn is extensively altered locally to a predominantly black-yellow serpentine with forsterite occurring only as intensly altered, relict grains.

Magnetite and forsterite replaced dolomite at the same time and later magnetite replaced forsterite-serpentine skarn. Pyrite and chalcopyrite occur only in small amounts as disseminated grains or in veinlets.

The Aleman Member of the Montoya dolomite is altered to distinctively banded marble, magnetite, serpentine, and chert rock (Fig. 12).

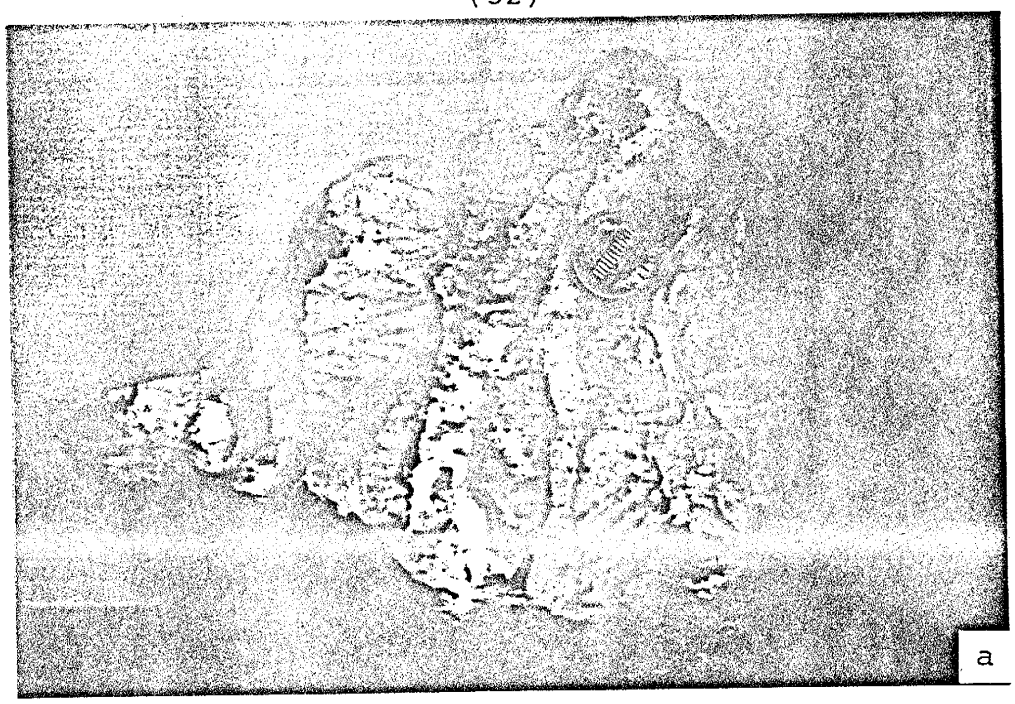

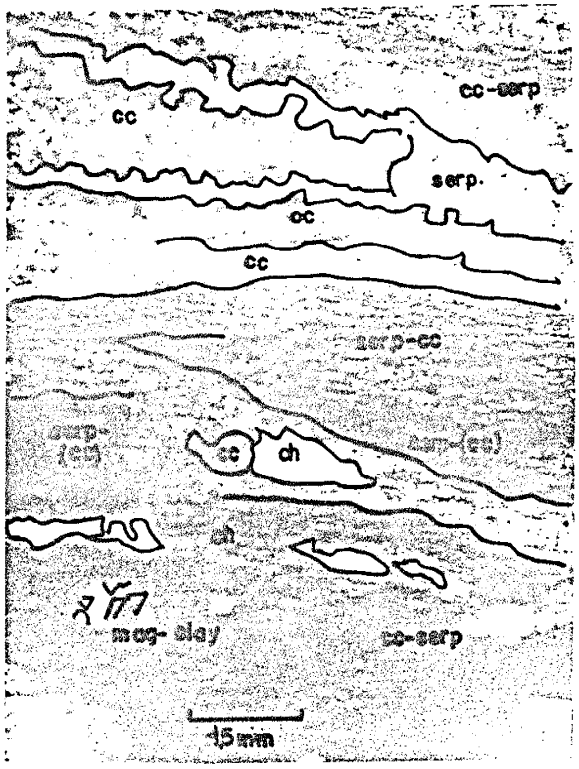

Figure 12. Hand sample and petrographic section of Aleman Chert Member (CMA-5).

a) Marble-chert-magnetite-serpentine skarn from the Aleman Chert Member of the Montoya Dolomite.

b) Banded serpentine (serp), massive and fine-grained calcite (cc), chert (ch), and serpentine+calcite +magnetite (mag). Some serpentine bands show remanent forsterite associated with serpentine and chlorite.

The El Paso Limestone is the lowermost limestone formation at the Continental orebody and is predominantly dolomitic. Samples collected were highly sheared and altered since they were close to the Barringer Fault. The El Paso Limestone is an extremely altered forsterite-clinopyroxene skarn. In thin section, massive, fractured, extremely veined, and altered, forsterite predominates with isolated occurrences of clinopyroxene. Irregular masses and veinlets of yellow green serpentine, unidentified oxides, clay, and biotite cut the massive skarn (Fig. 13).

Figure 13. Forsterite-serpentine-magnetite skarn with massive, highly fractured, forsterite (fo) with magnetite veins. Fibrous minerals (lower left) are actinolite (act) and biotite (bt). The irregular, masses and veinlets are primarily magnetite, amphibole, chlorite, epidote and fine-grained yellow clays. Sample is from the El Paso Limestone (CEP-3).

Shale Members

The lower shale horizons with the exception of the Percha shale have been altered to a fine-grained diopsidic hornfels close to the intrusive and to a biotite hornfels away from the intrusive.

The Percha shale unlike other shale formations is a biotite hornfels both close and away from the intrusive. In thin section fine-grained, quartz and feldspar predominate with lesser amounts of biotite associated with chlorite, actinolite and sericite. Numerous quartz + magnetite, quartz + magnetite + pyrite, and quartz + biotite veins cut the hornfels. Ore minerals occur predominantly in veins with minor occurrences of disseminated sulfides.

Shale horizons in the Syrena Formation, the Parting Shale at the base of the Oswaldo Formation and most of the Abo and Colorado Formations are altered to a fine-grained diopside hornfels close to the intrusive and a biotite or chlorite hornfels away from the intrusive. Sedimentary layering is preserved and distinguishable by differences in color related to the presence of magnetite. In thin section these hornfels are predominantly fine-grained quartz, feldspar, and iron oxides and lesser amounts of clinopyroxene altering to chlorite and epidote. Calcite, sphene, muscovite, and apatite are accessory minerals. Further from the intrusive biotite and chlorite occur and clinopyroxene is not present.

Shaly Limestone Members

The shaly limestones include the Syrena Formation and the similarily metamorphosed Augen Member of the Percha Shale. These shaly limestones form a garnet-diopside-quartz- feldspar hornfels close to the intrusive and a marble skarn away from the intrusive. In general, an increase in shale content of the limestone corresponds to an increase in clinopyroxene with respect to garnet. Therefore, the garnet diopside skarn described in the shaly limestones grades into the diopside hornfels characteristic of the shales.

The shaly limestone of the Syrena Formation is altered to a grey-green resinous garnet-diopside-quartz-feldspar hornfels. In thin section, large, euhedral to anhedral diopside occur in a fine-grained groundmass of predominantly quartz and feldspar. The diopside is replaced by irregular, light brown garnet, and altered to chloritic actinolite and granular diopside. Several plagioclase grains occur together in isolated areas and are dotted with numerous inclusions of diopside, garnet, and apatite (Fig. 14).

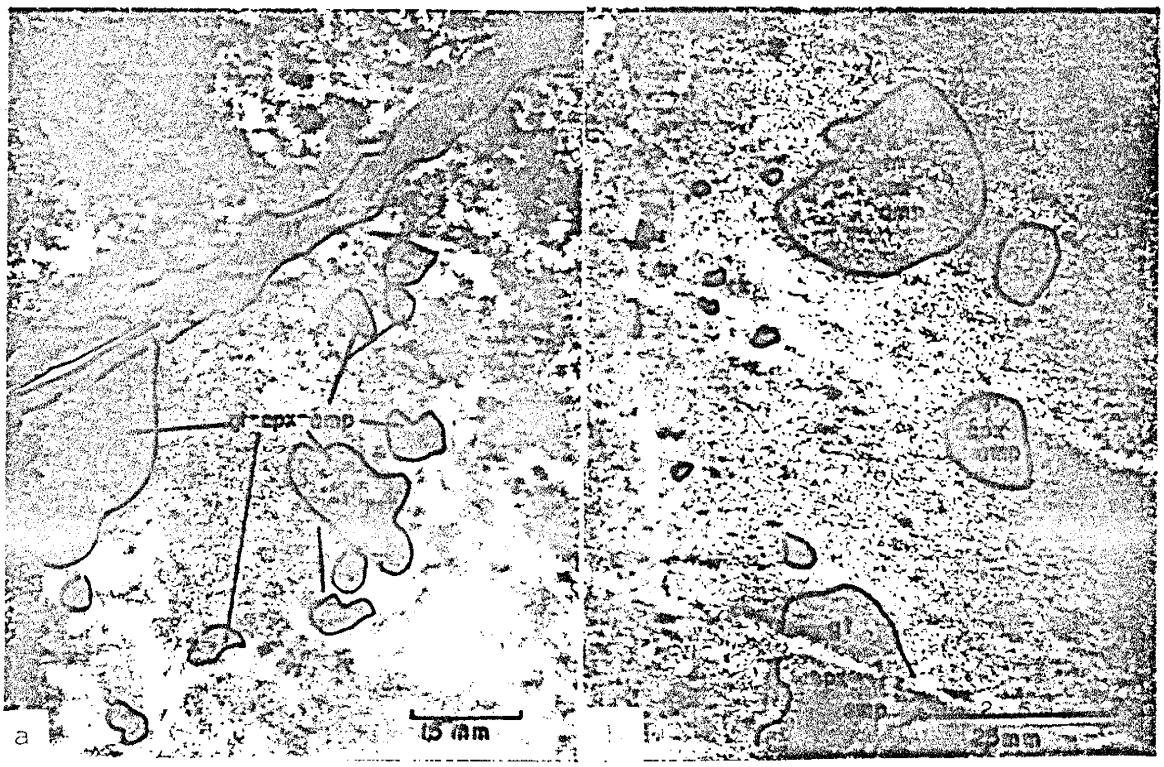

Figure 14. Samples from the Syrena Formation (CSY-127) and (CSY227).

a) Garnet-diopside-quartz-feldspar hornfels is comprised of extremely fine grained quartz (qtz) and feldspar (feld) with areas of anhedral to euhedral altered diopside (cpx) that is altered to granular diopside, chloritic actinolite (amp), and calcite and being replaced by irregular light-brown garnet (gt). The garnet veinlet is zoned, inclusion free, garnet (gt), chalcedony (ch), and calcite (cc) in the center, and diopside and magnetite towards the margins.

b) Garnet-diopside-quartz-feldspar hornfels showing a close-up view of the altered diopside grains (cpx). The altered diopside grains are coarser-grained towards the center with grain size decreasing outward. The diopside has primarily altered to granular diopside and chloritic actinolite (amp). Irregular, light-brown garnets are replacing the altered diopside. Surrounding the diopside is fine-grained quartz (qtz) and feldspar (feld).

Irregular bands of garnet skarn occur in the Syrena Formation between the garnet-diopside-feldspar-quartz hornfels. In thin section, anisotropic, highly fractured, garnet predominates and is surrounded by irregular areas of diopside and carbonate. Garnets have very fine-grained

inclusions of carbonate and diopside. These may be remanent minerals from the replacement of garnet.

The Augen Member of the Percha Shale is comprised of highly anisotropic, zoned, garnets that form irregular masses and veinlets in a groundmass of altered diopside, turbid calcite, quartz, epidote, secondary chlorite, actinolite accessory sphene, and apatite. Garnet replaces diopside and carbonate. However, the garnet is later altered to carbonate, clays, and granular epidote which is indicated by carbonate pseudomorphic after garnet (Fig. 15).

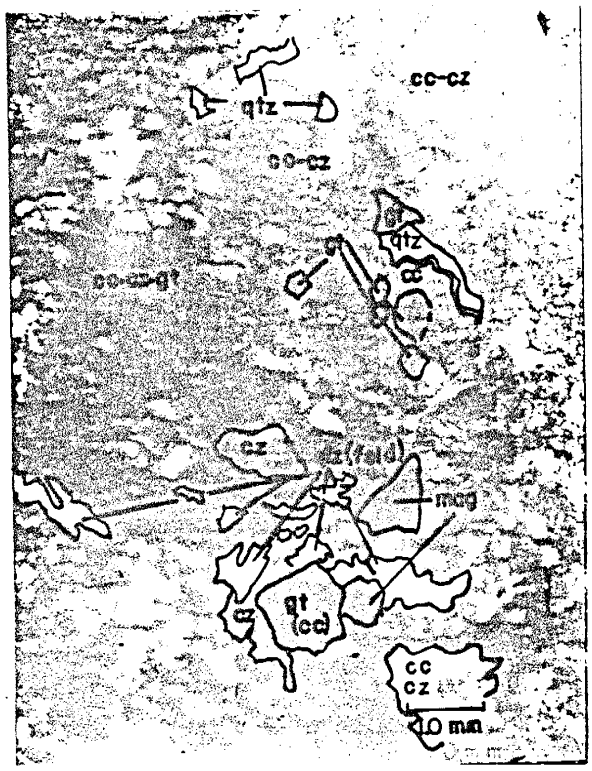

Figure 15. Garnet replaces carbonate and diopside and is later replaced by carbonate (arrow). The centers of the partially replaced garnet (gt) commmonly contain pyrite. The fine-grained hornfels (upper right corner) is predominately clinozoisite (cz), calcite (cc), and quartz (qtz). Garnets that have not been replaced by carbonate (lower left). From the Augen Member, Percha Shale (PS-AG-16).

The unaltered Augen Member is a limy shale with limestone nodules. In mineralized sediments the irregularly shaped, massive garnet replaces the more pure limestone nodules. Altering diopside, turbid calcite, quartz, and epidote replace the shaly limestone. Diopside and garnet were altered to epidote, amphiboles and chlorite. Magnetite replaces garnet and occurs in some veins. Other veins are comprised of coarse-grained calcite + quartz, and less commonly calcite + apatite.

Limestones

The relatively pure limestones such as the Hanover and Lower Blue Limestone of the Lake Valley Limestone, and, the Middle and Upper Blue Limestones of the Oswlado Formation, form massive garnet+magnetite skarn close to the intrusive and marble skarn away from the intrusive. Wollastonite skarn occurs locally adjacent to garnet skarn and marble skarn.

In thin section the garnet+magnetite skarn of the Oswaldo Limestone is predominantly massive, anisotropic, zoned, and fractured garnet. Minor chalcedony and calcite fill open spaces. Garnet replaces carbonate and may contain abundant minute inclusions of carbonate. Magnetite replaces garnet and fills open spaces. Pyrite and chalcopyrite fill open spaces and replace magnetite (Fig. 16).

Figure 16. Magnetite (mag) replaces garnet (gt) and fills open spaces. Garnets are small, zoned, and have very few carbonate inclusions. Iron-rich clays(?) commonly occur in the center of the garnets or are concentrated along growth zones (arrow). White areas are open spaces and less commonly chalcedony.
Sample from the Oswaldo Limestone (COS-15).

The unaltered Hanover Limestone is an extremely pure limestone with chert nodules. This member is the host to the major Fe-Cu-(Zn) ore of the Continental orebody. The Hanover Limestone is altered to garnet+magnetite skarn, diopside-garnet+magnetite skarn or locally magnetite-sulfide rock. In thin section magnetite skarn is comprised of approximately sixty percent magnetite surrounded by irregular areas of diopside, carbonate, quartz, magnetite, garnet, and secondary actinolite, tremolite, and chlorite. Pyrite and chalcopyrite occur as disseminated grains and in veins that fill fractures in the magnetite skarn (Fig. 17).

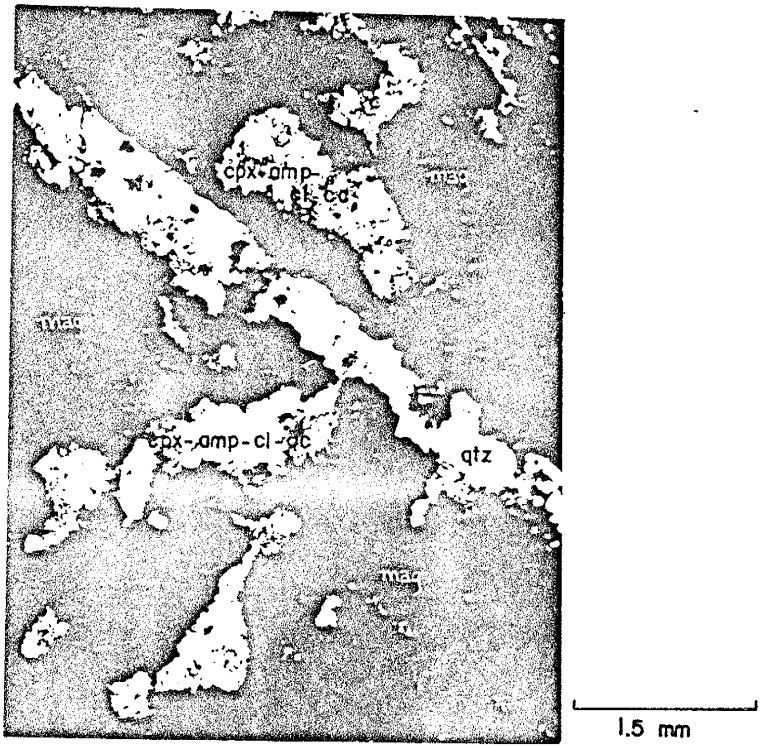

Figure 17. Magnetite skarn. Irregularly shaped shaped areas areas are unreplaced skarn comprised of carbonate (cc) and diopside (cpx) altering to amphibole (amp) and chlorite (cl). Vein is comprised of quartz+calcite+minor actinolite. Opaque areas are all magnetite (mag).
Sample is from the Hanover Formation (CLH-12).

The Lower Blue Limestone is a garnet skarn close to the intrusive contact. In thin section garnet predominates and is massive and fractured, with anisotropic margins and isotropic centers. Garnet replaces calcite and commonly contains minute included grains of carbonate and diopside. A reaction rim comprised of nontronite, calcite and epidote surrounds some garnets. Irregular stringers of quartz, quartz + garnet and garnet veinlets pinch and swell, cut the earlier garnet skarn, and locally replace skarn. Magnetite forms irregular veinlets that cut and replace garnet. Late stage quartz and quartz + magnetite veins cut entire rock.

Quartzite Formations

Two quartzite formations occur in the Continental orebody; the Lower Paleozoic Bliss Quartzite and the Upper Cretaceous Beartooth Quartzite.

The Beartooth Quartzite has not undergone significant alteration and occurs as a recrystallized orthoquartzite with minor disseminated pyrite. In thin section irregular quartz is ninety-five percent of the rock. with minor amounts of muscovite, chlorite, sericite, clay and pyrite.

The Bliss Quartzite sampled close to the Hanover-Fierro stock is altered and sheared due to the invasion of the Hanover-Fierro stock. The Bliss Quartzite occurs as a dark grey-green rock and in thin section is predominantly fine-grained quartz, poikolitic hornblende, actinolite, and magnetite. Poikolitic hornblende is being replaced by biotite, epidote, magnetite, quartz, and commonly contains abundant apatite inclusions. Zircon and sphene occur as important accessory minerals. Ubiquitous magnetite gives the rock its characteristic dark color.

Igneous Dikes And Sills

Two extremely metasomatized, granodiorite porphyry dikes invade the Montoya dolomite and predate mineralization. In thin section, most of the igneous texture has been obliterated and massive, anisotropic, irregularly zoned garnets have replaced most of the original rock. Garnet replaces plagioclase and is surrounded by a cryptocrystalline groundmass of remanent feldspar, carbonate, clays, and quartz. Sphene, epidote, muscovite, and apatite are important accessory minerals (Fig. 18).

Figure 18. Metasomatized granodiorite dike comprised primarily of zoned garnet (gt), which can be seen replacing plagioclase (pl). Carbonate occurs in the interior of most garnets. Growth zones are commonly observed around groups of garnet grains. Igneous texture has been obliterated. Sample from the Montoya Dolomite (CGD-9).

A felsic sill in the base of the Oswaldo Formation is extremely altered but igneous textures are observed. In thin section the groundmass is granular quartz, altered feldspar, hornblende, actinolite, and clays. Feldspar phenocrysts replaced by clay(?) and ragged hornblende(?) phenocrysts occur in the groundmass. Veins of actinolite + chlorite + magnetite + quartz, and quartz + actinolite + epidote cut the altered sill (Fig. 19).

Figure 19. Altered felsite sill. Fine-grained groundmass is primarily quartz (qtz) and feldspar (feld). Relict feldspar phenocrysts are altered almost entirely to clay. The north-south vein is massive magnetite (mag), quartz (qtz) and apatite (center) and epidote (ep) and chlorite (cl) (margins).
Sample from the base of the Oswaldo Formation (COSH13)

Numerous dikes and sills occur in the Colorado Formation Two altered, diorite porphyry sills and one amphibolite dike were sampled. The amphibolite dike in thin section is comprised of extensively altered hornblende phenocrysts in a green-yellow, aphanitic groundmass of actinolite, chlorite, epidote, clay, and indistinguishable minerals.

The least altered diorite sill is altered but igneous textures are evident. In thin section plagioclase and orthoclase altered to clays and sericite and hornblende altered to epidote, chlorite, magnetite and quartz. Apatite

and sphene are important accessory minerals. The more altered diorite sill is comprised of plagioclase and orthoclase phenocrysts that have have been entirely replaced by clays and minor epidote, sphene, and hornblende phenocrysts that are now chloritized actinolite with sphene and apatite. The groundmass is very fine-grained quartz, orthoclase, actinolite, clays, sphene and rare plagioclase grains.

Garnet Skarn

A brief discussion on garnet skarn is included because it is the most important host of the Fe-Cu-(Zn) ore and the most common skarn of the Continental orebody. Garnet skarn is variable and forms in several ways.

1. Coarse-grained, euhedral to subhedral, reddish-brown or green garnet that replace the more pure limestones such as the Hanover and Lower Blue Limestone of the Lake Valley Limestone and the Middle and Upper Blue Limestones of the Oswaldo Formation (Figs. 20 and 21). These garnets are the most important host of Fe-Cu-(Zn) ore and are always extremely brecciated. In thin section the garnet is light-brown to grey, extremely brecciated, and isotropic and/or anisotropic. Garnet replaces carbonate, and to a lesser extent diopside.

2. Garnet derived from shaly limestones and to a lesser extent in calcareous shales is fine to medium-grained subhedral to anhedral, usually reddish brown, and replaces primarily diopside and carbonate (Fig. 22). Garnets are typically extremely sheared.

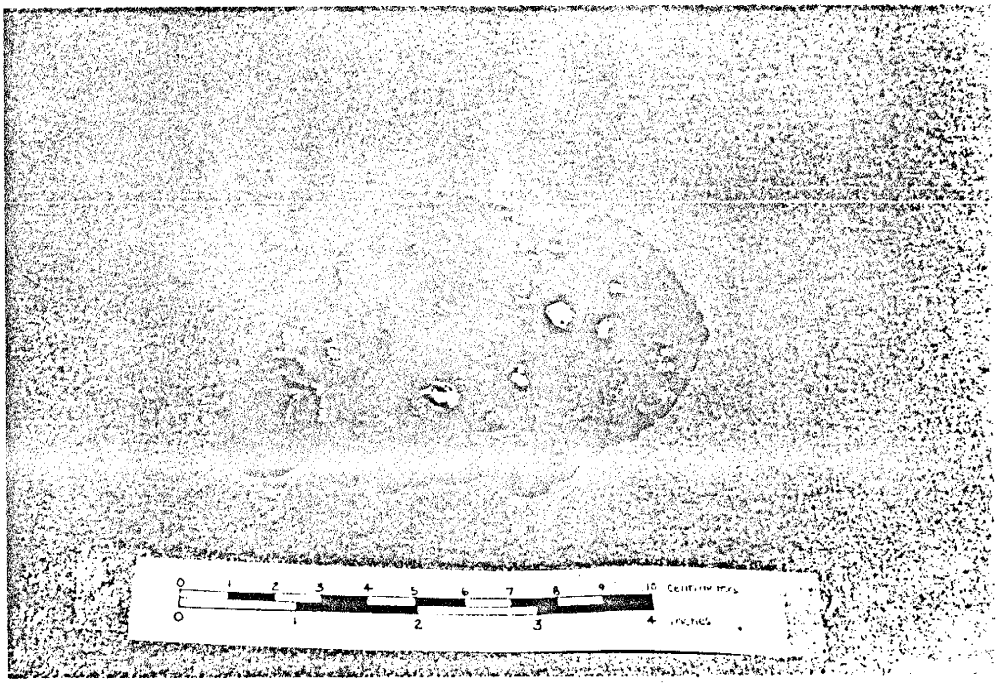

Figure 20. Massive, euhedral, green garnets associated with magnetite. Magnetite is filling open spaces and replacing garnets. From the Hanover Formation.

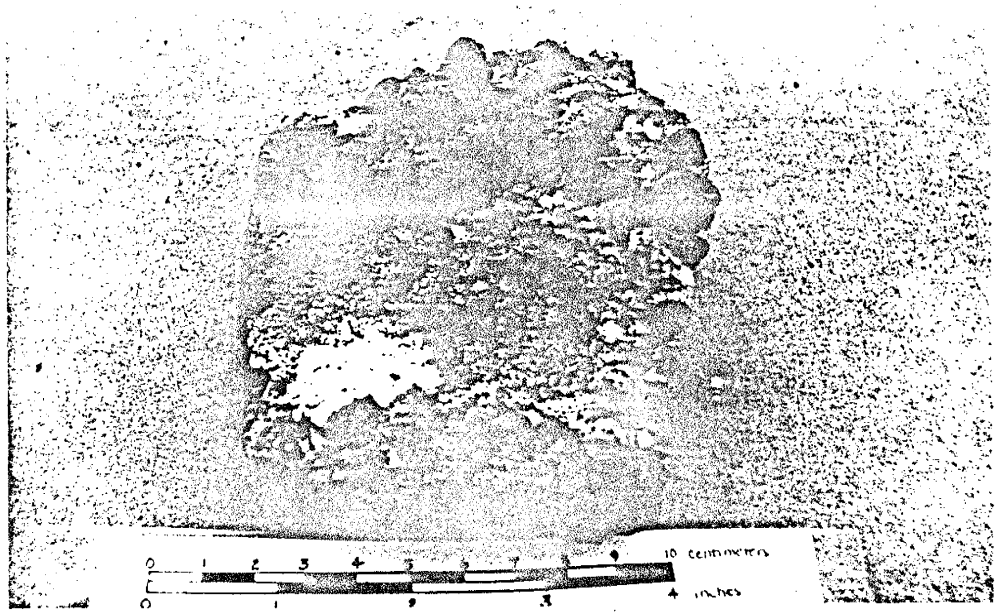

Figure 21. Massive, euhedral green garnets with magnetite, euhedral pyrite and chalcopyrite. The large, euhedral pyrite indicate the availability of open spaces during crystallization. Secondary calcite fills open spaces. From the Hanover Formation.

3. Garnet occurs in veins that cut earlier skarn formation and generally are anisotropic, zoned in the larger veins, and are free of inclusions. Garnet comprises the entire mineralogy of the vein or is associated with quartz, diopside, magnetite, and chlorite.

4. Massive garnet that is continuously zoned over several adjacent grains in the granodiorite dikes and replaced plagioclase (Fig. 18).

5. Locally garnet replaces wollastonite skarn.

Garnet compositions were approximately determined by color, refractive index, and X-ray diffraction analyses and range from andradite to grossularite. Commonly, the garnets have distinctively massive green centers and red-yellow zoned exteriors. Garnets range from uniaxial to biaxial and exhibit both positive and negative interference figures.

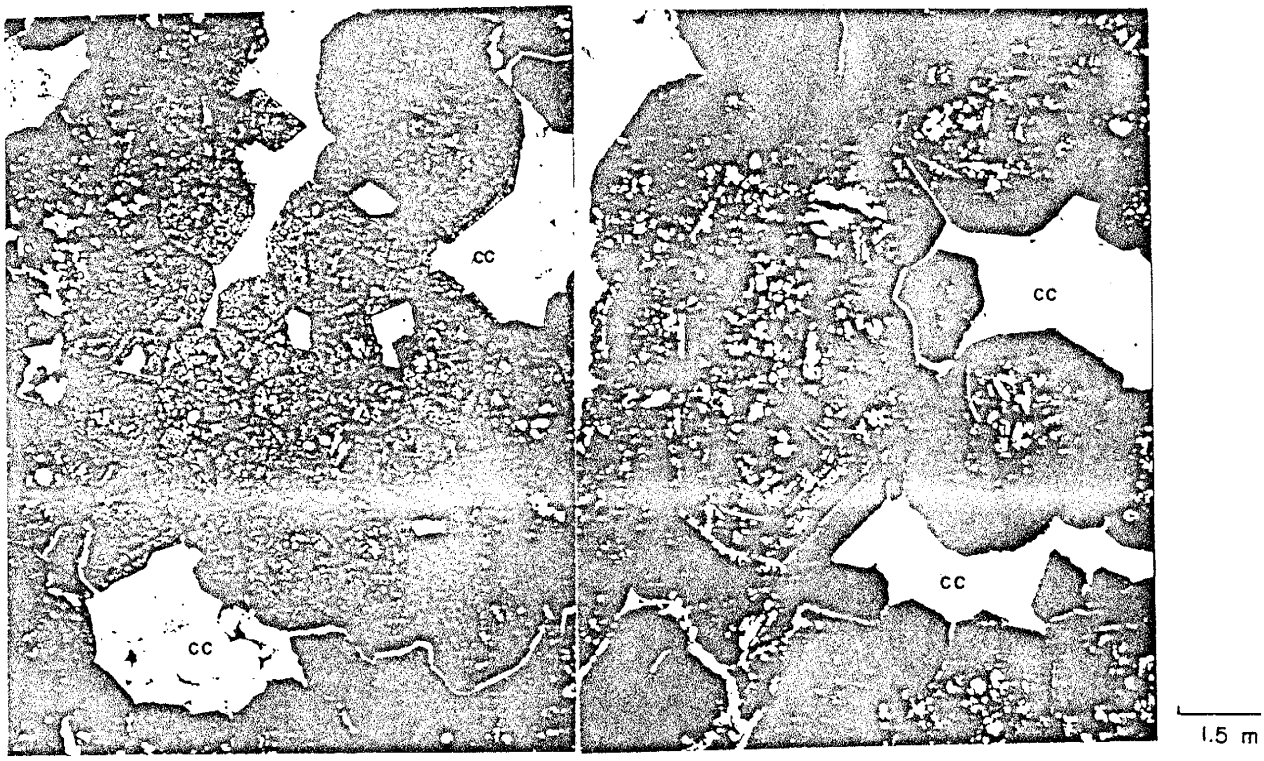

Figure 22. Garnet skarn from the Hanover Limestone
a) Euhedral garnets that are replacing calcite and diopside. Diopside inclusions are common in the center of the garnets (GT-4).
b. Euhedral, zoned garnets that are replacing calcite and diopside. Diopside inclusions are common throughout the garnets (GT-3).

Hydrothermal alteration

The general lithologic zonation described earlier has been modified by later propyllitic alteration which has affected the skarn to varying degrees. Alteration is most extensive along faults and fractures and where brecciation has occurred resulting in open spaces. Alteration of skarn includes:

1. Serpentinization of forsterite in the Fusselman-Montoya Dolomite.
2. Magnetite; magnetite occurs in veins, replaces forsterite and replaces garnet.
3. Periclase altering to brucite.

4. Chloritization; chlorite occurs in numerous veins, as an an alteration product of diopside and garnet, and associated with serpentine in the alteration of forsterite.
5. Epidotization; epidote occurs in numerous veinlets associated with magnetite+actinolite+chlorite+quartz veins, and quartz+pyrite veins (Fig. 19). Epidote is a common mineral in garnet-diopside-quartz-feldspar hornfels and is an alteration product of diopside and garnet.
6. Montmorillinite. Nontronite is a common alteration product of altering and brecciated garnets. Unidentified clays are intimately associated with the calcite and are responsible for the turbid appearance of the calcite.
7. Late stage quartz, quartz+calcite, quartz+calcite+chalcopyrite, and calcite veins cut skarn and most earlier formed veins.

Ore Mineralization

Magnetite, chalcopyrite, and pyrite are the most important ore minerals at the Continental deposit. Sphalerite is present but is not recovered. Magnetite is the only oxide mined and chalcopyrite is the most important sulfide mined.

Magnetite occurs disseminated and as massive ore interbedded with forsterite-serpentine skarn and forms as a primary mineral or replaces the forsterite-serpentine skarn. Magnetite also occurs in the garnet skarn but generally not as extensively as in the forsterite-serpentine skarn. In garnet skarn, magnetite replaces garnet and fills open spaces (Figs. 23-25).

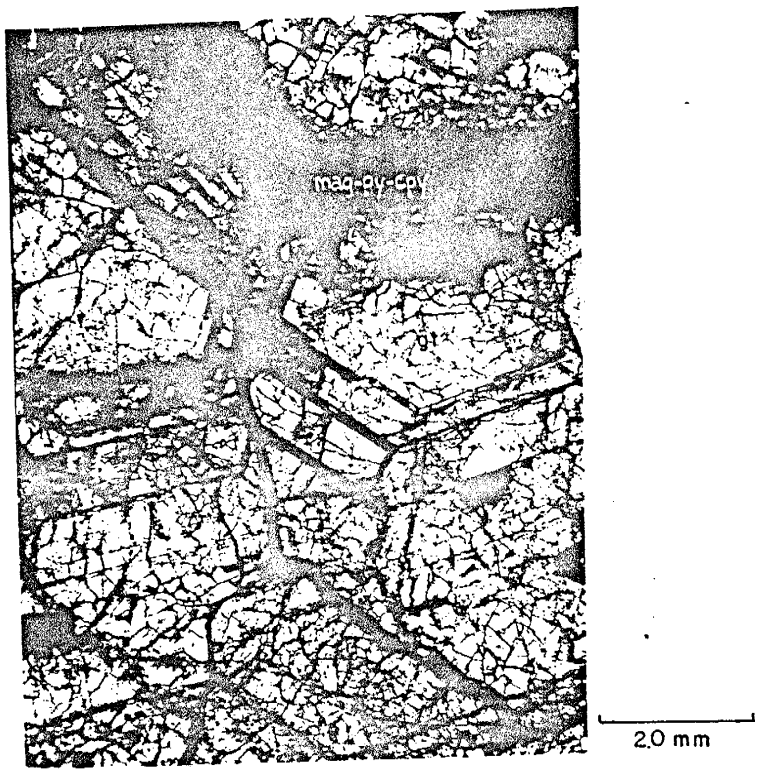

Figure 23. Large, massive, fractured, zoned garnets that are being replaced by magnetite (mag) along growth planes and along grain boundaries. All opaques are magnetite with the exception of the veinlet (top) that cuts the garnet (gt) and is comprised of magnetite, pyrite, and unidentified clay. Sample from the Hanover Limestone (GT-3).

Sulfide mineralization is essentially restricted to garnet skarn. Disseminated sulfides of minor importance occur in the forsterite-serpentine skarn. Chalcopyrite and pyrite cements brecciated garnet, fills open spaces and replaces magnetite, garnet and diopside (Fig. 25). Chalcopyrite and pyrite also occur as veins that cut massive magnetite skarn (Fig. 26a), as small, massive concentrations (Fig. 26b), and as disseminated grains replacing magnetite (Fig. 26c).

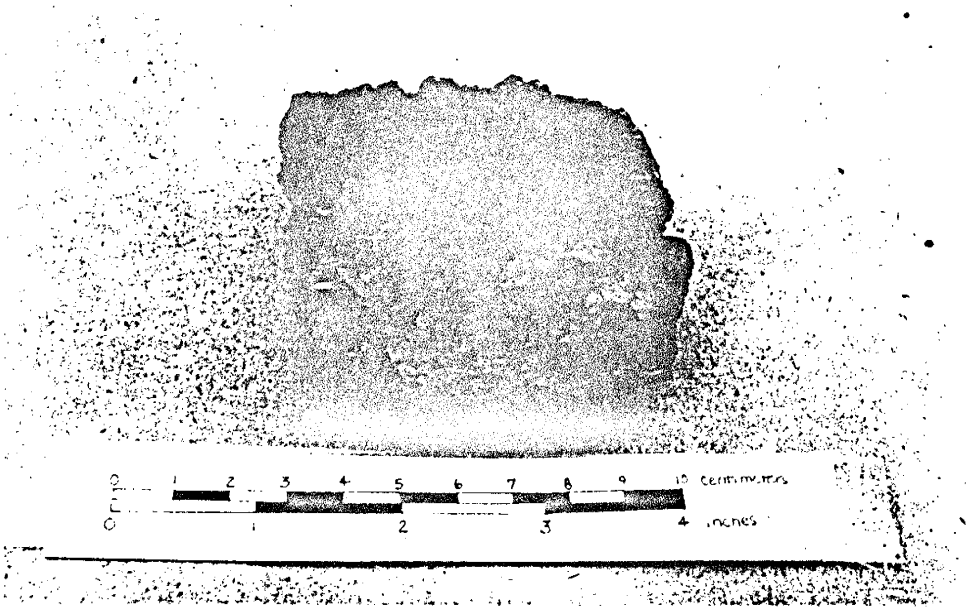

Figure 24. Finely zoned green garnet is partially replaced by magnetite. Magnetite and calcite fill open spaces. Note the porosity of this sample. From the Hanover Limestone GT-5.

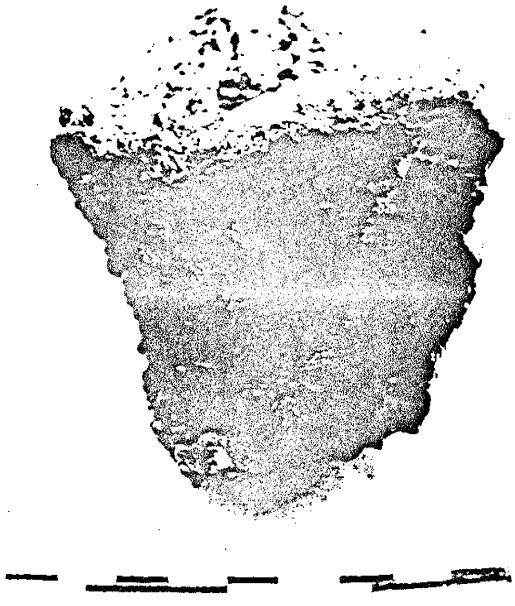

Figure 25. Red garnet and some green garnet with magnetite and chalcopyrite. The magnetite and chalcopyrite fill open spaces and replace garnet. From the Oswaldo Formation GT1-1.

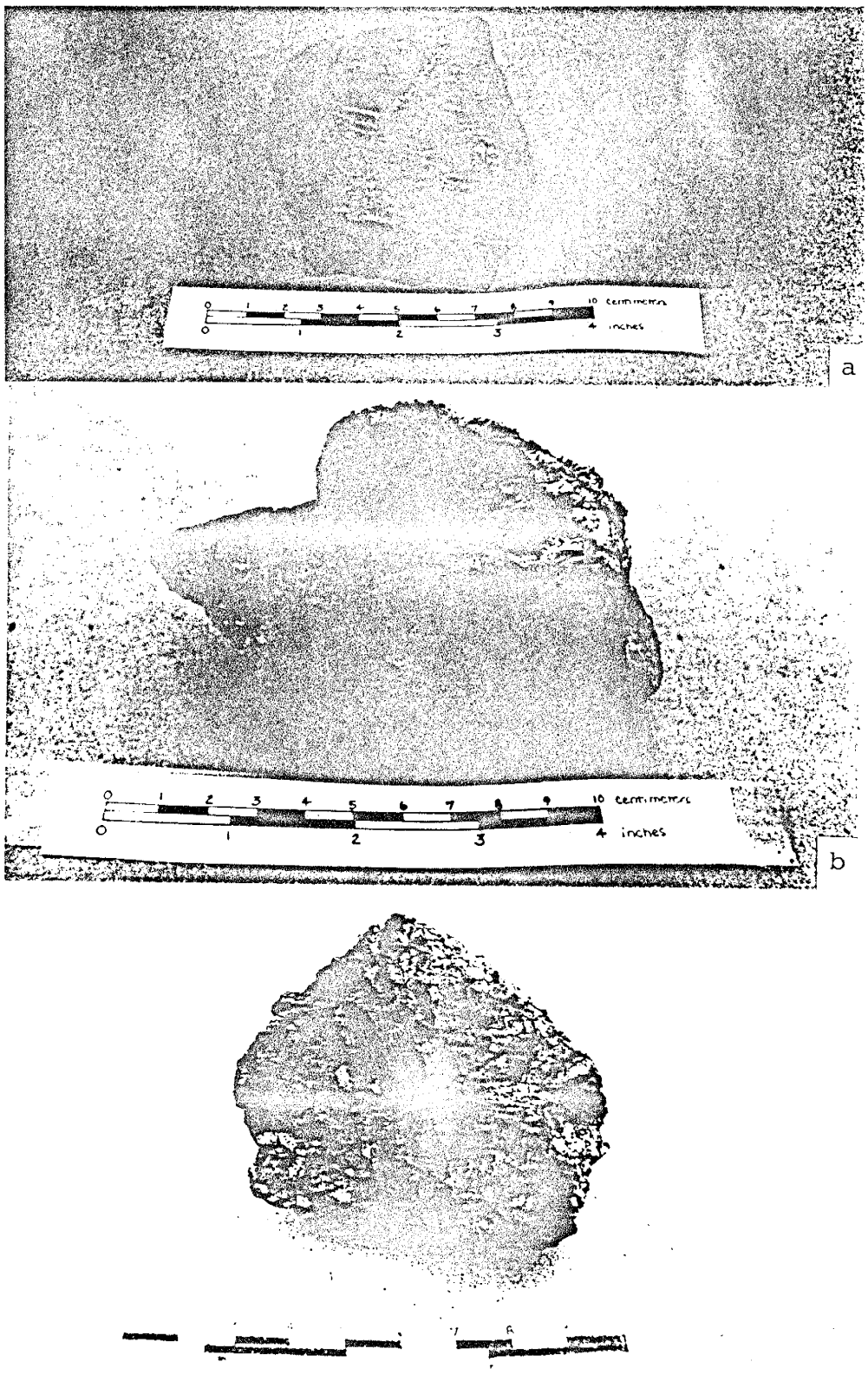

Figure 26. Ore samples from the Hanover and Oswaldo Limestones a) Chalcopyrite and pyrite veins fill fractures in massive magnetite skarn, b) massive chalcopyrite (top) and magnetite skarn (base) with pyrite occurring between (left), c) magnetite skarn with chalcopyrite and pyrite, Note boxwork structures probably after pyrite.

Hanover-Fierro Intrusive

The porphyritic facies (main mass) of the Hanover-Fierro intrusive occurs at the Continental mine and adjacent areas in this study.

In thin section, phenocrysts of euhedral-zoned plagioclase, hornblende, and less commonly biotite, orthoclase, and quartz occur in a groundmass of plagioclase, quartz, and orthoclase, with minor biotite and hornblende (Fig. 27).

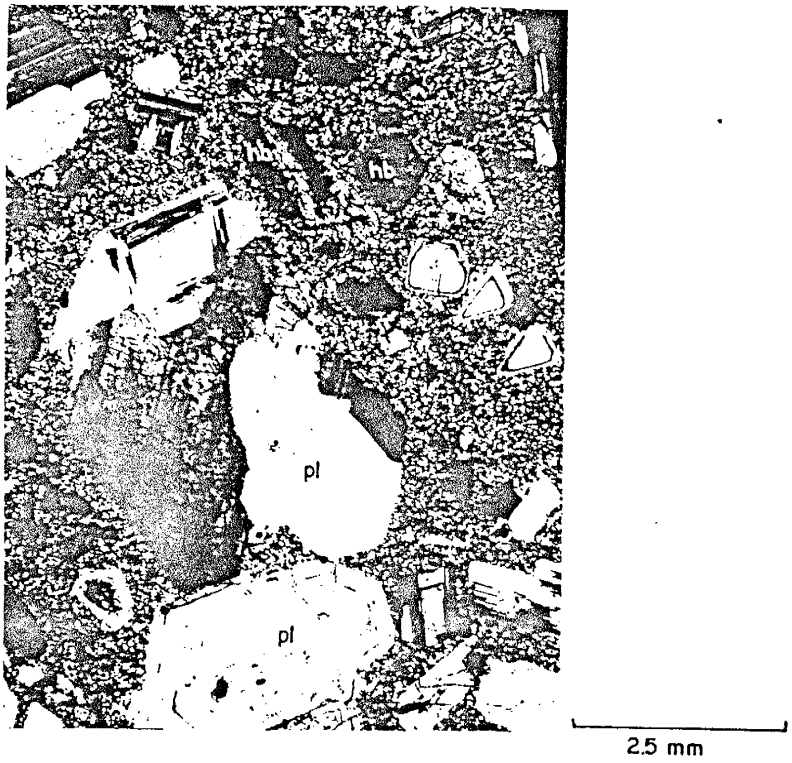

Figure 27. Main mass of the Hanover-Fierro intrusive. Large, euhedral, zoned plagioclase phenocrysts and hornblende phenocrysts altering to biotite and chlorite on the edges predominate. Biotite, quartz, and orthoclase also form phenocrysts. Groundmass consists of plagioclase, quartz, orthoclase and lesser amounts of biotite, hornblende, and magnetite. Porphyritic and glomerophyric texture. Sample from the Hanover-Fierro intrusive

Mineral Paragenesis

Based on textural evidence from hand sample and thin section observations, the following paragenesis is indicated (Table III). Early formation of forsterite, clinopyroxene, phlogopite and magnetite associated with forsterite skarn. Iron metasomatism resulted in magnetite deposition in the lower dolomitic formations. Garnet skarn formation followed with garnet replacing carbonate or earlier formed diopside. Veins assemblages of garnet and diopside indicate overlap in time of deposition. Following garnet mineralization magnetite once again became the stable phase and replaced garnet and filled open spaces between garnet. At this time iron-bearing fluids were responsible for serpentinization and veining of the forsterite skarn. Magnetite deposition was followed by sulfide deposition of copper, zinc and iron sulfides. Quartz and calcite veins cut both skarn and ore formation.

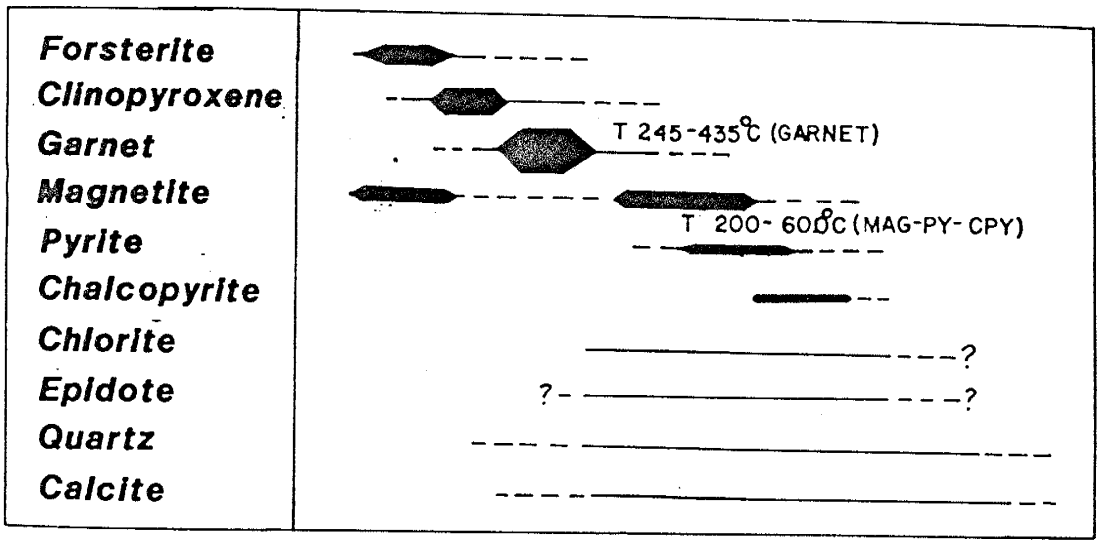

Table II. Paragenetic sequence of skarn minerals, important ore minerals, and later stage hydrothermal minerals.

FLUID INCLUSION ANALYSES

Seven-hundred and fifty fluid inclusions from 45 doubly polished sections were studied. Fluid inclusion measurements were made on garnet from skarn and on quartz from both quartz+magnetite and quartz+magnetite+sulfide veins that cut the skarn. All samples were collected from the Continental open pit (Fig. 2) and a brief description of the samples is in Appendix II. Homogenization temperatures and salinity measurements by freezing point depression were determined by microscopic observation using standard methods (Roedder, 1972). For those inclusions which contained a halite daughter, salinity was determined by solution temperature of the salt crystal. Microthermometry was performed utilizing the TH600 heating-freezing stage manufactured by LINKHAM Scientific Instruments of London, England.

General Observations of Fluid Inclusions in Garnet

Fluid inclusions from garnet are of the simple two phase type liquid-vapor with liquid>vapor (Figs. 28 and 29). About two percent of the fluid inclusions had a birefringent daughter mineral, possibly sulfate, that remained unchanged when heated or cooled (Figs. 28.2, 28.3 and 29.17). Fluid inclusions in garnet are divisible into three groups:

Type I Primary-type fluid inclusions that are isolated, range from elliptical to irregular in shape, and usually are not elongated. These inclusions appear to have dark, thick inclusion walls (Figs. 28.4, 28.7, 28.9, 28.10, 29.12 29.13, and 29.18).

Figure 28. FLUID INCLUSION PHOTOMICROGRAPHS
All fluid inclusions occur in garnet

1. GT-5 Oriented primary fluid inclusions elongated parallel to garnet growth zones.
2. GT-1 Secondary fluid inclusion that occurs along a fracture birefringent daughter mineral did not melt (sulfate?) (228°C,-14.5).
3. GT-1 High temperature primary, isolated fluid inclusion with birefringent daughter mineral that did not melt (sulfate?) (335°C)
4. GT-4 Two primary fluid inclusions (a. 261°C; b. 255°C, -5.0°C)
5. GT-5 Large, orientated, irregular fluid inclusions elongated parallel to garnet growth zones (a. 262°C, -10.4; b. 245°C, -8.0; c. 241°C, -6.7; d. 242°C, -6.7; e. 235°C, -5.7).
6. GT-5 Primary, elongated fluid inclusions parallel to garnet growth zones (a. 252°C,-6.7)
7. GT-1 Low temperature, isolated, primary fluid inclusion (205°C, -11.5)
8. GT-5 Secondary fluid inclusions (Type IIIb) appear extremely dark and occur on secondary fractures. Vapor bubble is difficult to distinguish (305°C, -12.5).
9. GT-1 Primary fluid inclusion, isolated, very dark inclusions with many shadows.
10. GT-5 Primary fluid inclusion, isolated, very dark inclusion walls are very typical of many garnet inclusions (267°C)

(All photomicrographs are taken under plane light)

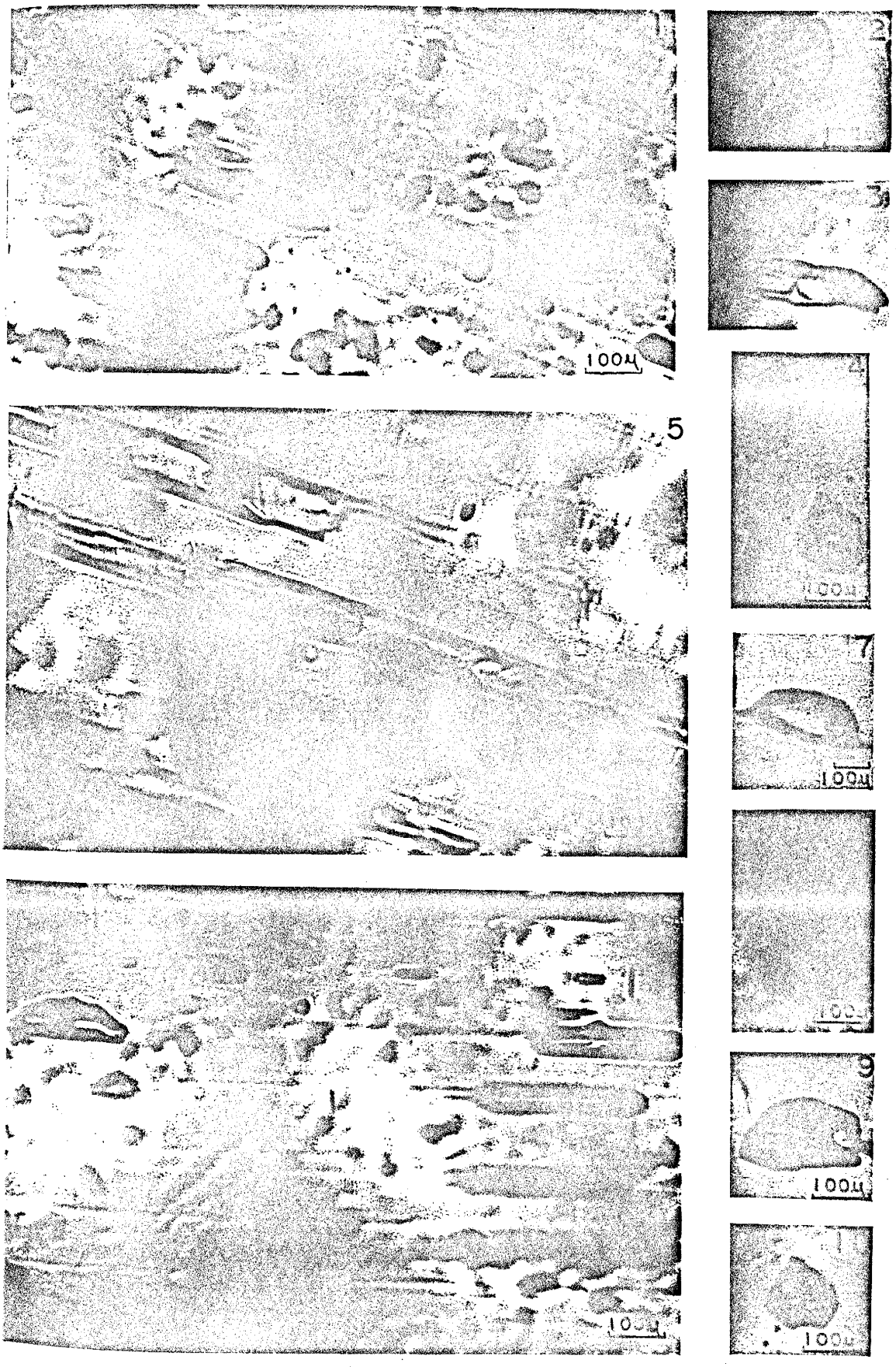
100μ
5
100μ
7
100μ
9
100μ
100μ

Figure 29. FLUID INCLUSION PHOTOMICROGRAPHS
All fluid inclusions occur in garnet

11. GT-5 Primary fluid inclusions parallel to garnet growth zones, irregular primary fluid inclusions (E-W direction) and another growth plane (NW-SE direction).
12. GT-5 Low temperature, primary fluid inclusion, (a. 224°C, -8.9)
13. GT-5 Primary fluid inclusion, isolated, 3-dimensional, with very dark inclusion walls (256°C, -7.3)
14. GT-5 Secondary-type (?) fluid inclusions, low temperatures (ranging from 190-230°C).
15. GT-5 Poorly developed, primary fluid inclusions that are parallel to garnet growth zones.
16. GT-4 Primary fluid inclusions, irregular in form, not parallel to garnet growth zones, the large vapor bubble in fluid inclusion a, homogenized to a liquid phase.
17. GT-4 Primary fluid inclusion, high temperature, parallel to garnet growth plane (330°C).
18. GT-1 Primary fluid inclusion, isolated.
19. GT1-1 Extremely dark fluid inclusion occurring parallel to several other similarly high temperature, very dark inclusions which may represent a secondary plane; this type of inclusion commonly formed in lines with other similar type of inclusions (a. 359°C, -0.1(?); b. 357°C,)

(All photomicrographs are taken under plane light)

12
100μ

13

100μ

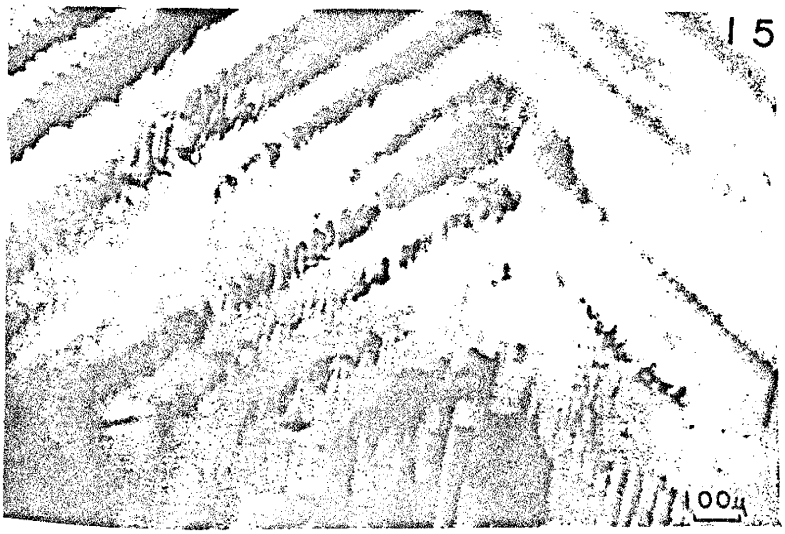
15
100μ

16
100μ

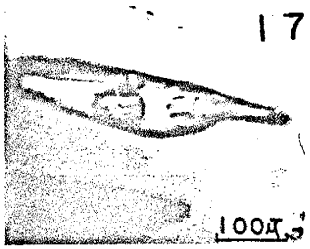
17
100μ

18
100μ

19
100μ

Type II Primary-type fluid inclusions that are elongated in form and occur parallel to garnet growth zones (Figs. 28.1, 28.5, 28.6, and 29.11).

TypeIII Secondary-type fluid inclusions that occur linarally associated with fractures. These inclusions are commonly elongated parallel to the fracture and have two forms: a) fluid inclusions that appear to have thick, dark walls and may be completely dark (Figs. 28.8 and 29.19), and b) fluid inclusions that have a flat appearance, thin walls, a relatively small vapor bubble and occur associated with secondary fractures. Type IIIb fluid inclusions also occurred isolated which made it difficult to determine whether they were primary or secondary.

Type I inclusions are ubiquitous throughout the entire garnet crystal with a higher density towards the interior of the garnet. Generally, these inclusions have thick-dark walls which made it difficult to measure the filling temperature and freezing point depression. Type II inclusions are usually restricted to the more zoned margins of the garnet. Type III inclusions are associated with fractures, that are extremely common throughout the entire garnet and are evidence of repeated and extensive fracturing. Some secondary-type inclusions are isolated.

Microthermomety For Fluid Inclusions in Garnet

Homogenization and freezing temperatures of garnet are diagramatically illustrated (Figs. 30 to 32). Homogenization temperature, salinity, and comments for individual

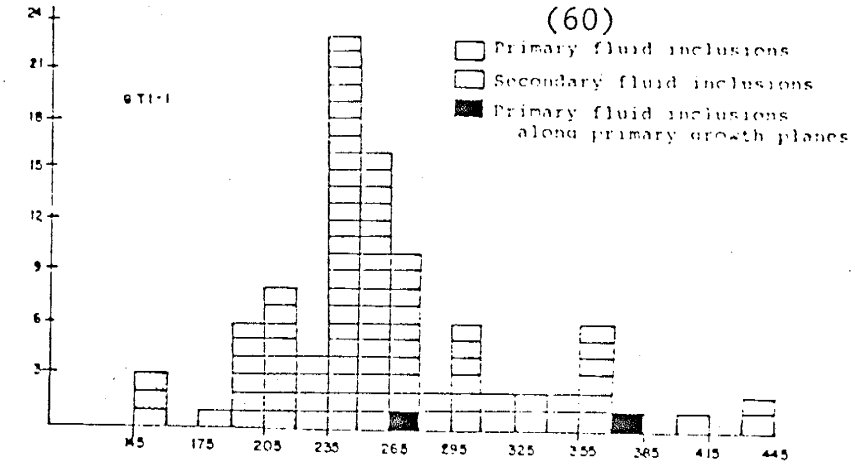

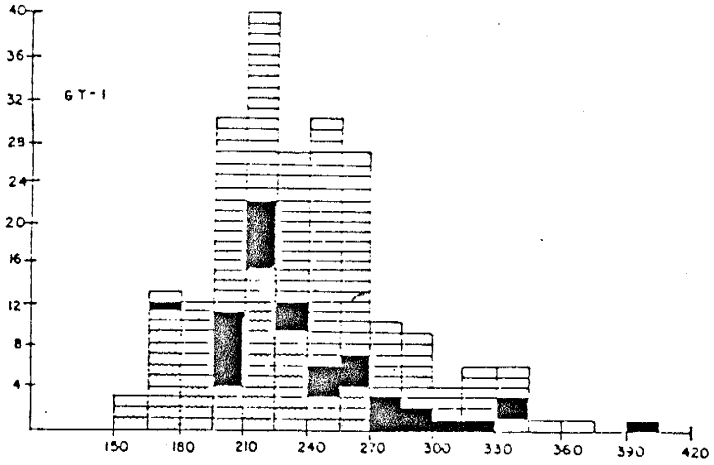

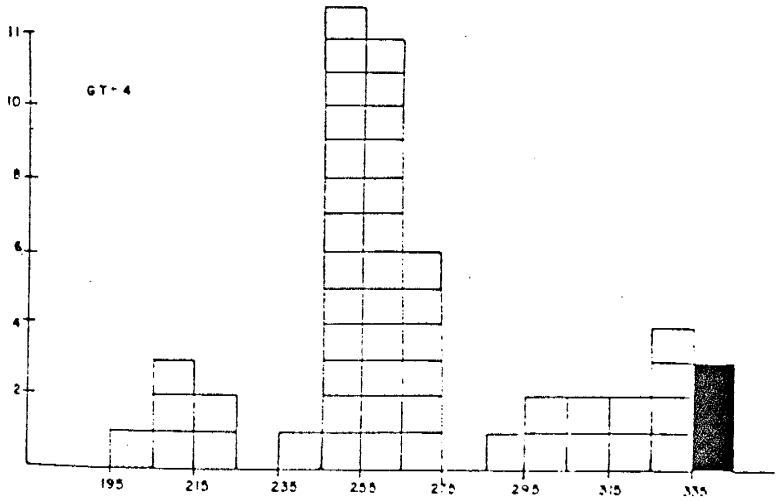

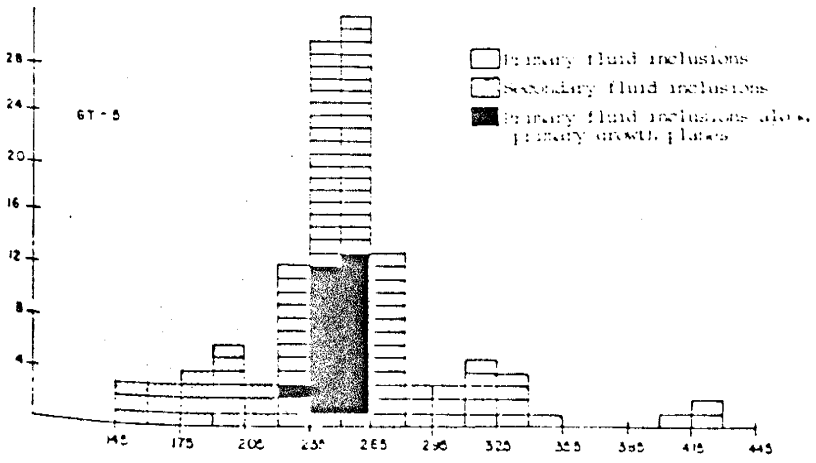

Fig.30 Homogenization temperatures of primary and secondary fluid

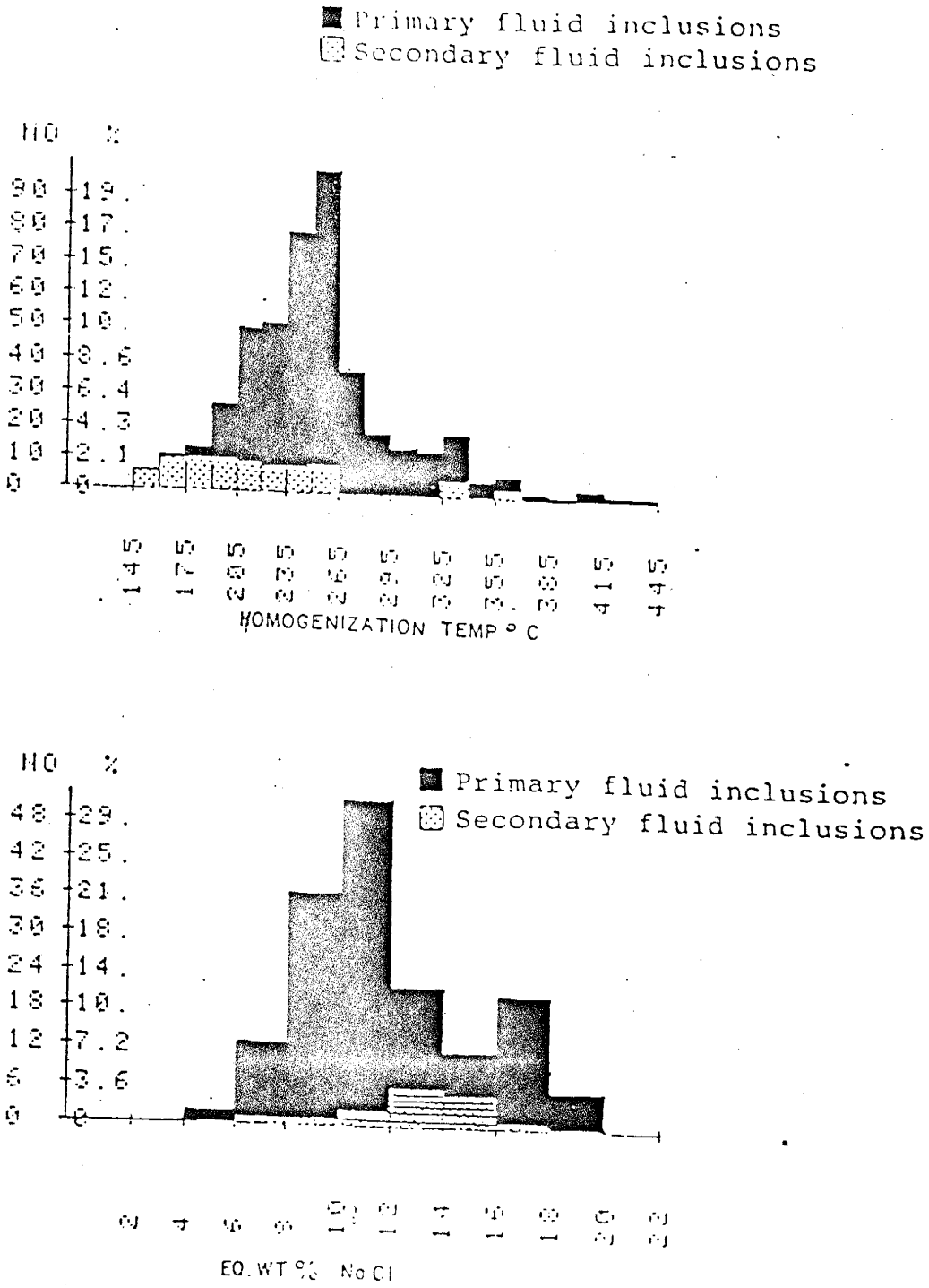

Fig.31 Summary of homogenization temperatures and salinities for primary and secondary fluid inclusions in garnet.

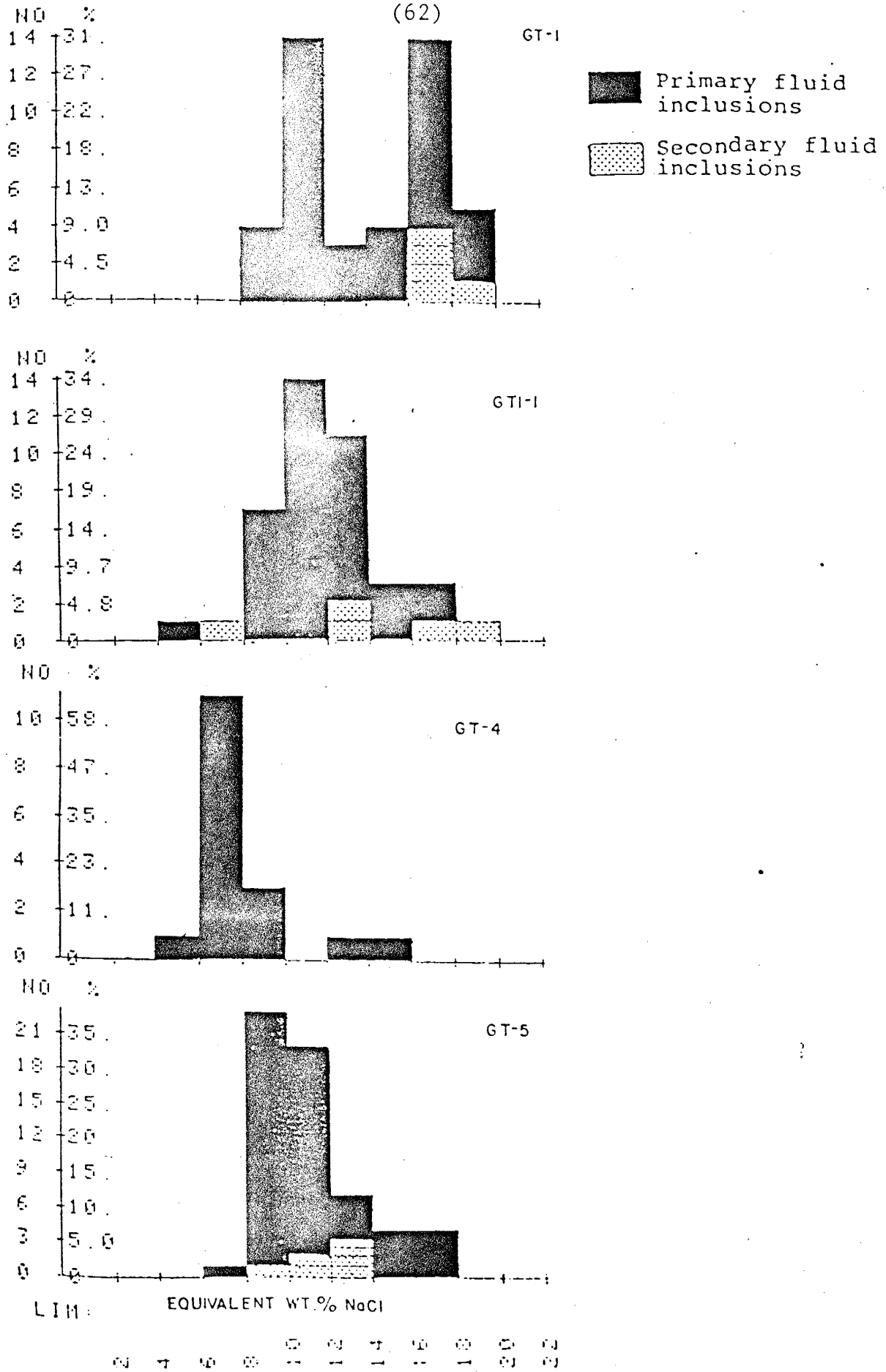
NO %
14 31.
12 27.
10 22.
8 18.
6 13.
4 9.0
2 4.5
0 0
GT-1
Primary fluid inclusions
Secondary fluid inclusions
NO %
14 34.
12 29.
10 24.
8 19.
6 14.
4 9.7
2 4.8
0 0
GTI-1
NO %
10 58.
8 47.
6 35.
4 23.
2 11.
0 0
GT-4
NO %
21 35.
18 30.
15 25.
12 20
9 15.
6 10.
3 5.0
0 0
GT-5
EQUIVALENT WT.% NaCl

fluid inclusions are listed in Appendix II. Salinities for individual inclusions in garnets were obtained from the freezing point of the liquid. The freezing point data was then related to salinities using data from Potter (1978).

Fluid inclusions in garnet filled to a liquid. Homogenization temperatures of primary fluid inclusions (Type I fluid inclusions ranged from 170°C to 435°C with a majority of the inclusions in the range of 205°C to 325°C (Figs. 30 and 31). Secondary-type fluid inclusions, (Type III) had low filling temperatures ranging from 145°C to 265°C (Type IIIb) or had higher filling temperatures around 330°C (Type IIIa) (Figs. 30 and 31). The lower filling temperature inclusions were the most common. The higher filling temperature group may represent another period of fracturing maybe at a later time associated with ore mineralization.

Distinction between primary and secondary fluid inclusions was difficult. Fluid inclusions of similar appearance to secondary fluid inclusions (Type IIIb) occurred in groups of between 25 to 100 inclusions and appeared unrelated to a fracture (Fig. 29.14). These groups of inclusions had low filling temperatures, on the order of 150°C to 220°C, and similar salinities. Possibly, they occurred on a flat-lying fracture plane and therefore would be interpreted as secondary. Because these fluid inclusions all had similar low filling temperatures, similar salinities, and looked similar to other secondary-type fluid inclusions, they were determined to be secondary.

Two fluid inclusions had vapor>liquid and homogenized to the vapor phase at 452°C and 410°C and had salinities of 9.0 and 7.5 eq. wt.% NaCl respectively. These were the only vapor-rich fluid inclusions observed in garnet. It is interesting to note that the two vapor-rich fluid inclusions in garnet had similar homogenization temperatures and salinities as the vapor inclusions that occur in the later quartz veins associated with ore mineralization. These two inclusions occurred together and could represent a secondary fracture that may have been related to the later ore mineralizing event.

Many fluid inclusions suitable for heating study were not suitable for freezing study because of their small size, the presence of wide and dark appearing inclusion walls, or because the entire inclusion was too dark. Most fluid inclusions froze between -45°C and -60°C, but all fluid inclusions were further frozen to approximately -90°C. Fluid inclusions in garnet samples had freezing temperatures of -14.0°C to - 2.7°C, corresponding to 19.0 to 4.5 eq. wt.% NaCl (Fig. 32). Most fluid inclusions, that occurred on garnet growth planes (Type II) had freezing temperatures ranging from -5.5°C to -10.0°C corresponding to salinities of 8.5 to 14.0 eq. wt.% NaCl (Figs. 28.5 and 28.6).

Homogenization temperature vs eq. wt. percent NaCl for individual fluid inclusions are plotted for the garnet samples (Fig. 33). There is indication that lower temperature fluid inclusions are characterized by higher salinities

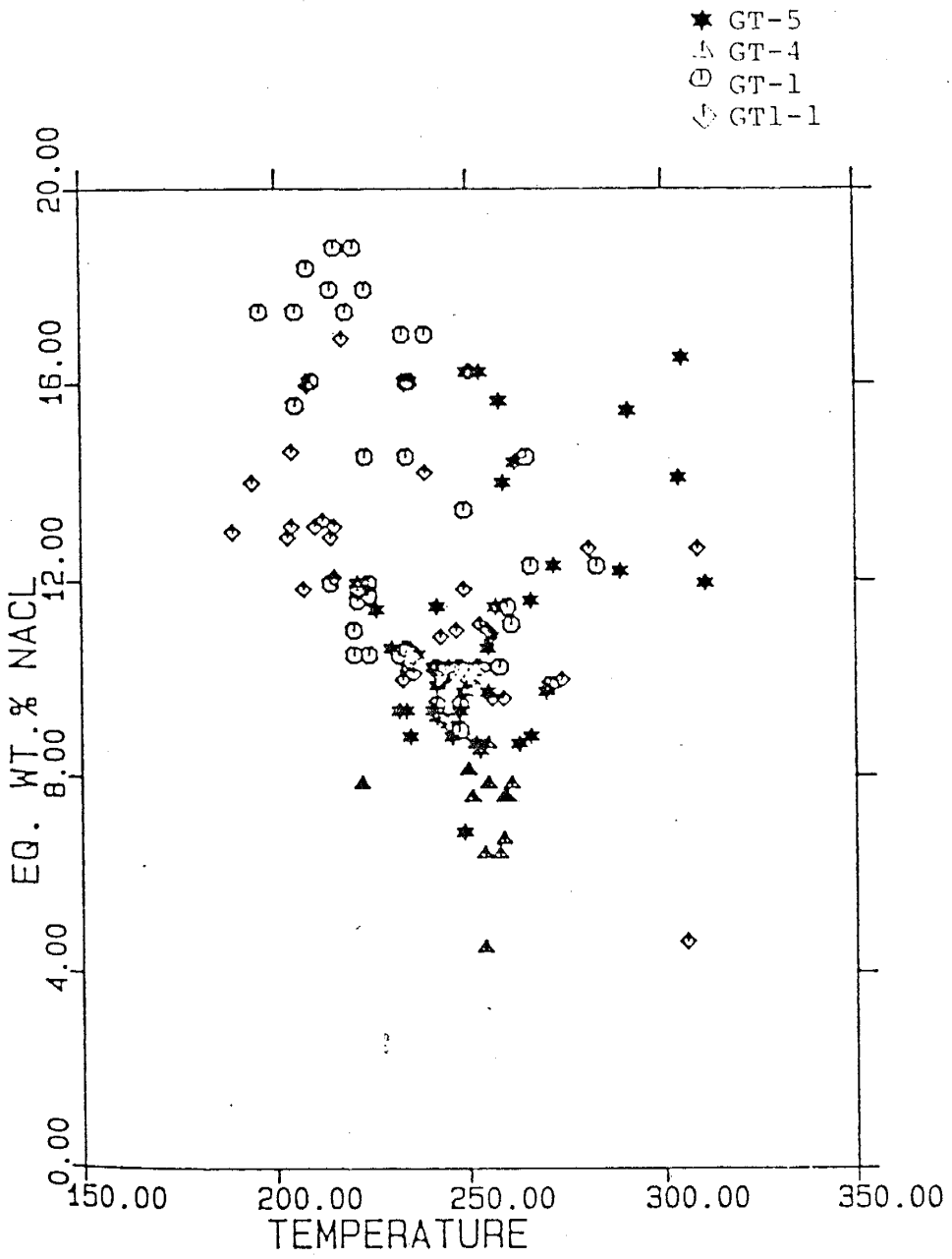

Figure 33. Equivalent wt.% NaCl vs homogenization temperature for individual fluid inclusions in garnet.

and higher temperature fluid inclusions are characterized by lower salinities. However, evidence for mixing is uncertain because there is a large variation of salinities for fluid inclusions with similar homogenization temperatures and there is also a wide variation of homogenization temperatures for fluid inclusions with similar salinities.

General Observations of Fluid Inclusions in Quartz from Quartz-Bearing Veins

Six different types of primary fluid inclusions were observed from quartz-bearing veins (Figs. 34 and 35) and include:

Type I Two phase liquid-vapor fluid inclusions with liquid>vapor that homogenized to the liquid phase (Figs. 34.21, 34.26, and 34.27).

Type II Two phase liquid-vapor fluid inclusions with vapor>liquid that homogenized to the vapor phase (Figs. 34.26, 34.27, and 34.28).

Type III Two phase fluid inclusions with variable liquid- vapor ratios that homogenized <400^{o}C and appeared to exhibit critical point behavior.

Type IV CO_2-rich fluid inclusions with three phases at room temperature or exhibited liquid CO_2 when cooled (Fig. 35).

Type V Three phase liquid-vapor-NaCl salt fluid inclusions with liquid>vapor.

Type VI Multiphase liquid-vapor-NaCl salt fluid inclusions with potassium chloride, magnetite, hematite, or

Figure 34. FLUID INCLUSION PHOTOMICROGRAPHS
All fluid inclusions occur in quartz-bearing veins

20. CLV-H-48 Apatite grain in quartz-magnetite-pyrite-chalcopyrite vein with liquid rich fluid inclusion.
21. CLV-H-48 Liquid rich and vapor rich fluid inclusions occurring together on microscopic scale.
22. CCF-22 Secondary plane of vapor rich fluid inclusions, most samples had abundant secondary planes containing vapor-rich inclusions or liquid+salt inclusions.
23. CCF-22 Primary fluid inclusion with vapor bubble (v), NaCl crystal (s), magnetite (m), and daughter (sulfate?) (d)
24. C-28 A group of fluid inclusions with similar shape and composition; all the fluid inclusions contain vapor bubble (v), NaCl crystal (s), KCl(?) crystal (k), magnetite (m) and daughters (d).
25. C-28 Primary fluid inclusions with vapor bubble (v), NaCl crystal (s) and magnetite (m); generally fluid inclusions that contain a NaCl crystal also have a magnetite daughter mineral present.
26. CLV-H-48 Various types of fluid inclusions occurring together on a microscopic scale, vapor dominated inclusions (v) and liquid dominated inclusions (l).
27. C-28 Liquid dominated (l) and vapor dominated (v) fluid inclusions occurring together, generally the vapor dominated inclusions are of larger size than the liquid dominated inclusions.
28. CLV-H-48 Two well defined vapor dominated primary fluid inclusions.
29. CLV-H-48 Primary liquid dominated fluid inclusion with NaCl crystal and shawdows.
30. C-28 Primary fluid inclusion with vapor bubble (v), NaCl crystal (s), magnetite (m) and daughter (sulfate?) (d).
31. C-28 Several fluid inclusions secondary(?) with similar form and composition, vapor bubble (v), NaCl crystal (s) and slightly isotropic daughter mineral (d).

(All photomicrographs are taken under plane light)

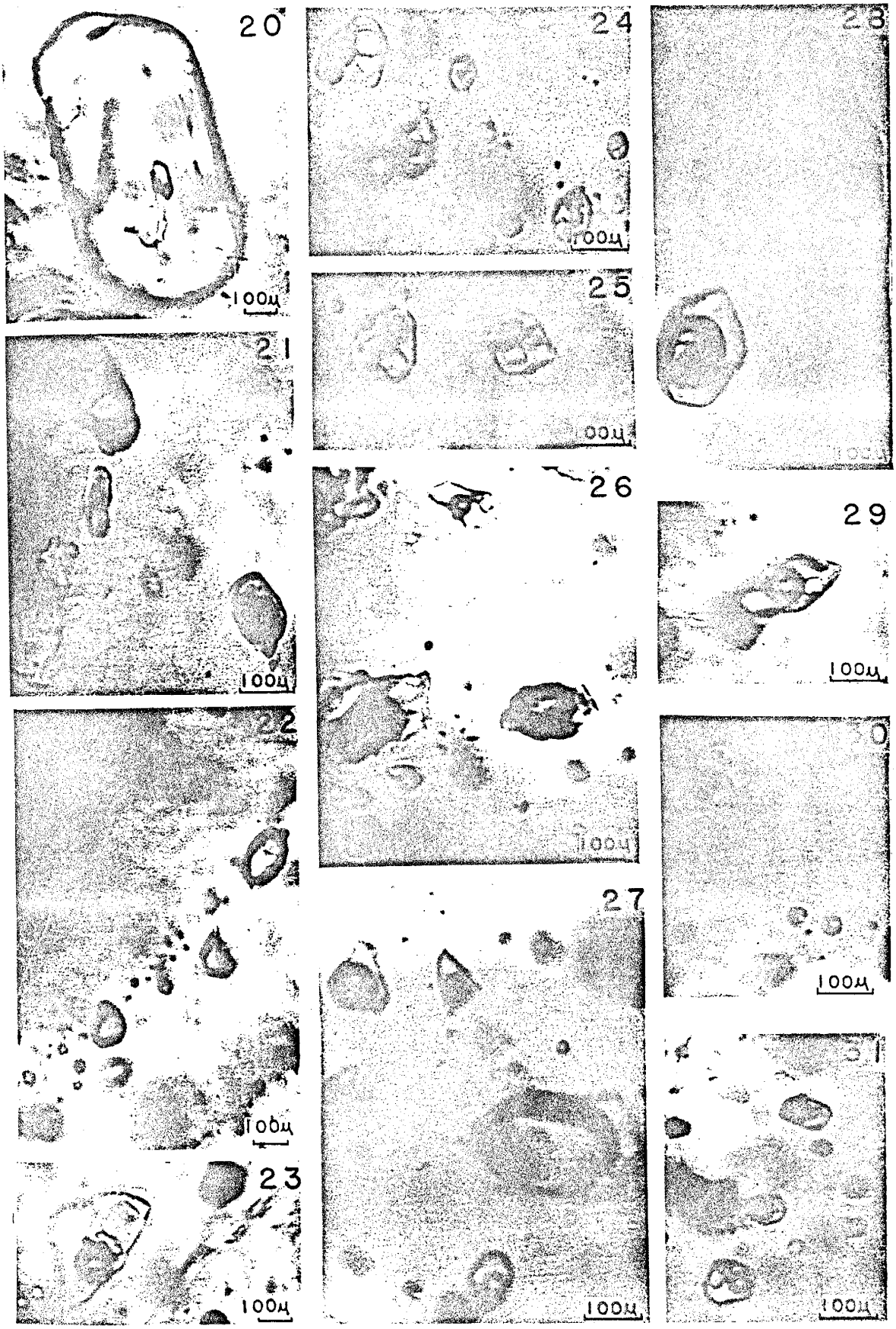
20
100μ
24
100μ
28
25
00μ
21
100μ
26
100μ
29
100μ
22
100μ
27
100μ
0
100μ
23
100μ
31
100μ

Figure 35. FLUID INCLUSION PHOTOMICROGRAPHS
All fluid inclusions occur in quartz-bearing veins
All fluid inclusions are CO_2-rich

32.-35. CLV-H-48D Photomicrographs of a CO_2-rich fluid inclusion; (32) at room temperature, a dark vapor bubble (v), and liquid water (lw); (33) frozen at -64.8°C; (34) at -7.0°C with a liquid CO_2 phase (lc), liquid water (lw), and vapor (v); (35) at 328°C the vapor bubble has decreased in size and the fluid inclusion homogenized to a liquid at 336°C.

36. CLV-H-48a Fluid inclusion with a CO_2 liquid phase that homogenized to a liquid at 322°C and the last liquid melted at +1.4°C.

37. CLV-H-48a Fluid inclusions with a CO_2 liquid phase that homogenized to a liquid at 352°C and the last liquid melted at +2.1°C.

(All photomicrographs are taken under plane light)

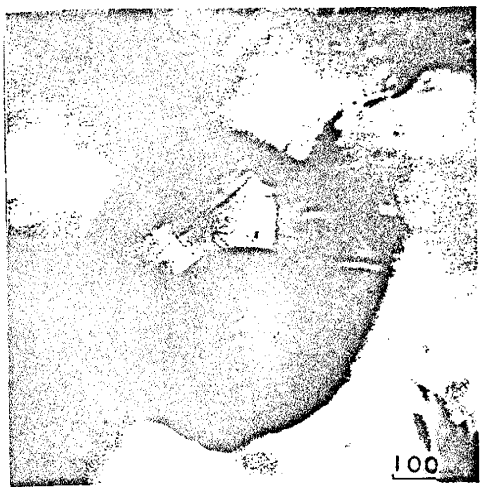
100

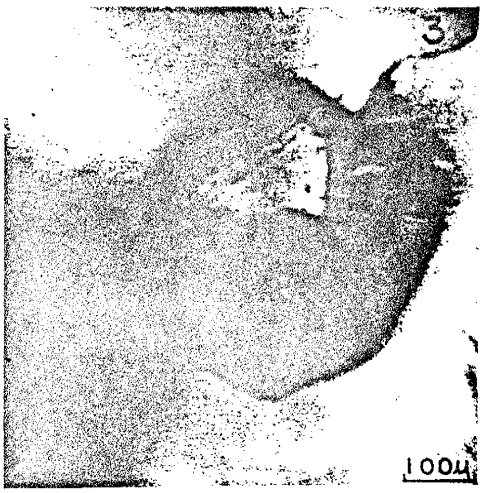
3
100μ

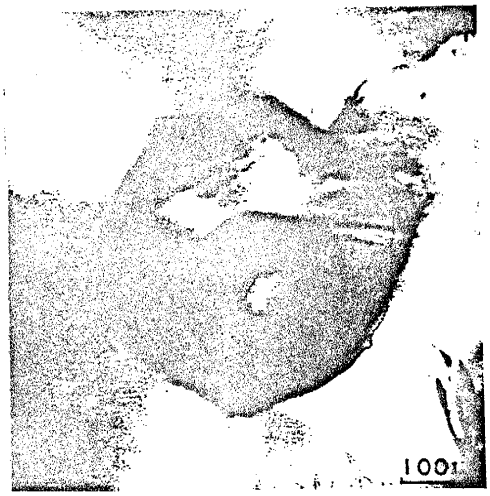
100μ

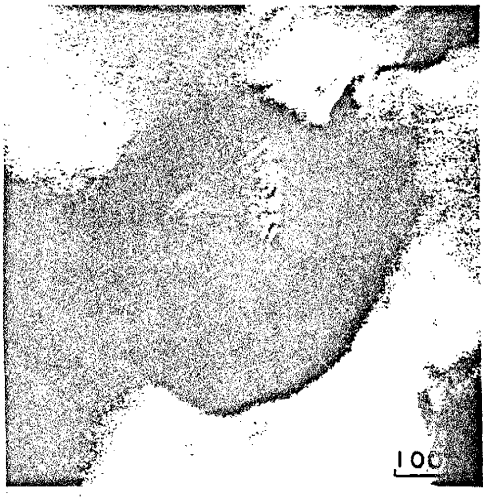
100

36

37

other unidentified daughters sulfates(?) with liquid>vapor (Figs. 34.23 to 34.26, 34.29 to 34.31).

Type III fluid inclusions were most common in sample C-28 and usually were vapor-rich. During heating, the vapor:liquid ratio remained almost constant and then within a few degrees the meniscus between the vapor and liquid phase faded rapidly.

Type IV, CO_2-rich fluid inclusions are of two types and were most common in samples CLV-H-48 and CLV-H-48D. One type has a vapor phase (v) and a liquid phase (l) and were most common (Figs. 35.32 to 35.35). The other type has a vapor phase (v) and an aqueous liquid phase (l) and a thin film of liquid rich C02 (lc). Presumably, the first type of inclusions did not have sufficient amounts of C02 present for a C02 rich liquid phase to be present. Both types of inclusions behaved similarly. Rapid cooling of two phase liquid (l) and vapor (v) CO_2-rich fluid inclusions revealed a thin ring of CO_2 that condensed to reveal this metastable assemblage between -10.0°C to -4.0 °C (Fig. 35.34). The fluid inclusions froze over a narrow range of temperatures ranging from -30°C to -35°C. but were further cooled to -90 C. During heating of the fluid inclusions an irregular interface between the vapor bubble (or the CO_2 liquid if present) was observed. This irregular interface is probably due to the formation of gas hydrate within the aqueous solution. From 0.2°C to 7.8°C motion of the gas bubble within the inclusion occurred on decomposition of the gas

hydrate at which time the vapor bubble returned to normal size.

Roedder, (1972) and Collins (1979), have observed similar behavior of fluid inclusions. This behavior is attributed to the formation of the clathrate compound carbon dioxide hydrate (CO2-5.75 H20) which freezes out prior to the freezing of the remaining aqueous solution to ice.

Identification and determination of a CO2 phase and/or the presence of other gases is not possible by cooling and heating procedures. Gas analyses were not performed on these inclusions and therefore the behavior of these fluid inclusions can only be interpreted as containing amounts of CO2 gas.

Both Type V and Type VI fluid inclusions that contained a NaCl crystal occurred in all samples. Disappearance of the NaCl crystal occurred both before and after the homogenization of the fluid inclusion. Fluid inclusions in which the vapor bubble homogenized before the disappearance of the NaCl crystal had a greater halite:vapor ratio as compared to those inclusions in which the NaCl crystal disappeared before the homogenization of the vapor bubble. Possible reasons for the persistence of halite above the filling temperature are necking down of inclusions, (Roedder, 1972); trapping solid NaCl; the need of a large pressure correction, or may be explained by the trapping of high salinity inclusions at high pressures (Erwood and others, 1979).

Potassium chloride, magnetite, and hematite usually occur in high salinity-type fluid inclusions that have a NaCl crystal. KCl occurred in some Type VI fluid inclusions, however, accurate measurements were difficult because of poor visibility and because of other daughter minerals present (Figs. 34.24 and 34.25). Magnetite was the most common daughter mineral in Type VI fluid inclusions and was identified by its color, euhedral form, and magnetitic properties (Figs. 34.24, 35.25, and 35.30). Less commonly, Type VI fluid inclusions had a red, slightly opaque mineral, presumably hematite. Neither magnetite nor hematite dissolved at the filling temperature.

Some fluid inclusions had a small, cubic, birefringent daughter mineral (Fig. 34.24, 34.25, 34.26, and 34.30) or a small, elongated, birefringent daughter mineral (Fig. 34.23) that did not change during heating or freezing. Possibly, this is a sulfate mineral.

Microthermometry of Fluid Inclusions from Quartz-Bearing Veins

Homogenization temperatures and salinities for fluid inclusions from quartz-bearing veins are diagramatically illustrated (Fig. 36 and 37). Homogenization temperatures, salinities, an comments for individual fluid inclusions are listed in Appendix II. Salinities of fluid inclusions in quartz-bearing veins were obtained both from relating freezing point data to salinities using data from Potter (1978) and by determining the temperature of halite

Fluid Inclusion Types

- Liquid dominated
- Vapor dominated
- Liquid dominated secondary
- Vapor dominated secondary
- Liquid + NaCl
- Liquid + NaCl secondary
- CO_2 liquid phase
- Critical point behavior

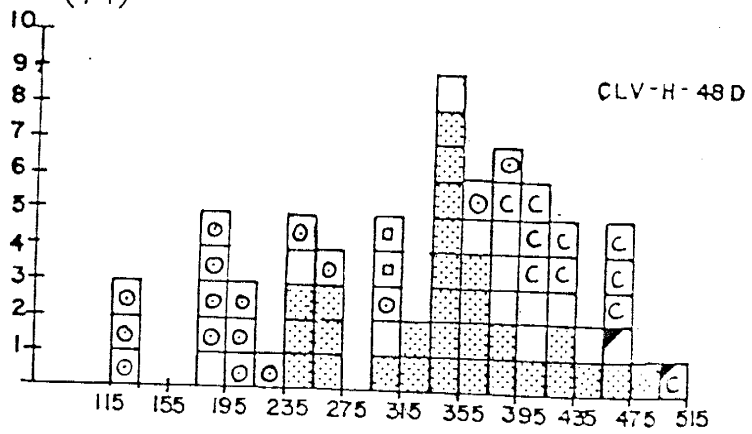

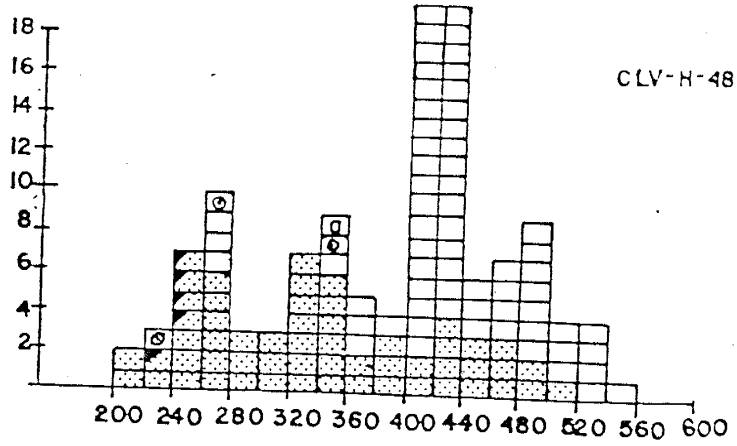

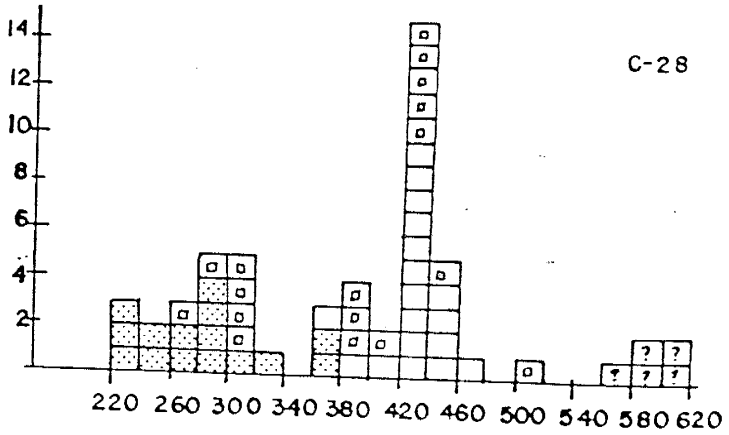

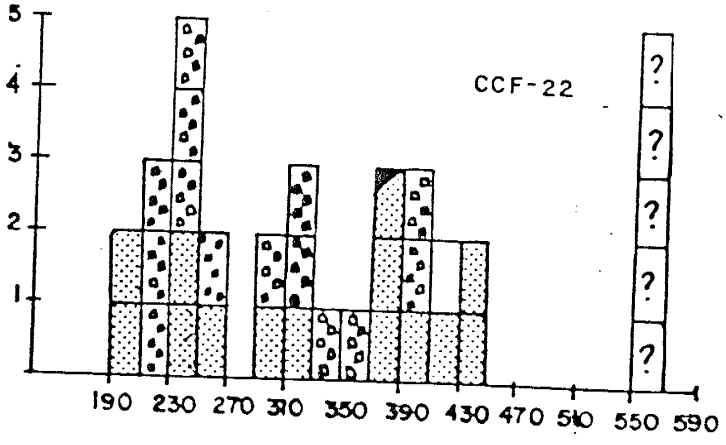

Figure 36. Homogenization temperatures for fluid inclusions in quartz + magnetite ± sulfide veins.

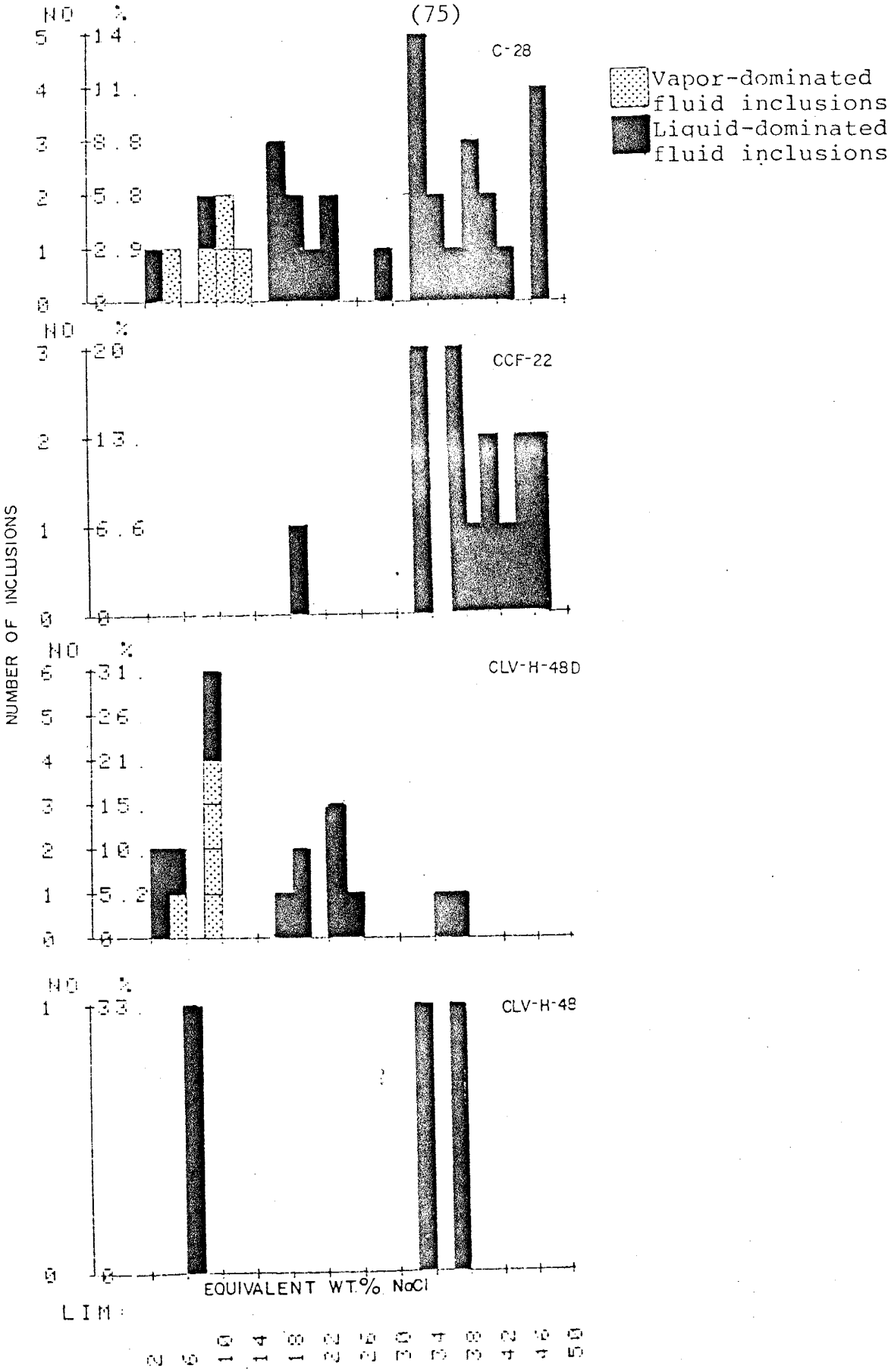

Fig.37Equivalent wt.% NaCl for individual fluid inclusions in quartz-bearing veins.

disappearance and relating this temperature to salinity data from Keevil (1942).

Homogenization temperatures vary from 115°C to >600°C. However, different types of inclusions exhibit a narrower range of filling temperatures (Fig. 36). Fluid inclusions are grouped into the same types as discussed earlier.

Type I Liquid-vapor fluid inclusions with liquid>vapor homogenize to a liquid between 190°C and 513°C. Freezing temperatures ranged from -24.0°C to -0.9°C corresponding to salinities of 25.0 to 1.5 eq. wt. % NaCl. The presence of CO_2 in some of these fluid inclusions is not clear because identification of CO_2 and salinity measurements were difficult to obtain because of poor visiblity.

Type II Liquid-vapor fluid inclusions with vapor>liquid homogenize to a vapor between 240°C and >600°C. A majority of these inclusions have filling temperatures ranging from 400°C to 460°C. Generally, Type II fluid inclusions have higher filling temperatures than Type I inclusions. Freezing temperatures are generally higher in Type II fluid inclusions when compared to Type I inclusions and range from -9.0°C to -3.6°C corresponding to salinities of 12.8 to 5.4 eq. wt. % NaCl.

Type III Fluid inclusions appeared to have critical points of the supercritical fluids ranging from 394°C to 430°C. Three secondary fluid inclusions had critical points between 459°C and 504°C. All fluid inclusions that appeared to exhibit critical point behavior had vapor>liquid.

Freezing temperatures were very difficult to obtain for these kinds of inclusions; however, the most reliable measurement was made on a fluid inclusion that had a critical point of 403°C and a freezing temperature of -6.2°C corresponding to a salinity of 9.4 eq. wt.% NaCl. The high salinities of these fluid inclusions suggests that they probably only approached critical point behavior. Data from Sourijan and Kennedy (1962) indicate a salinity of 2.5 eq. wt.% NaCl for vapor-rich fluid inclusions at 400°C and a salinity of 4.5 eq. wt.% NaCl for vapor rich fluid inclusions at 425°C. This suggests that the fluid inclusions from this study probably also contained small amounts of liquid and were not pure vapor.

Type IV CO_2-rich fluid inclusions homogenized to a liquid or a vapor phase. Those fluid inclusions that homogenized to a vapor phase generally had lower filling temperatures ranging from 115°C to 120°C than those that homogenized to a liquid phase and had filling temperatures ranging from 175°C to 361°C. Freezing temperatures varied from between approximately 0.0°C to +7.8°C.

Type V and VI NaCl-bearing fluid inclusions homogenized to a liquid and had filling temperatures ranging from 210°C to 520°C. The lower homogenization temperatures were most common in sample CCF-22 (Fig. 37). Salinities were variable and ranged from 32.5 to 47.0 eq. wt.% NaCl. In some inclusions the vapor bubble disappeared at a lower temperature than the NaCl crystal and these fluid inclusions

had a narrow range of homogenization temperatures from 303°C to 317°C with the exception of one inclusion that had a filling temperature of 279°C. Two inclusions in which NaCl disappeared before homogenization of the vapor bubble also had another crystalline solid that disappeared approximately 15 degrees before the disappearance of the NaCl. This could possibly be KCl.

Some fluid inclusions could not be frozen, usually these inclusion were fairly small in size and had a relatively small vapor bubble.

Evidence of boiling comes from all quartz-bearing veins. Type I inclusions (liquid>vapor) and Type II inclusions (vapor>liquid) homogenized to the liquid and vapor phase respectively at about the same temperature, indicating that the trapped fluid was on the liquid-vapor curve (Figs. 34.21, 34.26, and 34.27). Figure 36 indicates that liquid-rich and vapor-rich fluid inclusions filled at 245°C and 241°C to a liquid and vapor respectively. The presence of CO_2 in some of the fluid inclusions was not determined until late in the study and whether CO_2 was present in these fluid inclusions is not known. The presence of CO_2 in some of the fluid inclusions would affect the boiling temperatures and salinites of the inclusions and also greatly affects the pressure estimatation of the fluids. Fluid inclusions that were boiling at approximately 425°C to 450°C with salinities on the order of 15 eq. wt.% NaCl do not indicate that CO_2 is present. These inclusions

are used for a pressure estimate.

Pressure Determinations From Fluid Inclusion Data

A fluid of 15.0 eq. wt.% NaCl and a boiling temperature of 425°C, yields a pressure of 322 bars using data from Sourijan and Kennedy (1962). Extrapolation of boiling point curves from Haas (1971) yields a pressure estimate of 315 bars which is in close agreement to the data from Sourijan and Kennedy (Table III).

Table III. Pressure Estimates

Temperature of boiling	Salinity (eq.wt. % NaCl)	Pressure (bars)	
425°C	15.0	322	(Sourijan and Kennedy, 1962)
425°C	15.0	315	(Haas, 1971)

Temperature Correction for Fluid Inclusions

Temperature corrections for fluid inclusion homogenization temperatures in garnet can be estimated from the data of Potter (1977) providing pressure, salinity and homogenization temperature of the fluid inclusion is known.

The pressures during skarn formation can be assummed to be similar to those during ore mineralization or be estimated by reconstructing the overburden of sediments above the intrusion during skarn and ore mineralization. The following evidence suggests that pressures during skarn formation approached hydrostatic conditions: a) the shallow

depth of the intrusion, b) skarn formation greatly increases permeability allowing more open channels to the surface, c) the formation of garnet requires that the CO_2 pressures not be high and therefore suggests that CO_2 must have had a way to escape from the system, and, d) the numerous fractures and faults present of which many probably connected to the surface.

Applying the pressure estimate determined from fluid inclusions from quartz-bearing veins to fluid inclusions in garnet yields a temperature correction of approximately 30°C for filling temperatures of 265°C and a temperature correction of 45°C for filling temperatures of 170°C in garnet. If the system was not open to the surface during garnet skarn formation pressures would be approximately three times higher or approximately 900 bars. Nine hundred bars pressure yields a temperature correction of 85°C for most fluid inclusions in garnet. Therefore, depending on the geologic conditions during skarn formation the temperature correction for fluid inclusions from garnet is between 30°C to 85°C. Because, the system probably more closely approached hydrostatic conditions a temperature correction on the order of 30°C to 45°C for filling temperatures of fluid inclusions in garnet is reasonable.

Forrester (1972) has determined from drill core data and stratigraphic relations that the maximum pressure at the base of the El Paso Limestone was approximately 300 bars and approximately 100 bars if water-filled fractures existed

open to the surface.

Relationship Between Fluid Inclusions From Garnet And Fluid Inclusions From Quartz-Bearing Veins

Fluid inclusions from earlier skarn formation differ in composition, salinity, and temperature from fluid inclusions in later quartz-bearing veins. Most fluid inclusions from garnet have lower homogenization temperatures and salinities than fluid inclusions from quartz-bearning veins. Also, fluid inclusions from quartz-bearing veins commonly contain magnetite, whereas magnetite is not present in any of the fluid inclusions from garnet.

The differences in composition, homogenization temperatures, and salinities of fluid inclusions from garnet and from quartz-bearing veins suggests that the fluid inclusions are filled with fluids from differing origins. An alternative possibility is that the same fluid may have been responsible for both earlier skarn formation and later ore mineralization but the fluid changed composition with time.

REE Analyses

Introduction

The REE (Rare Earth Elements) comprise elements with atomic numbers 57-71 and include the elements from La to Lu in Group IIIA of the Periodic Table. The REE group exhibits a decrease in ionic radius from 1.02 (La) to 0.85A (Lu) and are usually octahedrally coordinated. The REE generally have a plus three valence state; however, some of the REE also have charges of plus two (Sm, Eu, Yb) or plus four (Ce, Pr, Tb) (Felsche, 1970). In general the REE have a similar chemistry so that whenever one REE appears the others also occur. Therefore, the chemical separation within the REE group generally occurs as a smooth function of atomic number.

The partitioning of REE is a function of temperature, pressure, and composition of the phases. The partioning of REE into one of two phases has been extensively studied in igneous processes for crystal/melt systems. However, the partioning of REE between crystal/aqueous fluid has not been well studied. The effects of other components in the aqueous fluid such as fluorine, chlorine, and CO_2 may greatly affect the partioning of the REE between the aqueous fluid/crystal. Presently, data is not available for modeling studies in hydrothermal systems.

A major problem in the correct interpretation of REE distribution patterns lies in the understanding of their mobility. Recent studies have led to the view that the REE

can be mobile in the presence of a fluid phase (Mitchell and Brunfelt, 1975; Martin and others, 1978). It has been suggested that enchanced mobility of the REE can be caused by the presence of a CO_2-rich fluid during metamorphism (Wendlandt and Harrison, 1979; Hynes, 1980).

Sample Preparation and Chemical Analyses

About 50 mg. of crushed sample was subjected to (Instrumental Neutron Activation Analysis) to determine their REE concentrations. Forty-eight whole rock samples were analyzed. In addition, REE concentrations were determined on six garnet samples. Garnet samples were hand-picked, isolated by heavy mineral separation, checked optically and by x-ray diffractometry.

RESULTS

Appendix IV lists the REE concentrations and chondrite normalized values for each sample and Appendix V lists the concentrations of other trace elements for each sample. REE concentrations for each sample are plotted on standard chondrite normalized plots (Figs. 38 to 51). Each figure shows the REE patterns of samples from a particular formation and usually includes an unaltered sample, a thermally altered sample and a metasomatically altered sample from the Continental orebody. In some instances a complete suite of samples was not available. An attempt was made to collect more than one group of samples in formations in which the lithology varied. When there is no point for a particular REE this means that that particular REE has no

determined value and is extrapolated.

The REE concentrations and fractionation pattern of each sample is directly related to the mineralogy of the sample. Appendix I gives a complete mineralogical description of each sample analyzed.

REE Geochemistry Of The Limestones

The REE patterns of all the limestones show increases in absolute REE concentrations and an enrichment in the lREE (light REE) from the least to the most altered limestones. All the unaltered limestone samples are characterized by low absolute concentrations of REE and positive Eu anomalies (Figs. 38-40).

The skarns of the Oswaldo Formation have higher absolute REE concentrations and show an enrichment in the lREE relative to the unaltered limestone (Fig. 38). Both skarn samples have small negative Eu anomalies.

Both skarn and unaltered limestone of the Lower Blue Limestone are characterized by lREE enrichment and positive Eu anomalies (Fig. 39). The two altered samples have higher absolute REE concentrations with the more altered sample having the highest absolute concentration of REE. Both samples have REE patterns similar to the garnets (Fig. 42).

The Hanover Limestone is the principal ore-bearing formation. Similar to the other limestones, the skarn has the highest absolute concentration of REE, the recrystallized limestone has intermediate REE concentrations and the unaltered limestone has low absolute REE

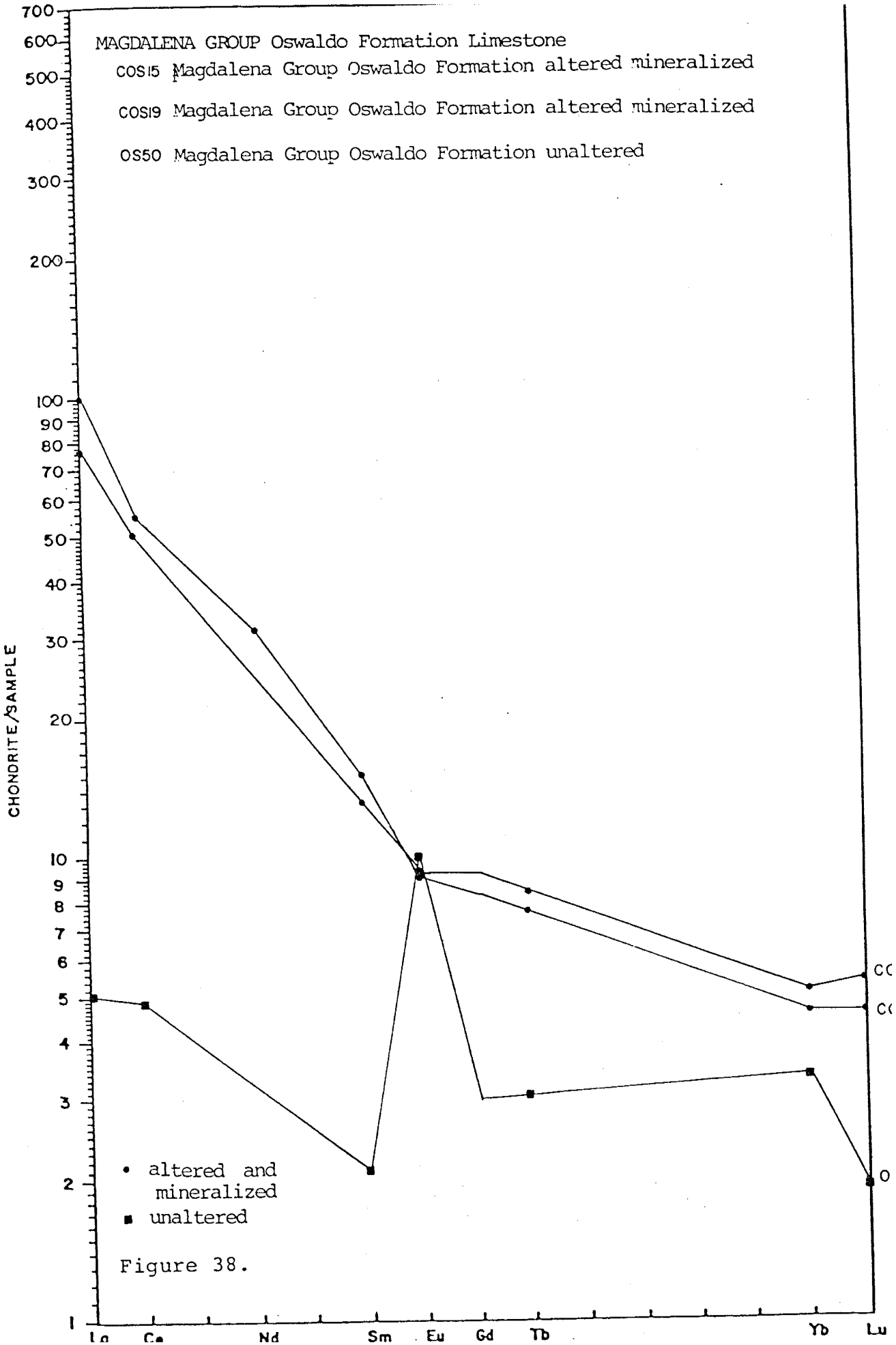
MAGDALENA GROUP Oswaldo Formation Limestone
COS15 Magdalena Group Oswaldo Formation altered mineralized
COS19 Magdalena Group Oswaldo Formation altered mineralized
OS50 Magdalena Group Oswaldo Formation unaltered
CHONDRITE/SAMPLE
700
600
500
400
300
200
100
90
80
70
60
50
40
30
20
10
9
8
7
6
5
4
3
2
1
La
Ce
Nd
Sm
Eu
Gd
Tb
Yb
Lu
• altered and mineralized
■ unaltered

Figure 38.

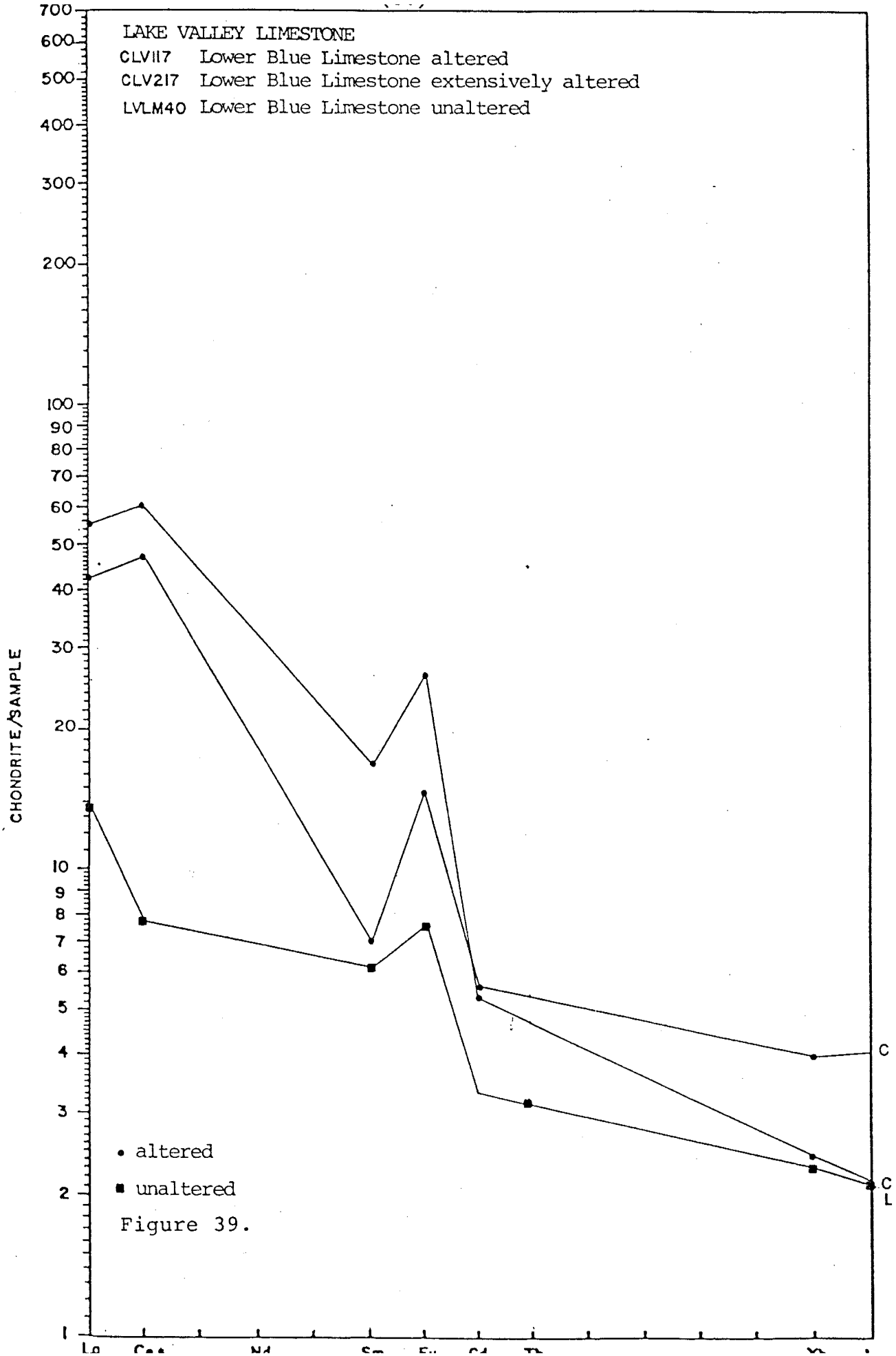
LAKE VALLEY LIMESTONE
CLV117 Lower Blue Limestone altered
CLV217 Lower Blue Limestone extensively altered
LVLM40 Lower Blue Limestone unaltered
CHONDRITE/SAMPLE
700
600
500
400
300
200
100
90
80
70
60
50
40
30
20
10
9
8
7
6
5
4
3
2
1
C
C
L
• altered
■ unaltered

Figure 39.

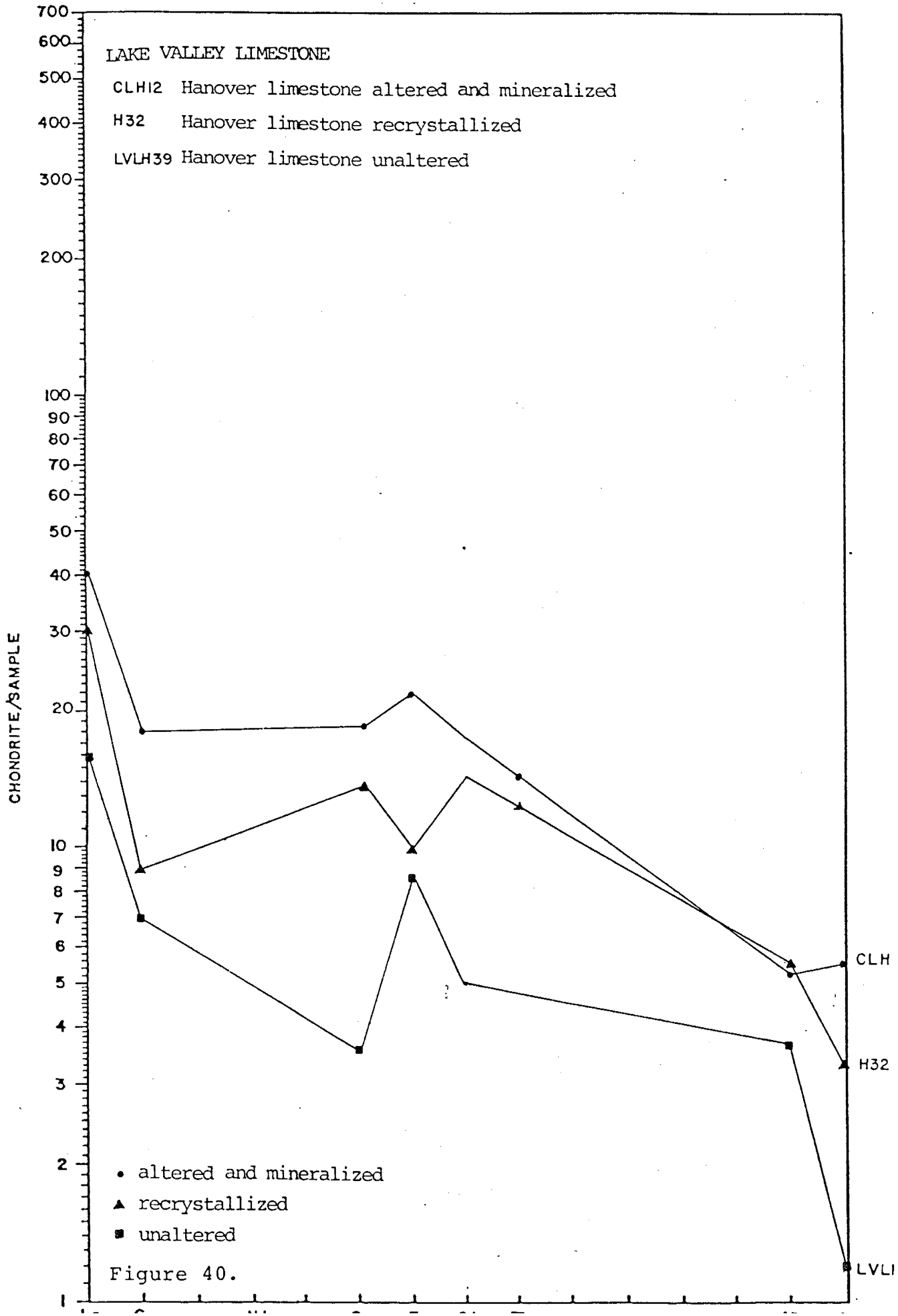
LAKE VALLEY LIMESTONE
CLH12 Hanover limestone altered and mineralized
H32 Hanover limestone recrystallized
LVLH39 Hanover limestone unaltered
CHONDRITE/SAMPLE
700
600
500
400
300
200
100
90
80
70
60
50
40
30
20
10
9
8
7
6
5
4
3
2
1
CLH
H32
LVLI
• altered and mineralized
▲ recrystallized
■ unaltered

Figure 40.

concentrations (Fig. 40). The recrystallized sample differs from the other samples by having a negative Eu anomaly.

REE Geochemistry Of The Shaly Limestones

Two metasomatized samples from the Syrena Formation have REE patterns characterized by lREE enrichment, high absolute concentrations of REE and negative Eu anomalies (Fig. 41). The most altered sample has the greatest absolute concentration of REE. A garnet skarn band from the Syrena Formation has a REE pattern similar to the garnets (Fig. 42).

REE Geochemistry Of Garnet

Six garnet separates were analyzed (Fig. 42). The REE patterns of all the garnet samples are similar and characterized by an enrichment in lREE, very low concentrations of hREE, show a positive Eu anomaly, and may show a positive Ce anomaly.

The garnets have a REE fractionation pattern similar to the limestones they replaced with the major difference being the higher absolute REE concentrations of the garnets.

REE Geochemistry Of The Dolomites

The REE patterns for the unaltered, recrystallized, and the metasomatized Montoya and Fusselman Dolomite are all similar (Fig. 43). All samples are characterized by low absolute REE concentrations; positive Eu anomalies; and a positive or no Ce anomaly which may be analytical error. Four of the samples show no values for Sm. This is because the Sm values for these samples was interpreted to be

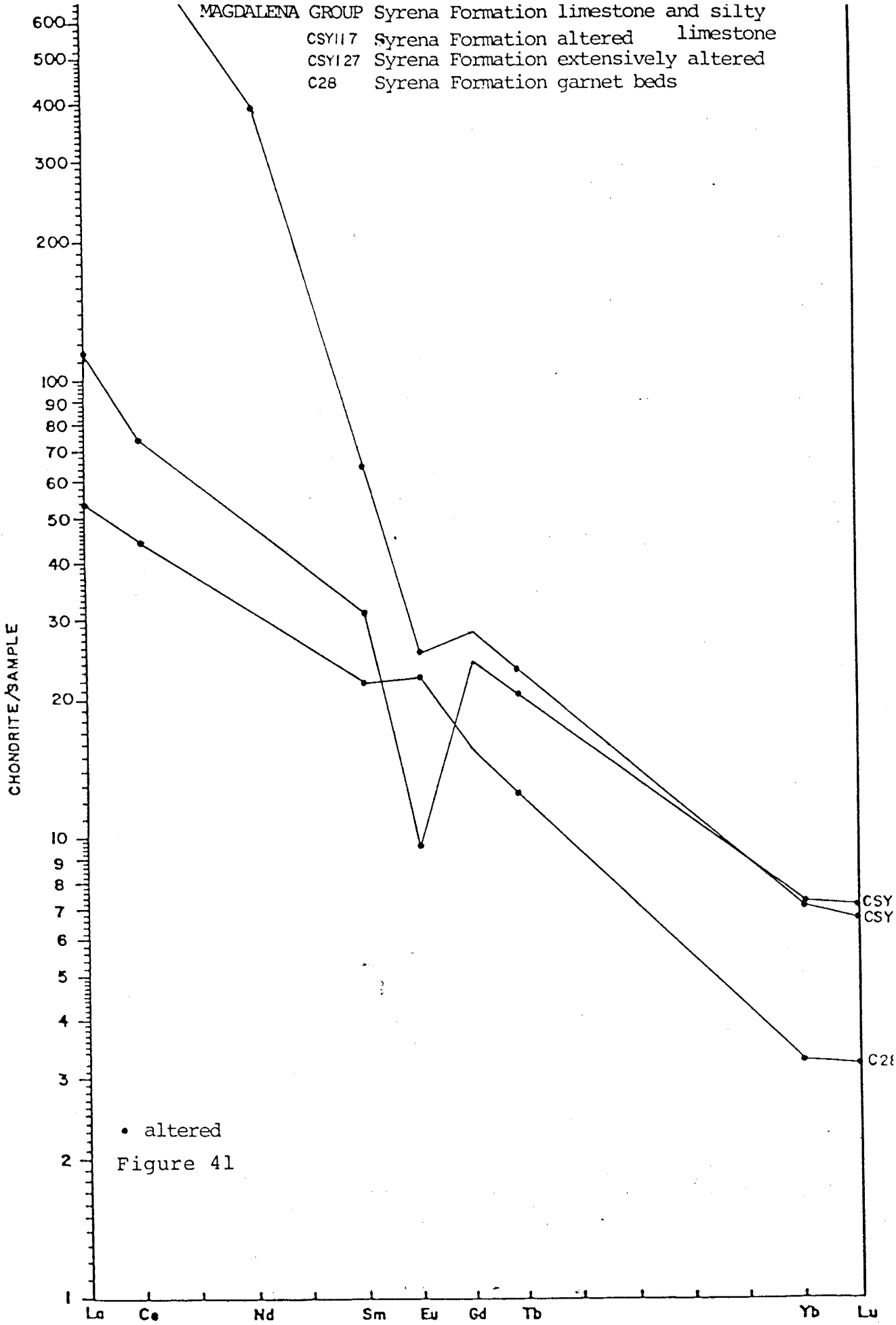
MAGDALENA GROUP Syrena Formation limestone and silty
CSY117 Syrena Formation altered limestone
CSY127 Syrena Formation extensively altered
C28 Syrena Formation garnet beds
CHONDRITE/SAMPLE
600
500
400
300
200
100
90
80
70
60
50
40
30
20
10
9
8
7
6
5
4
3
2
1
La
Ce
Nd
Sm
Eu
Gd
Tb
Yb
Lu
CSY
CSY
C28
• altered

Figure 41

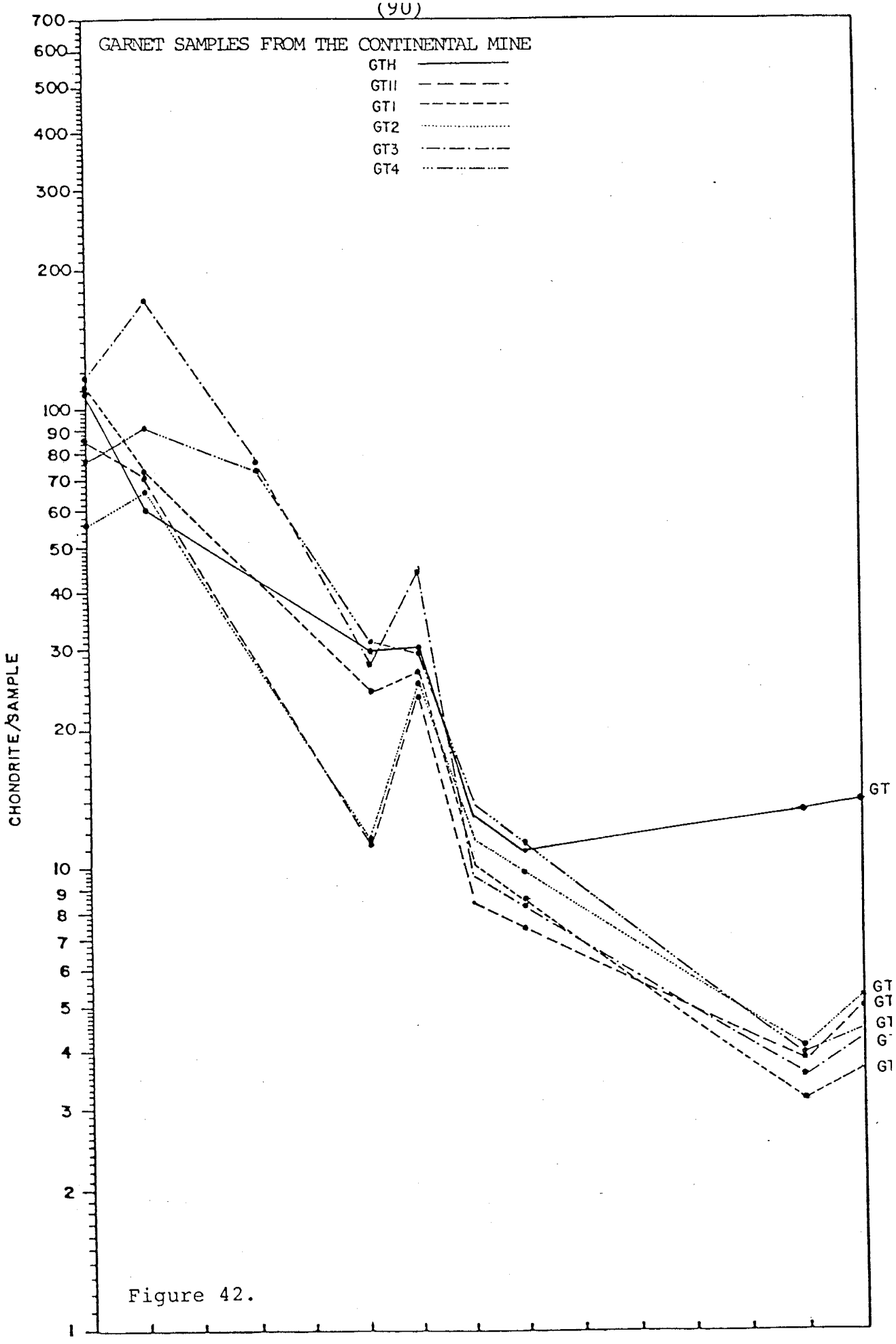
GARNET SAMPLES FROM THE CONTINENTAL MINE
GTH
GTII
GTI
GT2
GT3
GT4
CHONDRITE/SAMPLE
700
600
500
400
300
200
100
90
80
70
60
50
40
30
20
10
9
8
7
6
5
4
3
2
1
GT
GT
GT
GT
GT

Figure 42.

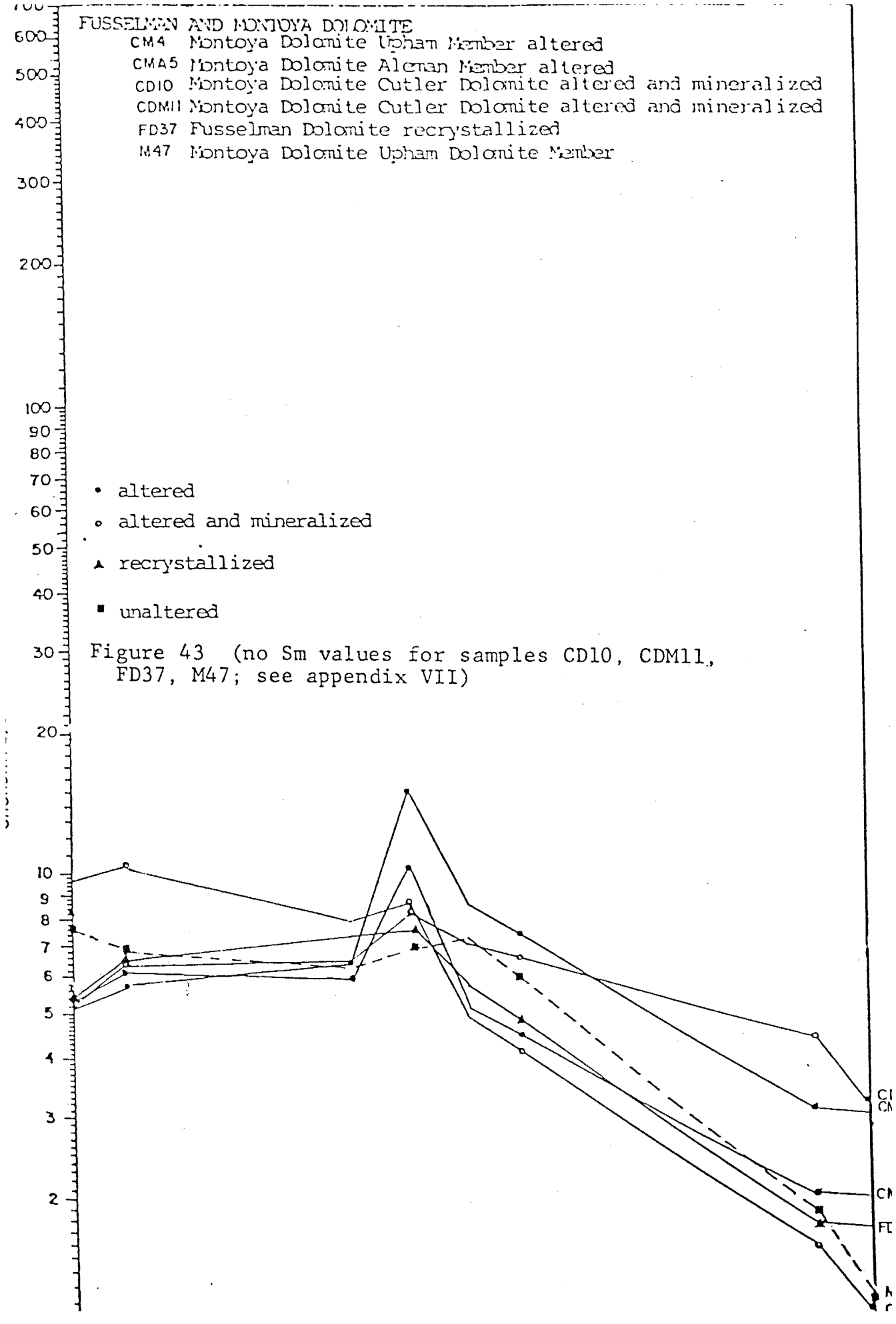

Figure 43 (no Sm values for samples CD10, CDM11, FD37, M47; see appendix VII)

analytical error. The Sm values for these samples are shown in Appendix VII.

The unaltered dolomite is characterized by low absolute REE concentrations similar to the unaltered limestone samples. Similar low absolute REE concentrations have been determined on carbonate rocks in others studies (Haskin and Gehl, 1962; Haskin and others, 1966; Balaschov and others, 1964; Ronov and others, 1967, 1972, 1974).

Metasomatically altered samples (CM4, CMA5, CD10) are very similar mineralogically and comprised of primarily carbonate (95%) and altered forsterite (5%). Sample (CDM11) differs in that it is mineralized and comprised of approximately equal amounts of forsterite, phlogopite-actinolite-tremolite, carbonate and clays, and magnetite and sulfides. All four samples have similar REE patterns despite differences in mineralogy.

The metasomatically altered sample from the El Paso Limestone has a much higher absolute REE concentration than the unaltered sample and shows an enrichment in the lREE (Fig. 44). The skarn sample is characterized by a negative Eu anomaly and the unaltered sample by a positive Eu anomaly. The unaltered sample has a REE fraction pattern that is similar to the fractionation patterns of the other unaltered carbonate rocks. However, the absolute REE concentration of the unaltered El Paso Limestone is higher than most of the other carbonate rocks.

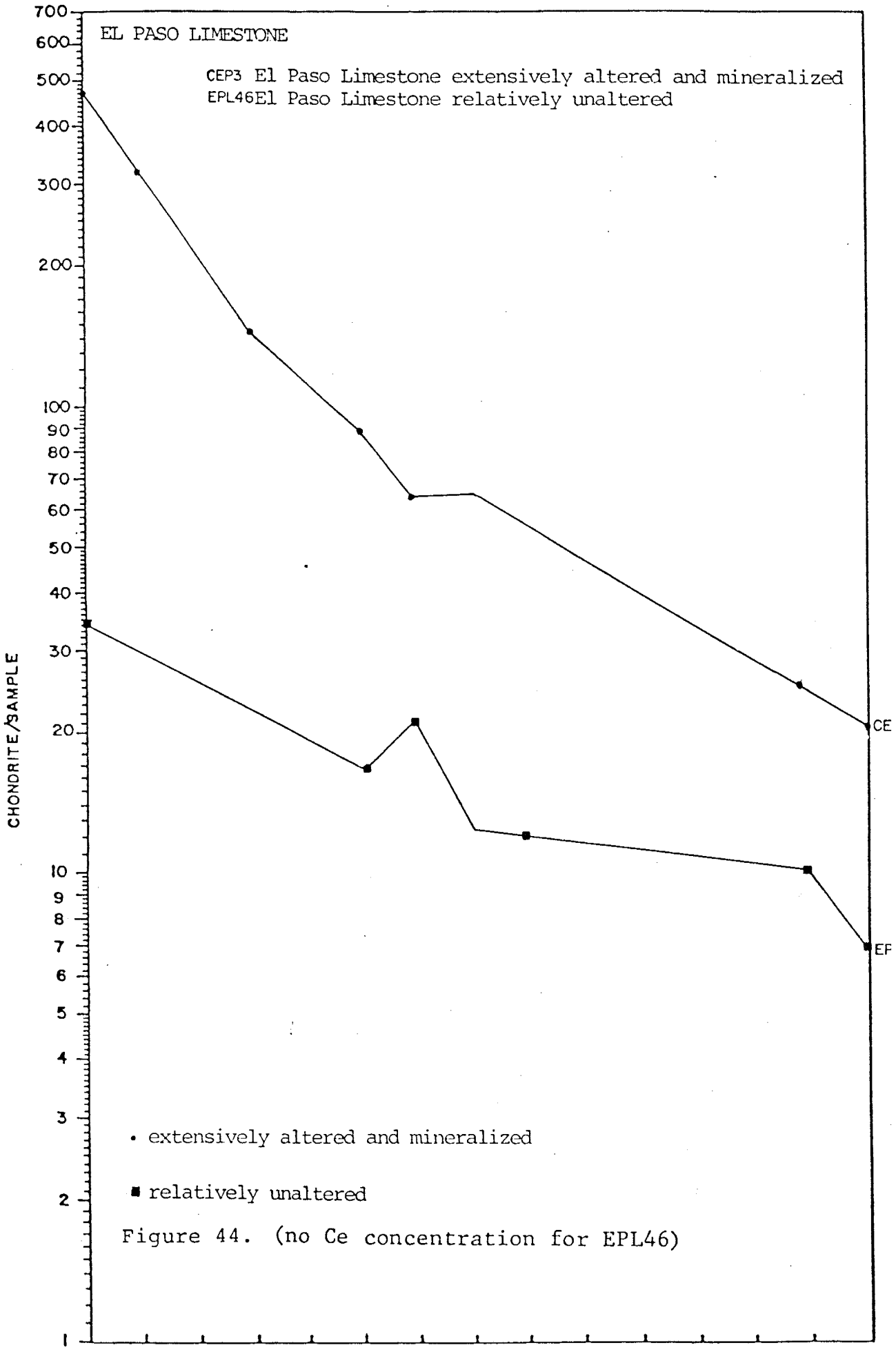

Figure 44. (no Ce concentration for EPL46)

REE Geochemistry Of The Shales

REE patterns of samples from the Ready Pay Member of the Percha Shale indicate that the REE concentrations of the shales have not changed significantly from the unaltered to the most altered samples (Fig. 45). All samples are characterized by lREE enrichment and a negative Eu anomaly. Both unaltered and partially recrystallized samples have REE patterns similar to North American Shales (NAS). (Fig. 46). The altered sample has a slightly greater absolute REE concentration, a smaller negative Eu anomaly, and slightly higher hREE concentrations than the less altered samples.

The REE patterns of the Augen Member (Box Member) of the Percha Shale (Fig. 47) are similar to that of the Ready Pay Member (Fig. 45) with the exception of the unaltered Augen Member sample. It has a REE fractionation pattern similar to the REE patterns of the unaltered carbonate rocks. The unaltered and recrystallized samples have REE patterns similar to NAS (Fig. 46).

The metasomatically altered samples from both the Augen Member (Fig. 47) and Ready Pay Member (Fig. 45) of the Percha Shale have no Eu anomaly and a very small Eu anomaly respectively.

A hornfels sample of the Parting Shale (Fig. 48) has a REE pattern that is flatter with a smaller concentration of lREE and a greater concentration of hREE as compared to the shale samples from the Percha Shale and NAS.

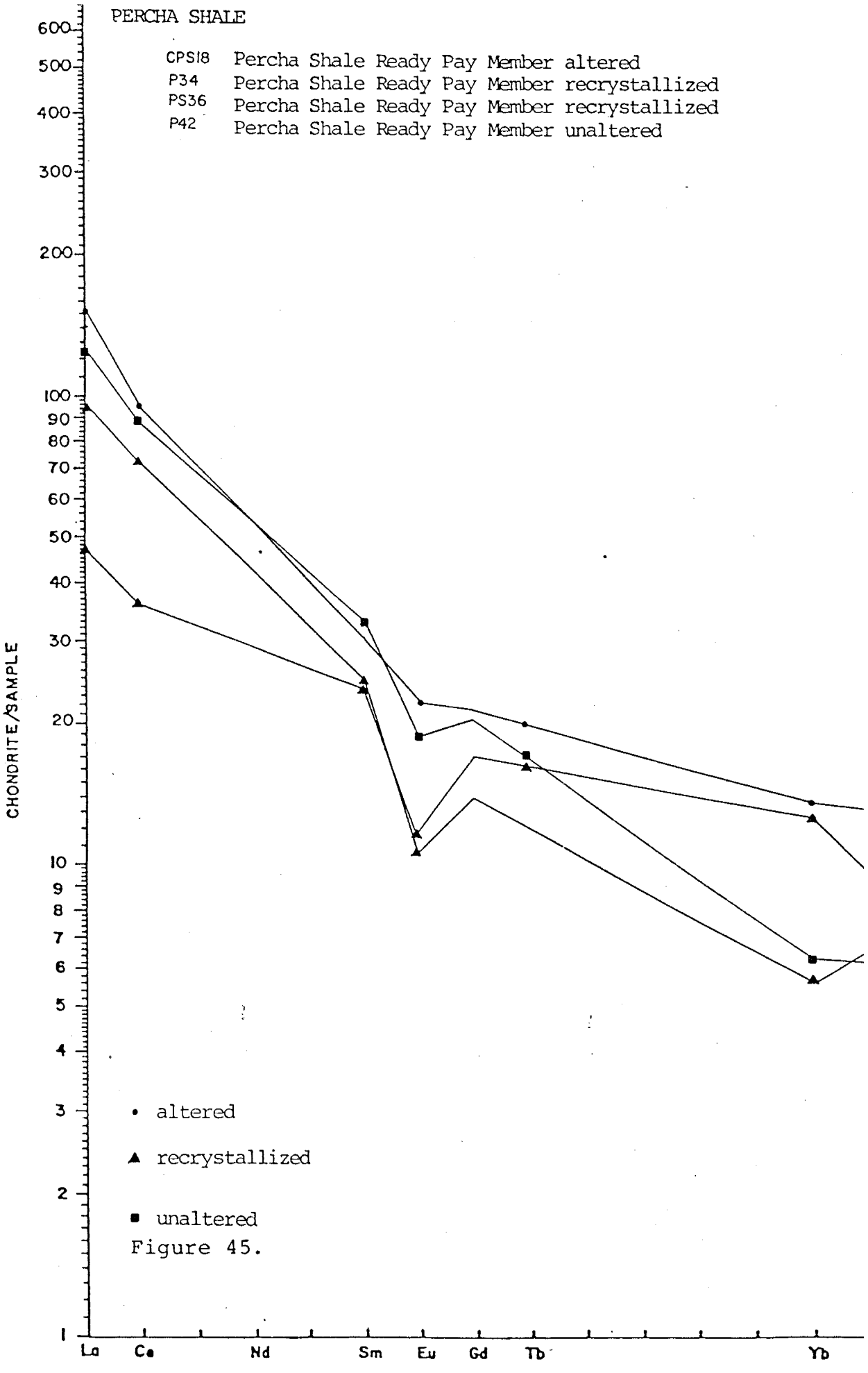
PERCHA SHALE
CPS18 Percha Shale Ready Pay Member altered
P34 Percha Shale Ready Pay Member recrystallized
PS36 Percha Shale Ready Pay Member recrystallized
P42 Percha Shale Ready Pay Member unaltered
CHONDRITE/SAMPLE
600
500
400
300
200
100
90
80
70
60
50
40
30
20
10
9
8
7
6
5
4
3
2
1
La
Ce
Nd
Sm
Eu
Gd
Tb
Yb
• altered
▲ recrystallized
■ unaltered

Figure 45.

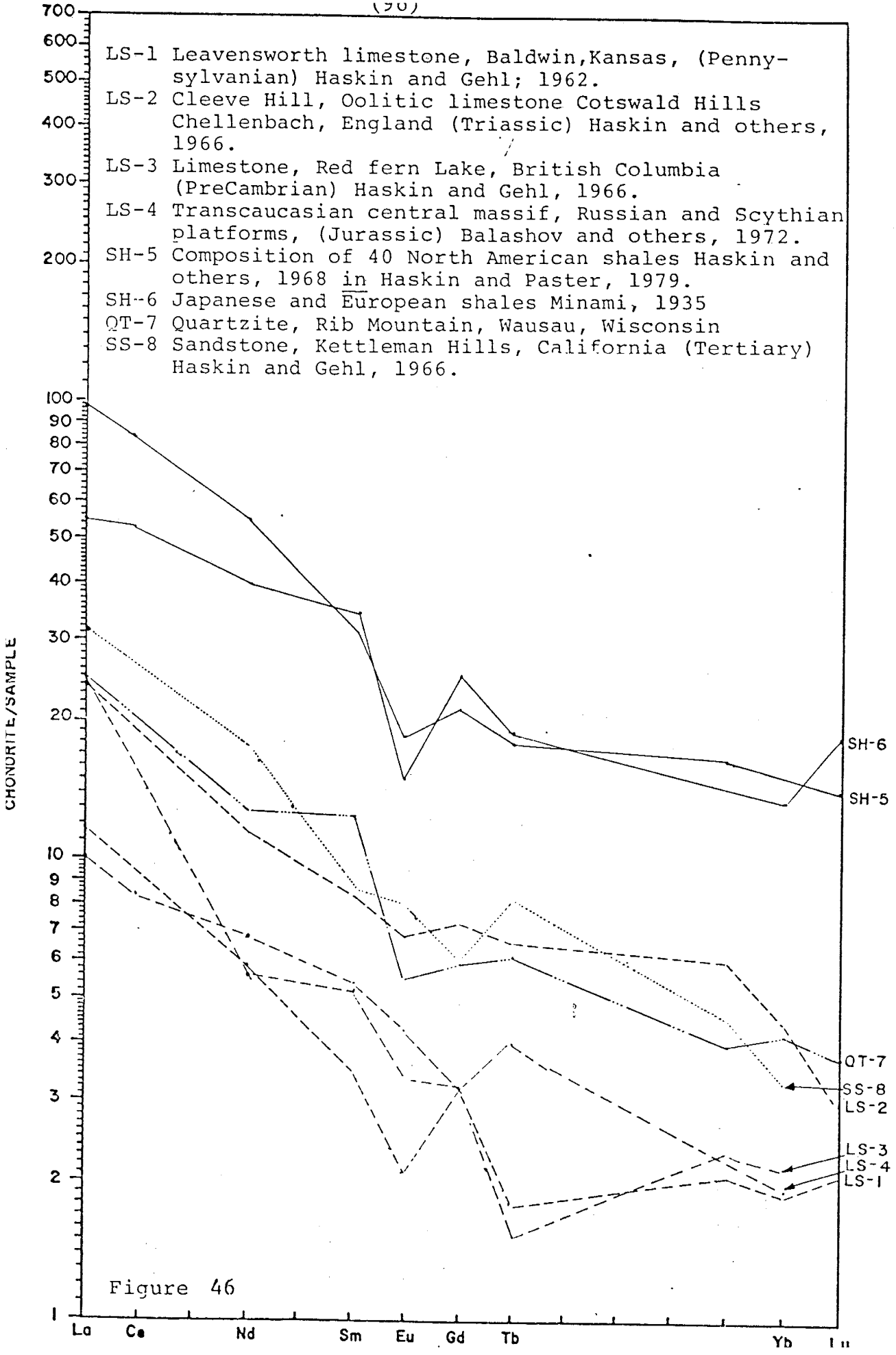
LS-1 Leavensworth limestone, Baldwin,Kansas, (Pennsylvanian) Haskin and Gehl; 1962.
LS-2 Cleeve Hill, Oolitic limestone Cotswald Hills Chellenbach, England (Triassic) Haskin and others, 1966.
LS-3 Limestone, Red fern Lake, British Columbia (PreCambrian) Haskin and Gehl, 1966.
LS-4 Transcaucasian central massif, Russian and Scythian platforms, (Jurassic) Balashov and others, 1972.
SH-5 Composition of 40 North American shales Haskin and others, 1968 in Haskin and Paster, 1979.
SH-6 Japanese and European shales Minami, 1935
QT-7 Quartzite, Rib Mountain, Wausau, Wisconsin
SS-8 Sandstone, Kettleman Hills, California (Tertiary) Haskin and Gehl, 1966.
CHONDRITE/SAMPLE
700
600
500
400
300
200
100
90
80
70
60
50
40
30
20
10
9
8
7
6
5
4
3
2
1
La
Ce
Nd
Sm
Eu
Gd
Tb
Yb
Lu
SH-6
SH-5
QT-7
SS-8
LS-2
LS-3
LS-4
LS-1

Figure 46

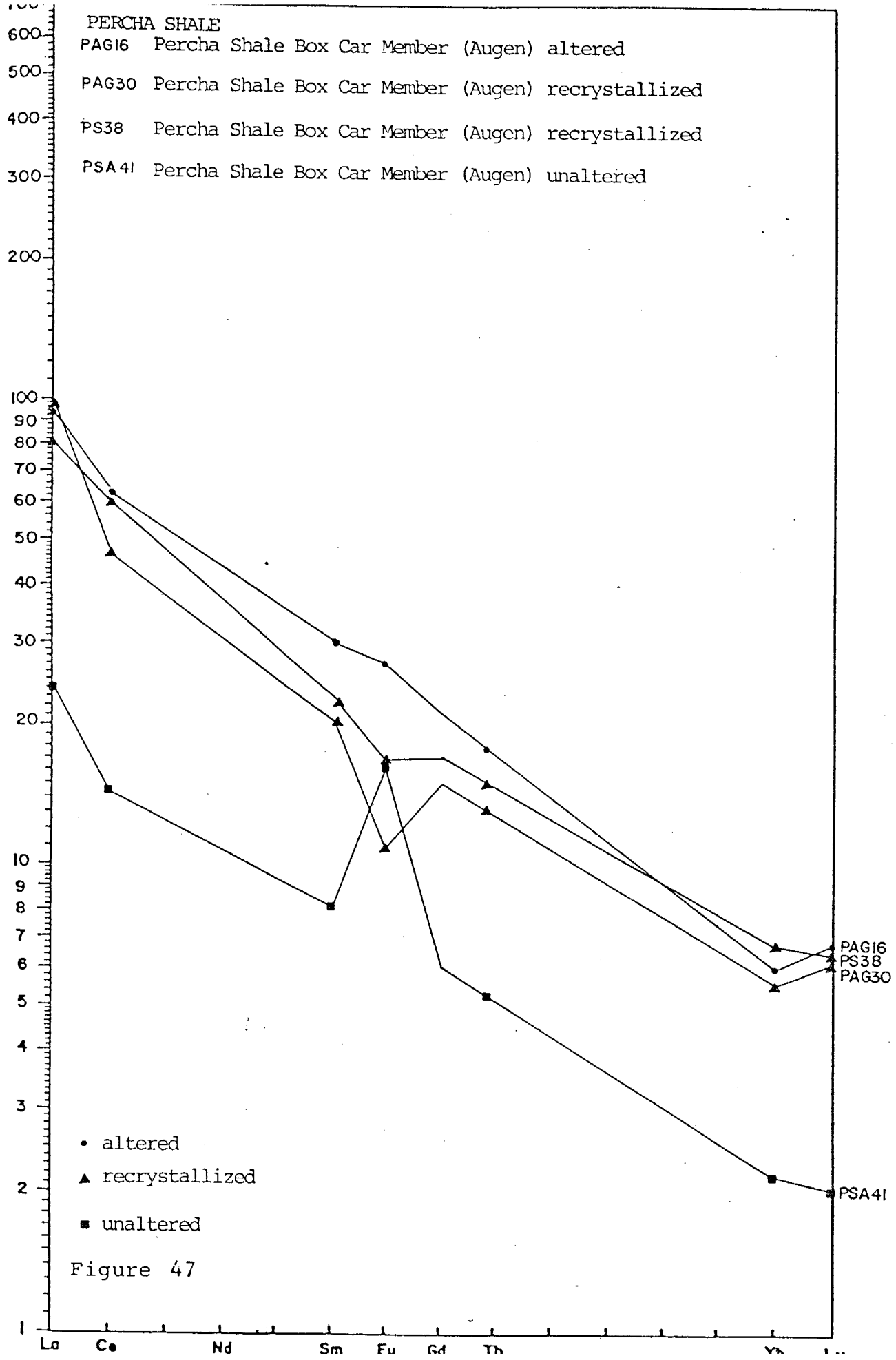
PERCHA SHALE
PAG16 Percha Shale Box Car Member (Augen) altered
PAG30 Percha Shale Box Car Member (Augen) recrystallized
PS38 Percha Shale Box Car Member (Augen) recrystallized
PSA41 Percha Shale Box Car Member (Augen) unaltered
600
500
400
300
200
100
90
80
70
60
50
40
30
20
10
9
8
7
6
5
4
3
2
1
PAG16
PS38
PAG30
PSA41
• altered
▲ recrystallized
■ unaltered
La
Ce
Nd
Sm
Eu
Gd
Tb
Yb

Figure 47

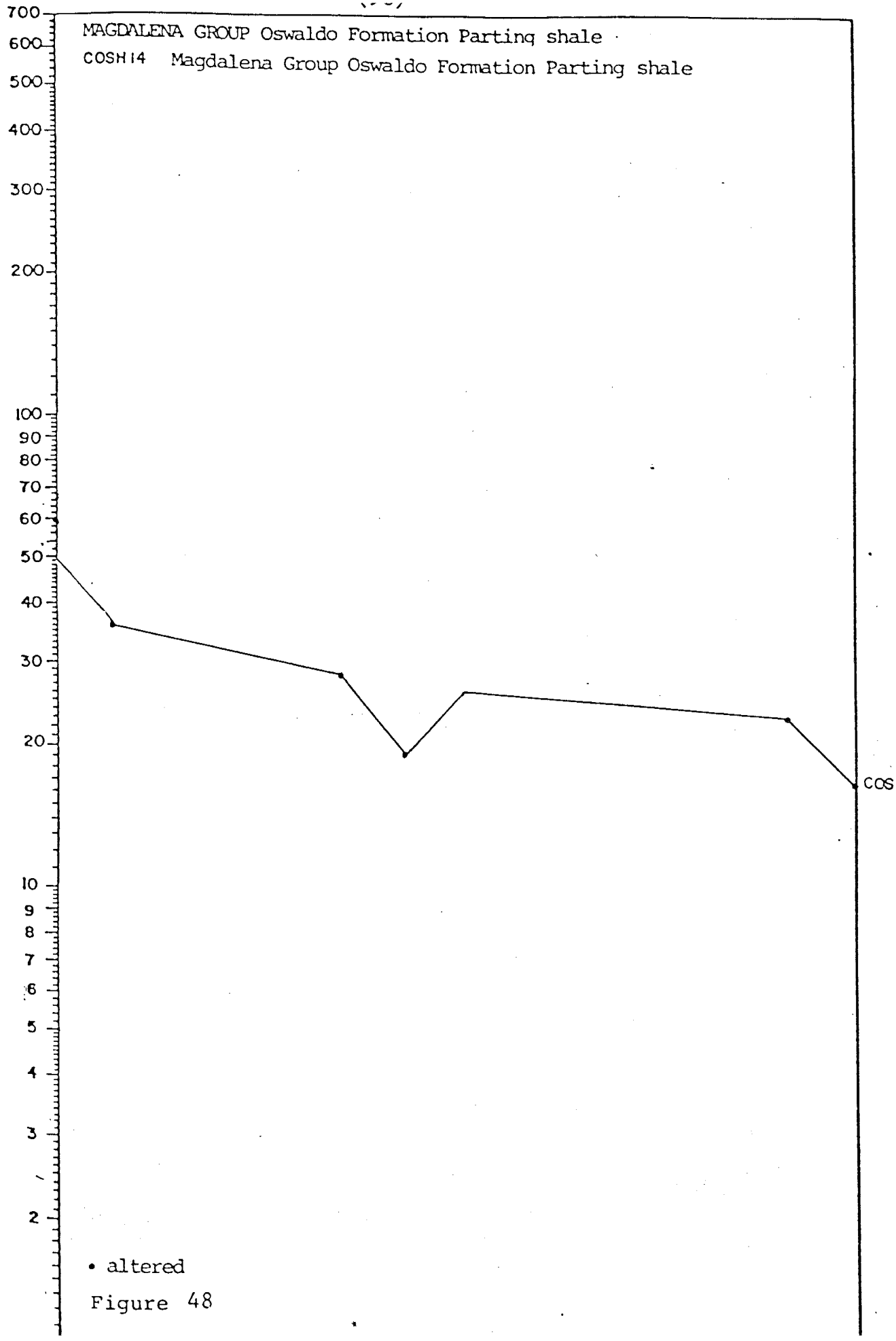

• altered

Figure 48

REE Geochemistry Of The Bliss Quartzite And The Beartooth Quartzite

The Bliss Quartzite shows an increase in absolute REE concentrations, especially in the lREE from the least altered quartzites to the most altered quartzite (Fig. 49). The REE patterns of the least altered quartzites are probably related to the REE concentrated in the hematite, chlorite, carbonate and clays that occur in both samples (Appendix I). Values for Sm and Tb are extrapolated for sample CBQ1 because the values reported are interpreted as being in error (Appendix VII).

One sample of the Beartooth Quartzite from the Continental orebody, was analyzed. The REE pattern is characterized by a low absolute REE concentration and a positive Eu anomaly. In thin section, this sample is 95% quartzite with 5% clays. The low absolute REE concentration probably reflects the relatively pure composition of this sample and suggests that it has not been greatly affected by the Hanover-Fierro intrusive.

REE Geochemistry of the Abo and Colorado Formations

A hornfels sample of the Abo Formation has a REE pattern characterized by lREE enrichment, relatively high absolute concentrations of REE and no Eu anomaly (Fig. 50). A hornfels sample from the Colorado Formation has a lREE enriched pattern and no Eu anomaly. A quartz + chalcopyrite + chalcocite vein from the Colorado Formation and has a lREE enriched pattern with a significant drop in the interval of

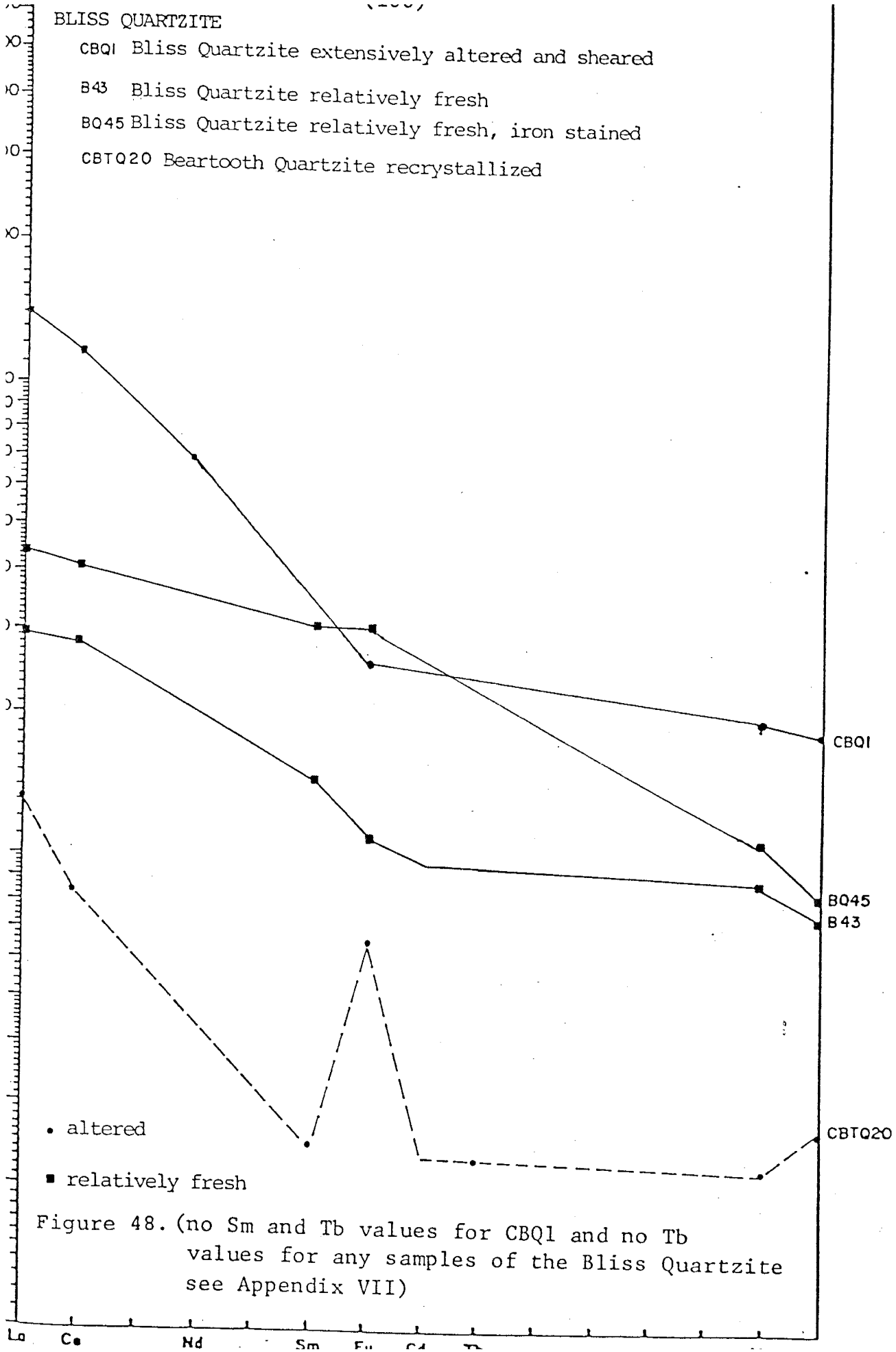

Figure 48. (no Sm and Tb values for CBQ1 and no Tb values for any samples of the Bliss Quartzite see Appendix VII)

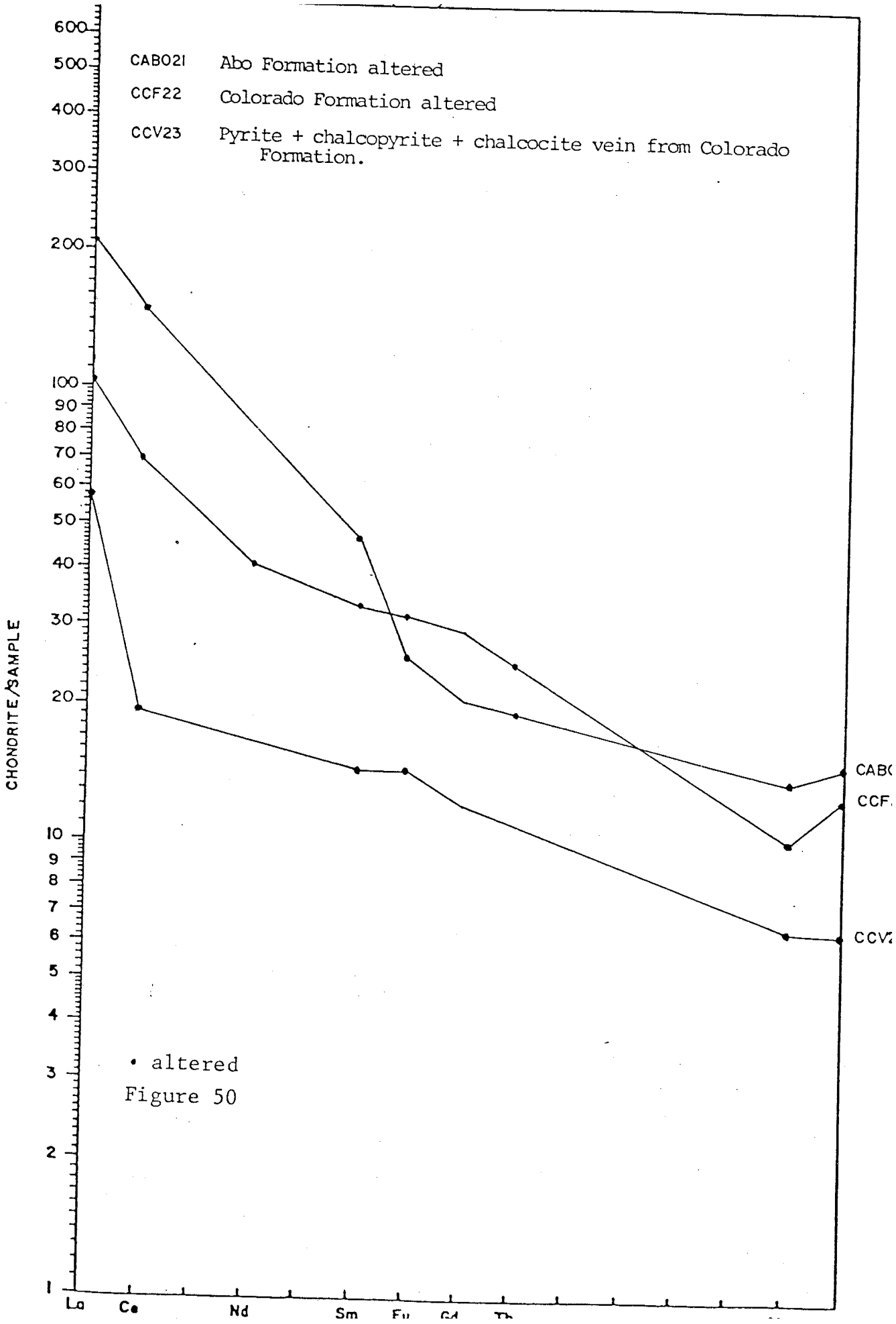
CAB021 Abo Formation altered
CCF22 Colorado Formation altered
CCV23 Pyrite + chalcopyrite + chalcocite vein from Colorado Formation.
CHONDRITE/SAMPLE
600
500
400
300
200
100
90
80
70
60
50
40
30
20
10
9
8
7
6
5
4
3
2
1
La
Ce
Nd
Sm
CAB(
CCF
CCV
• altered

Figure 50

La to Ce and a very small positive Eu anomaly.

REE Geochemistry Of Altered Granodioritic Dikes, Felsite Dike and Diorite Sills

Four intrusive samples have similar REE patterns and are characterized by enrichment in lREE and positive Eu anomalies (Fig. 51) despite differences in their mineralogies (Appendix I). Two granodiorite dikes have been altered to predominantly garnet. The other two samples are a propyllitically altered felsite dike and a propyllitically altered diorite sill. The REE fractionation patterns of all four samples are similar to the REE fractionation patterns of the garnets (Fig. 42).

REE Geochemistry Of The Granodioritic Hanover-Fierro Intrusive

The REE patterns of the unaltered granodiorite and the altered granodiorite of the Hanover-Fierro stock are characterized by lREE enrichment and a negative Eu anomaly (Fig. 52). The altered granodiorite is more depleted in the hREE and has a smaller absolute REE concentration than the unaltered sample. This is the only sample in which the altered rock shows a depletion in absolute REE concentration.

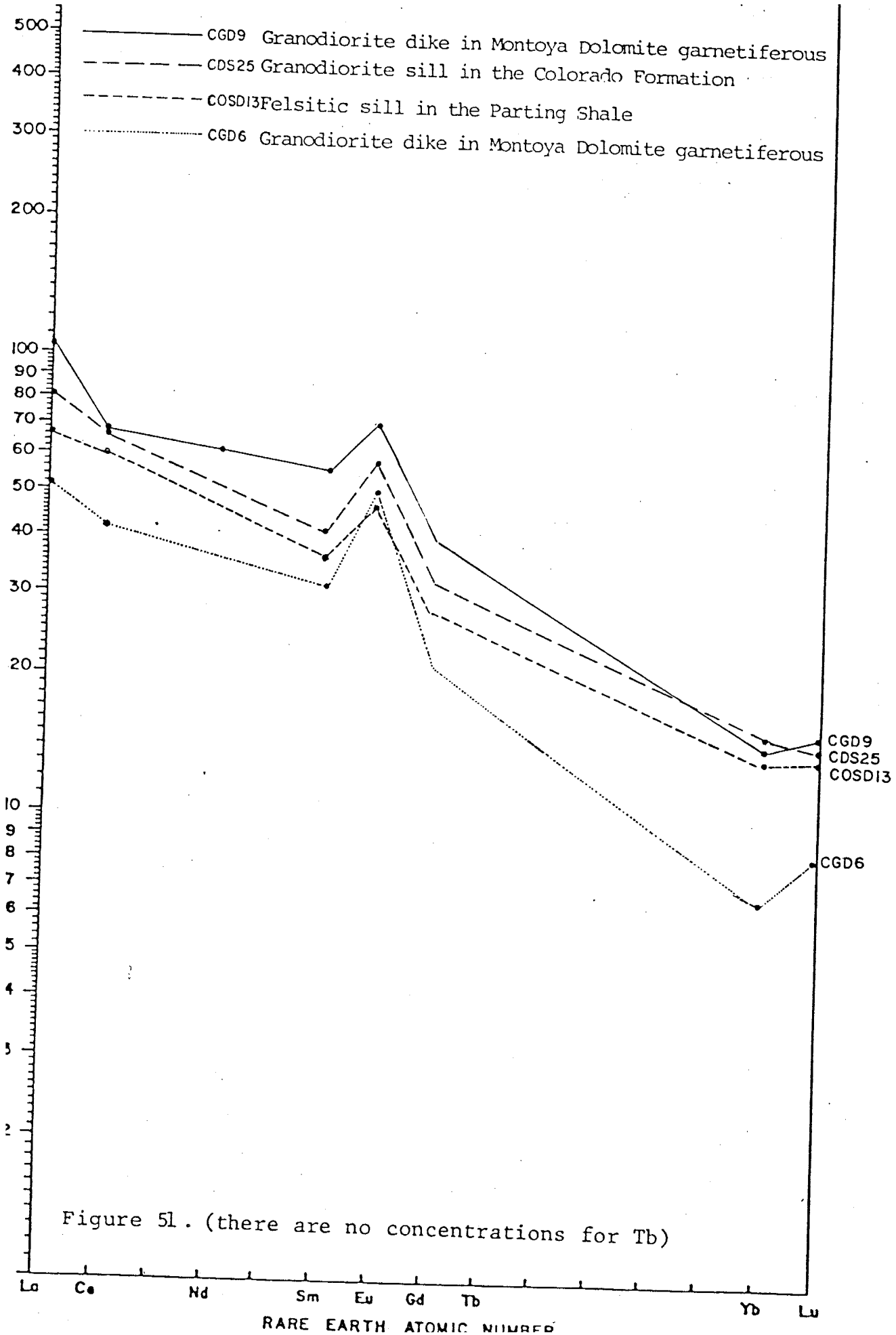

Figure 51. (there are no concentrations for Tb)

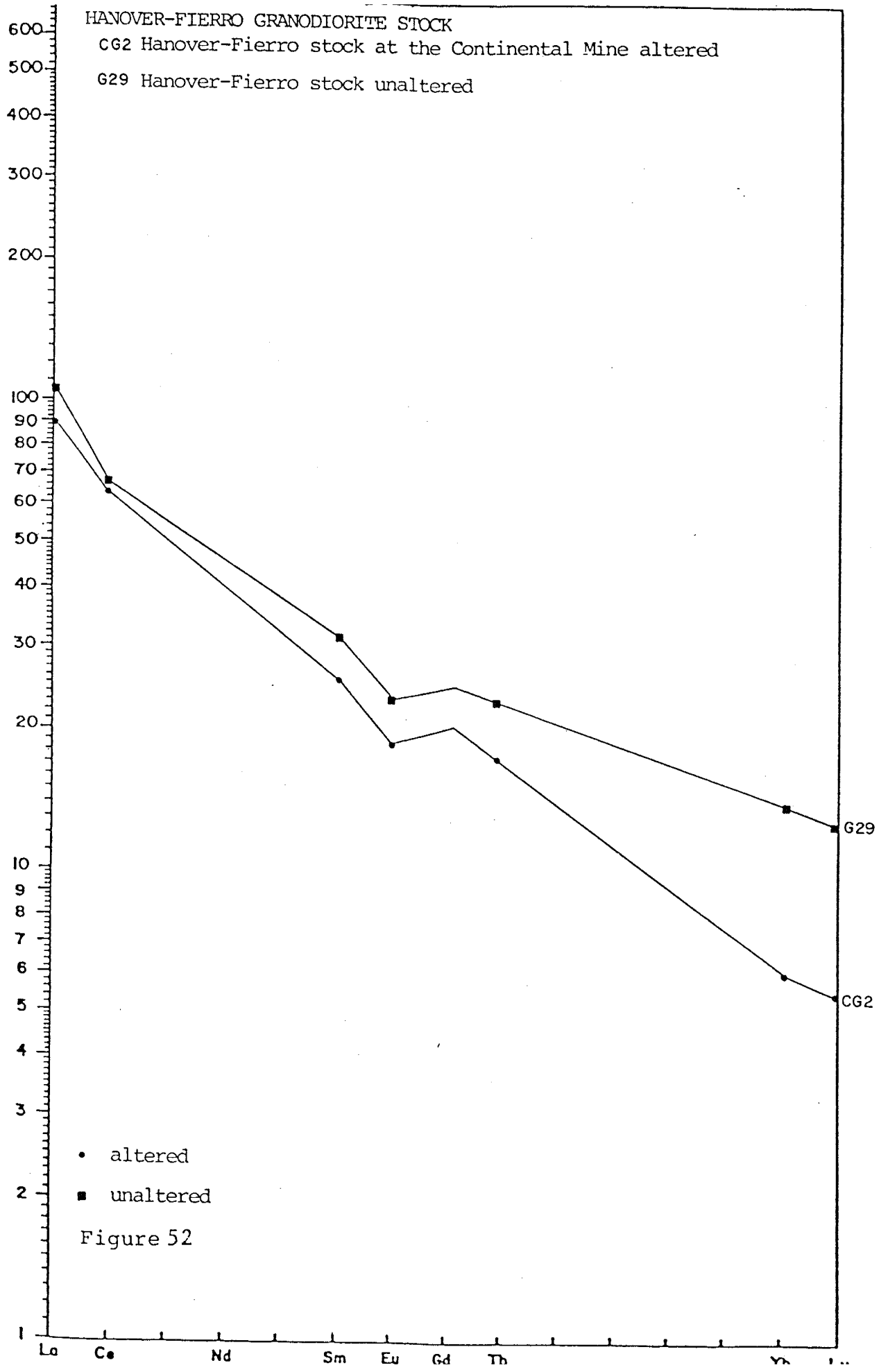
HANOVER-FIERRO GRANODIORITE STOCK
CG2 Hanover-Fierro stock at the Continental Mine altered
G29 Hanover-Fierro stock unaltered
600
500
400
300
200
100
90
80
70
60
50
40
30
20
10
9
8
7
6
5
4
3
2
1
G29
CG2
• altered
■ unaltered
La
Ce
Nd
Sm
Eu
Gd
Tb
Yb

Figure 52

DISCUSSION

Skarn Mineralization at the Continental Mine

Metamorphic reactions have been determined for carbonate and quartz-bearing carbonate rocks (Bowen, 1940; Turner, 1968; Metz and Trommsdorf, 1968). However, the experimental work does not account for high water/ rock ratios or the presence of salts especially NaCl that may be present in the fluids which may affect these reactions. Therefore, metamorphic reactions are not used in this study.

The formation of large quantities of andradite garnet required the addition of Fe and Si. Mg, Al, Cu, Zn, S, F, and H20 were also added to the sedimentary rocks.

The Fe could not have come from the limestone as no significant iron-bearing minerals are present in the unaltered rocks. Formations that could contribute Fe such as Percha Shale are altered to Fe-bearing assemblages such as biotite and clinopyroxene. Forrester (1972) suggests that the Fe originated from the Hanover-Fierro stock because xenoliths in the Hanover-Fierro granodiorite are strongly repaced by magnetite and because the contact of the pluton is marked by fine-grained magnetite in both the granodiorite and country rock. This is not conclusive evidence that the Fe originated from the intrusive because you could also get Fe deposited at the contact of the intrusive by fluids coming inward toward the cooling intrusive.

The addition of silica was necessary to form garnet.

Some of the silica may have been derived from the siliceous horizons in the dolomite, chert nodules in the limestones and from the Bliss and Beartooth Quartzites. However, this can not account for all the silica necessary to form the garnet. The formation of forsterite in the lower dolomitic formations probably did not require the addition of silica. Chert associated with the dolomite could have been the source of the silica. Forrester (1972) suggests that the Si was derived from the Hanover-Fierro intrusive because of the silicification of the granodiorite along major faults such as the Barringer Fault.

A mass-volume calculation indicated that the water evolved from the cooling Hanover-Fierro intrusive is less than the amount necessary to transport the silica required to form the skarn (Appendix VIII). A problem with this calculation is that the volume of the intrusive can only be estimated because its extent at depth is not well known. Schmitt (1939) decided that the Hanover-Fierro pluton was too small to supply the amount of Fe and Si necessary to form the skarn deposit to the south of the intrusive at the Lewabic mine.

Iron and silica can be transported in hydrothermal waters in significant quantities (Barnes, 1979) therefore, evolved waters (connate and/or meteoric) are possible sources of Si and Fe.

It can not be conclusively determined from this study where the Fe and Si originated. A magmatic and/or evolved fluid source(s) agree with the data from this study.

Origin of Skarn and Ore Mineralization in Light of Fluid Inclusion Evidence

Data from fluid inclusions are not adequate to determine the source of the fluids responsible for skarn and ore mineralization at the Continental orebody. However, the data do present constraints for the origin of the fluids.

The differences in fluid composition, homogenization temperatures, and salinities of fluid inclusions in garnet and in the quartz-bearing veins suggests that the fluid inclusions are filled with fluids from differing origins. An alternative possibility is that the same fluid may have been responsible for both skarn formation and later ore mineralization but the fluid changed composition with time.

Possible Origins Of The Fluids Responsible For Garnet Formation

Possible origins for the fluids responsible for earlier garnet formation include: a) heating of saline connate or meteoric water by the intrusive, or b) heating of lower salinity meteoric and/or connate water by the intrusive causing boiling of the fluids which may increase the salinity, or, c) dilution of high-temperature, magmatic water with lower-temperature, evolved waters All three possibilities agree with the fluid inclusion data from this study.

Possible Origins Of Fluids Responsible For Quartz-Bearing Veins

Possible origins of the more saline fluid characteristic of the quartz-bearing veins are a) saline fluids derived from the Hanover-Fierro intrusive, b) by boiling of less saline fluids from the Hanover-Fierro intrusive, or c) by high temperature solutions of evaporites in meteoric water. The high temperature, high salinity fluid inclusions in the later quartz-bearing veins suggests a magmatic origin for the fluids responsible for ore mineralization. The writer has examined magmatic fluid inclusions associated with porphyry copper deposits. These fluid inclusions had homogenization temperatures and salinities similar to the fluid inclusions associated with ore mineralization in this study. The only major difference was that the fluid inclusions associated with porphyry copper deposits commonly had daughter chalcopyrite grains and the fluid inclusions associated with ore mineralization from this study commonly had daughter magnetite grains.

Suggested Origin of the Fluids Responsible for Skarn and Ore Mineralization

The Hanover-Fierro intrusive is considered to be a composite pluton (Spencer and Paige, 1935; Jones and others, 1967 Fig. 53). The southern equigranular facies intruded first and the porphyritic facies that occurs at the Continental ore deposit intruded into the earlier equigranular facies. The earlier intrusive may have been responsible for most of the skarn formation. This earlier intrusive is south and further from the Continental ore deposit than the later intrusive and the fluids would have had time to cool and mixing with meteoric and/or connate waters would have been likely. The second intrusion would provide a mechanism for the later increase in temperature and probably was the source of the ore mineralizing fluids that are characterized by higher temperature and higher salinity fluids. Mixing with meteoric and/or connate waters at a later time may explain some of the lower temperature and lower salinity fluid inclusions in the quartz-bearing veins. Some secondary fractures in garnets are filled with higher temperature inclusions which may be related to filling of fractures during this later higher temperature ore mineralization event.

As mentioned earlier, garnet formation may be related to heated saline or heating of low salinity meteoric and/or connate waters causing boiling of the fluids. Fluid inclusions data is not able to conclusively determine the origin of the fluids responsible for skarn formation.

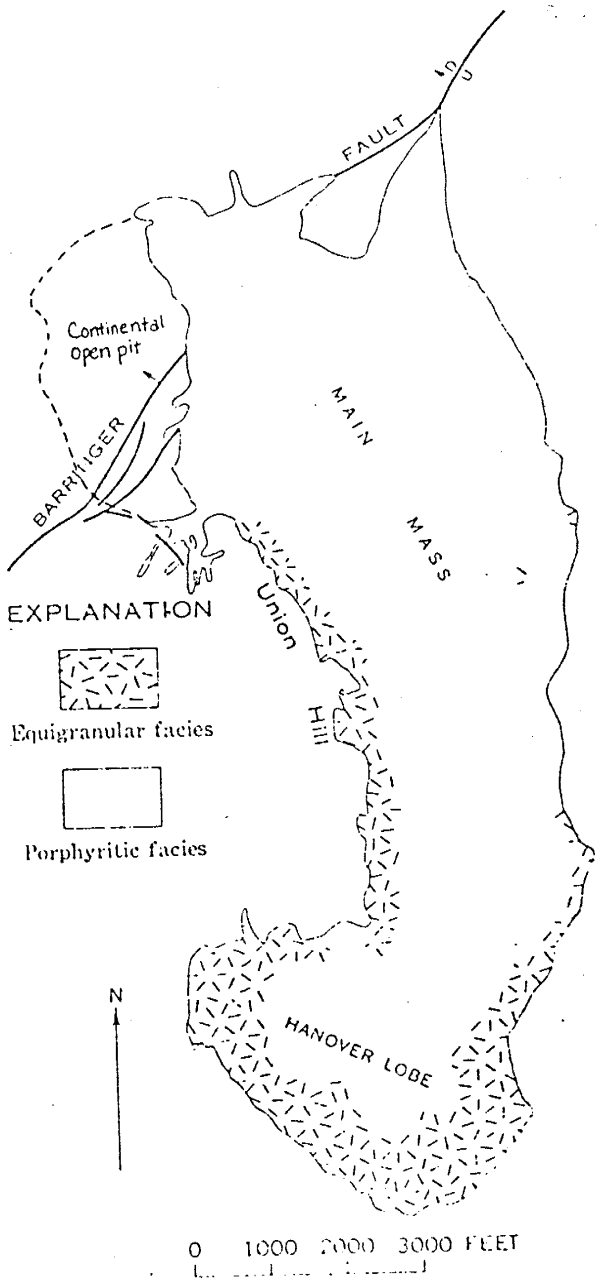

Figure 53. The equigranular and porphyritic facies of granodiorite of the Hanover-Fierro stock (from Jones and others, 1967).

REE GEOCHEMISTRY

REE Geochemisty Of The Limestones and Shaly Limestones

The REE patterns of the limestones and shaly limestones exhibit increases in absolute REE concentrations and show an enrichment in the lREE, from the unaltered samples to the most altered samples. The initially low absolute REE concentrations of the unaltered limestones suggests that the REE were added to the thermally altered and the metasomatically altered rocks.

The enrichment in lREE may a) reflect lREE enrichment of the source, or, b) may be caused by the REE partition coefficients of the skarn minerals that replaced the limestones e.g the minerals tend to partition the lREE relative to the hREE, or, c) be due to lREE fractionation caused by remobilization processes.

The positive Eu anomaly characteristic of all the unaltered limestones from this study is generally not present in pure limestone (Fig. 52) and is not caused by feldspar since it is not observed in thin section. Clay minerals present in the limestone may cause a positive Eu anomaly (Cullers and others; 1975) and since Fe-oxides and clay minerals are observed in thin section, this can explain the positive Eu anomaly.

The thermally altered Hanover limestone is the only limestone sample that has a significant negative Eu anomaly. In thin section, this sample is essentially pure limestone (marble). Limestones analyzed from other studies may have

negative Eu anomalies (Fig. 52).

Most limestones that have been replaced by garnet skarn have similar REE fractionation patterns to the garnets (Fig. 42). This suggests that garnet may be controlling the REE patterns of these rocks. Two garnet skarns (COS15, COS19) have the same lREE enrichment and hREE depletion as the garnet but do not have the positive Eu anomaly. The lack of a positive Eu anomaly may be due to some differences in the mineralogies of these garnet skarns.

The metasomatically altered, shaly limestone (CSY127) from the Syrena Formation has extreme lREE enrichment. This sample has significant apatite and since apatite tends to concentrate the REE, especially the lREE, (Towell and others, 1965; Haskin and Frey, 1966) the apatite in the rock can explain the extreme lREE enrichment.

REE Geochemistry Of The Garnet

The REE fractionation patterns of the garnets are similar to the REE fractionation patterns of the limestones, with the garnets having a greater absolute REE concentration. The REE fractionation pattern of the garnet may be influenced by the REE fractionation pattern of the limestone they replaced. The positive Eu anomaly of all the garnet samples may be due to the positive Eu anomaly of the original carbonate rocks that they replaced. The relationship between the REE patterns of the limestone and garnet depend upon the REE partition coefficients between the aqueous fluid/garnet.

The REE fractionation patterns of the garnets from this study differ markedly from the REE fractionation patterns from other studies (Frey and Haskin, 1964; Schnetzler and Philpolts, 1968, 1970; Schmizu and Kushiro, 1973; Irving and Frey, 1976, 1978; and Mysen, 1978) which indicate that the hREE tend to partition into the garnet relative to the lREE. Garnets analyzed from most other studies are pyrope-almandine in composition and formed under high temperature and pressure conditions. The garnets from this study are grossularite-andradite in composition and formed under low pressure and temperature conditions by the replacement of carbonate rocks. In addition, the hREE enrichment characteristic of garnet from other studies reflects the partition coefficient of the REE between garnet/silicate melt. This is not applicable to this study because partition coefficients between garnet/aqueous fluid are needed to understand the partitioning of the REE into garnet.

REE Geochemistry Of The Dolomites

The Montoya-Fussleman Dolomite does not show any major changes in absolute or relative REE concentrations over the entire range of samples. Unaltered, thermally altered, and metasomatized samples all have similar low absolute REE concentrations and similar REE fractionation patterns.

The unaltered and the thermally altered samples are predominantly carbonate and a low absolute REE concentration is expected. However, the metasomatically altered samples

also have low absolute REE concentrations. Magnesian skarn that replaced dolomite differs mineralogically from the skarn that replaced the limestones. Garnet usually does not occur in magnesian skarn. This study suggests that in the garnet skarn, the garnets and other Ca-bearing minerals tend to concentrate the REE, especially the LREE. The lack of Ca-bearing minerals in the magnesian skarn may explain the lack of increase in the REE in the metasomatically altered samples.

Skarn minerals that replaced the dolomites may have small partition coefficients for the REE and therefore not accept the REE. Three of the metasomatically altered dolomites are forsterite-marble skarns. Carbonate as determined from this study has low absolute REE concentrations. Forsterite and magnetite have small partition coefficients (~ 0) for silicate melt/mineral. Similar behavior of the REE between forsterite/aqueous fluid and magnetite/aqueous fluid may occur. If this is true, the magnesian skarn would not accept REE which could result in REE concentrations and patterns similar to the dolomite. A sample of magnesian skarn, has a complex mineral assemblage with actinolite, phlogopite, wollastonite, magnetite and sulfides in addition to forsterite and carbonate. Despite differences in mineralogy, all the samples have similar absolute REE concentrations and REE fractionation patterns. This suggests that the skarn minerals that replaced the dolomites were not REE acceptors. Another possibility is

that the aqueous fluid that interacted with the dolomites had a very low absolute REE concentration and therefore could not donate significant amounts of REE. The problem with this second possiblity is that it suggests that the aqueous fluid that interacted with the dolomites differed in composition from the fluid that interacted with the limestones, shaly limestones and quartzites.

The REE patterns of the El Paso Limestone indicate an increase in the absolute concentration of REE with a lREE enrichment from the unaltered to the metasomatized sample. The metasomatically altered sample was collected in close proximity to the Barringer Fault which served as a major channelway for the mineralizing fluids. The REE concentrations of this sample provides information on the REE composition of the mineralizing fluids that moved along the fault. The increase in absolute REE concentration and the lREE enrichment in the altered sample as compared to the unaltered sample suggests that the fluid was transporting REE and possibly was preferentially enriched in the lREE.

REE Geochemistry Of The Shales

Except for PSA41, the unaltered shales, recrystallized shales, and the hornfels all have similar absolute REE concentrations and similar REE patterns. The similar REE patterns of these samples indicates that metamorphism has little influence on the abundances and fractionation of the REE in the shales. Other studies have similar results (Haskin and others, 1968).

The similarity in REE fractionation patterns between most of these samples may be explained by the lack of introduction of new elements into these rocks during alteration. Most of the hornfels formed by reconstitution of previously existing elements and therefore REE may not have been subtracted or added.

The Augen Member of the Percha Shale is a shale with limestone nodules when unaltered. Samples collected varied in their shale:carbonate ratio. The samples that were mostly shale have a REE pattern similar to NAS and the shales of the Ready Pay Member of the Percha Shale.

The unaltered sample of the Percha Shale (PSA41) is predominately carbonate with some shale. The REE pattern of this sample differs from the REE patterns of the other Augen samples and has a REE fractionation pattern similar to the carbonate rocks.

Garnet is present in the hornfels sample of the Augen Member of the Percha Shale. In thin section, the garnet is replacing areas of limestone which probably represent the limestone nodules in the shale. The presence of garnet seems to be influencing the REE pattern of this rock causing an increase in Eu concentration and deviation from the recrystallized Augen samples.

The Parting Shale hornfels has no LREE enrichment unlike the hornfels samples from the Percha Shale. This is probably related to the different mineralogy of this sample, which is not understood.

From a structural viewpoint, the shale horizons are relatively impermeable as compared to the carbonate rocks and perhaps less interaction with an aqueous fluid occurred and REE were not added or subtracted from the original rocks.

REE Geochemistry Of The Bliss Quartzite And The Beartooth Quartzite

The accessory minerals and clays are probably responsible for the REE patterns of the the Bliss Quartzite. The metasomatically altered, magnetite-rich sample has a higher absolute REE concentration and a greater lREE enrichment than the less altered samples. This suggests that the REE were introduced into the altered Bliss Quartzite.

The low absolute REE concentrations of the Beartooth Quartzite suggests that this formation has not been greatly affected by metasomatism. The positive Eu anomaly could be due to small amounts of clays that are present. Some clays isolated from shales have REE patterns characterized by a positive Eu anomaly (Cullers and others, 1975).

REE Geochemisty Of The Abo And Colorado Formation

A hornfels sample from the Abo Formation has a high absolute REE concentration with an enrichment in the lREE. Unaltered, this sample is a shale and may have had a REE pattern similar to shales from this study and shales from other studies (Fig. 52). The hornfels sample shows an increase in absolute REE concentrations with an enrichment in the lREE. This enrichment may be explained by the

presence of apatite, fluorite, and (zircon?) that occur in the numerous veins that cut the hornfels.

A hornfels sample from the Colorado Formation has a REE pattern characterized by lREE enrichment and no Eu anomaly. Unaltered, this sample is also a shale. The REE pattern of the hornfels sample is similar to shale but differs in having no negative Eu anomaly. The lack of a negative Eu anomaly is probably explainable by the mineralogy of the sample (Appendix 1) which is not clearly understood.

The sulfide vein (CCV23) from the Colorado Formation has a REE pattern characterized by having a significant drop in the interval La-Ce and a small positive Eu anomaly. The REE pattern of this sample is not explainable since there is no information on the partitioning of REE between aqueous fluid/ore mineral.

REE Geochemistry Of The Altered Dikes, Felsite Dike and Diorite Sill

Granodiorite dikes altered to predominantly garnet have REE fractionation patterns that are similar to the REE fractionation patterns of the garnets suggesting that the garnets are the major REE acceptors. A propyllitically-altered diorite sill and felsite dike have REE patterns similar to the garnetiferous dikes despite major differences in mineralogies.

Both the garnetiferous dikes and the propyllitically altered sill and dike have positive Eu anomalies. The garnet present in the two garnetiferous samples is probably

responsible for the positive Eu anomaly. The presence of orthoclase may explain the positive Eu anomaly in the two propyllitically-altered samples. However, unaltered granodiorite has a REE pattern characterized by lREE enrichment and a negative Eu anomaly (Haskin and Pasters, 1969) that is similar to the unaltered granodiorite of the Hanover-Fierro intrusive.

REE Geochemistry Of The Hanover-Fierro Intrusive

The propyllitic-sericitic altered granodiorite and the unaltered granodiorite have similar REE fractionation patterns suggesting that alteration has not caused extensive REE fractionation. However, the decrease in the absolute REE concentrations, especially the hREE from the unaltered to the altered sample suggests that the REE were subtracted from the altered sample. Other studies (Mineyev, 1963; Aleksiyev, 1970; and Bowden and Whitney, 1974) show steep increases in hREE which have been attributed to interactions with hydrothermal fluids either associated with their formation or as a result of later interactions. These results differ from this study.

The Hanover-Fierro intrusive is the only example in this study in which the altered sample shows a decrease in absolute REE concentration relative to the unaltered sample. The altered granodiorite has not been metasomatized in the Continental mine area. This may explain why the granodiorite sample does not show an increase in absolute REE concentrations similar to the metasomatized sedimentary samples.

Possibly, the enrichment in hREE in the unaltered sample may be explained by the presence of accessory zircon which tends to concentrate the hREE and flatten the REE pattern of the granodiorite.

REE GEOCHEMISTRY AT THE CONTINENTAL MINE

REE concentrations of the recrystallized and metasomatically altered sediments show two types of behavior: a) sediments that show no or only a very small change in REE concentrations such as the dolomites and shales, b) sediments that show significant increases in the absolute concentration of REE with an enrichment in the lREE such as the limestones, shaly limestones, and the quartzites (Fig. 54). The changes in the REE concentrations for this second group of sediments can be summarized as: REE concentration of the metasomatically altered samples > REE concentrations of the recrystallized samples > REE concentrations of the unaltered samples.

If the fluid that interacted with the different sediments was of the same composition, then the sediments reacted differently to this fluid. Several possiblities can explain these differences: a) the aqueous fluid did not interact to the same degree with all the sedimentary rocks, (hornfels that replaced shale and magnesian skarn that replaced dolomite did not require the introduction of new elements and may have not reacted to a great extent with any fluid), b) locally, different fluids may have interacted with a particular formation, c) dolomites and shales were not greatly affected by metasomatic processes whereas limestones, shaly limestones and quartzites were greatly affected, d) the mineral assemblages that replaced the limestones tended to partition the REE with respect to the

Figure 54. REE concentrations of altered and recrystallized sediments compared to the unaltered sediments. Samples are normalized to the unaltered sedimentary rock. Each graph represents a particular formation and shows the relative change in REE concentrations with increased alteration. The limestones, shaly limestones, and quartzites all show increases in the absolute concentration of REE, especially the LREE. The shales and dolomite show very little changes in concentrations. The composition of the Augen Member of the Percha Shale made it difficult to sample equivalent altered recrystallized and unaltered samples and therefore the graph is difficult to interpret.

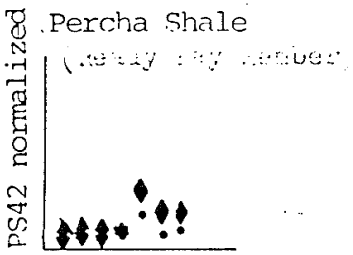

▲ CPS-18 altered/ hornfels
▼ P34 recrystallized/ hornfels/slate
• P36 recrystallized/ hornfels/slate

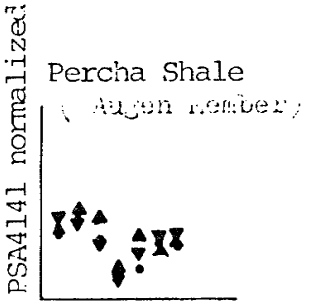

▲ P-AG-16 altered/ hornfels
• PAG30 recrystallized/ shale (limestone)
▼ PS38 recrystallized shale

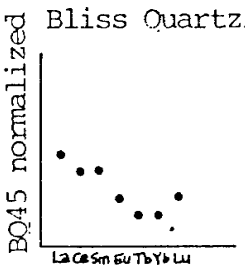

• CBQ1 altered/ magnetite-bearing

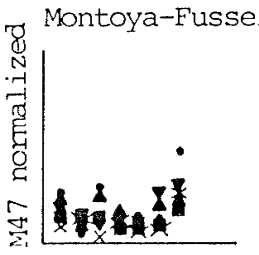

▲ CM4 altered/forsterite-marble skarn
• CMA5 altered/forsterite-marble skarn
■ CD10 altered/forsterite-marble skarn
▼ CDM11 altered/forsterite-marble-phlogopite-wollastonite-magnetit skarn
x FD37 recrystallized/marble-dolomi

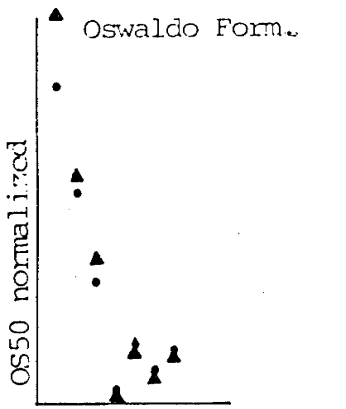

▲ COS15 altered/garnet-magnetite skarn
• COS19 altered/garnet-magnetite skarn

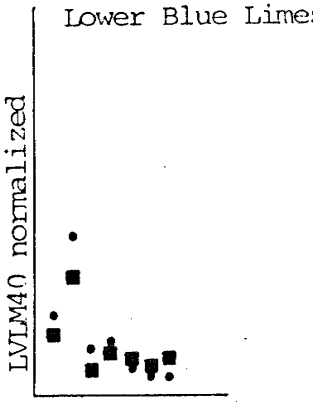

• CLV117 altered/garnet-magnetite skarn
■ CLV217 altered/garnet-magnetite skarn

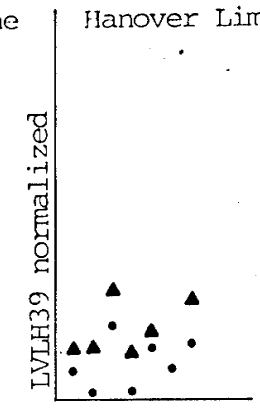

▲ CLH12 altered/magnetite-diopside (garnet)-carbonate skarn.
• H32 recrystallized/marble

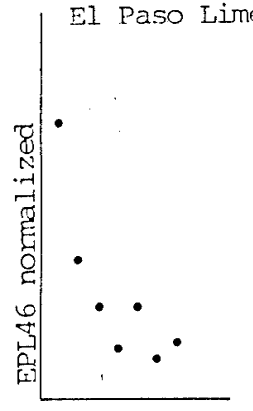

• CEP3 altered/forsterite-diopside-hornfels-magnetite

fluid whereas the minerals that replaced the dolomites and formed in the shales did not partition the REE with respect to the fluid, e) the shales were rather impermeable and therefore had little interaction with the aqueous fluid(s), f) secondary processes may have drastically redistributed the REE.

REE concentrations and fractionation patterns of the altered rocks may be related to several sources and/or processes and include: a) the composition of the fluid e.g. the fluid may have been enriched in the lREE, b) the partition coefficients of the REE between the fluid and the minerals that replaced the sediments e.g. the minerals that replaced the sedimentary rocks tended to partition the lREE, c) may be partly governed by REE concentrations of the original rock, or, d) related to remobilization of the REE at a later time.

Remobilization of the REE in the presence of CO2-rich fluids under crustal conditions has been documented by Wendlandt and Harrison (1979). Hynes (1980) concluded that usually immobile elements (Ti, Y, Zr,) were mobile under high CO2 levels in the fluid phase during metamorphism. The numerous metasomatic reactions that resulted in the formation of the skarn assemblages were primarily decarbonization reactions. The excess CO2 may have greatly remobilized the REE after they were introduced and/or while they were being introduced.

There is much disagreement concerning the differences in mobility of the various REE. Studies by Balashov and Sharas'kin (1966), Kasputin, (1966) and Cullers and Medaris (1970) suggest that the hREE are more mobile than the lREE. Other studies, Wendlandt and Harrison (1979), Martin and others, 1978, and Mitchell and Brunfelt (1975) do not support this. If the hREE form more stable complexes, then possibly they would be carried in the fluid longer and therefore the lREE would more likely precipitate. Also, a fluid that preferentially partioned the hREE could explain the lack of increases in the hREE in the altered sedimentary rocks.

Anomalous fractionations within the REE group such as the occurrence of Ce, Eu or other REE anomalies may be caused by a) the presence or absence of mineral(s) in the altered sediments that preferentially partition a particular REE, or, b) an effect of remobilization processes, or, c) the REE composition of the fluids that were responsible for altering the sediments, or, d) analytical error.

POSSIBLE AND SUGGESTED ORIGINS OF THE REE AT THE CONTINENTAL OREDEPOSIT

The addition of REE to the metasomatized and to a lesser extent the recrystallized limestones, shaly limestones and quartzites occurred in an open system and requires an available source of REE. The enrichment of lREE in the skarn that replaced the limestones and shaly limestones and the lREE enrichment of the altered quartzite suggests that the source may have been enriched in the lREE.

The carbonates have very low REE concentrations which suggests that they are not the source. Possibly, a process which increases the REE concentration in the carbonate rocks by concentrating REE from a large quanitity of carbonate rocks into a smaller area of carbonate rocks can occur. It is not known whether processes such as this are applicable to the REE or how the REE would behave during such a process. In this study, pure limestones such as the Hanover Limestone, has been recrystallized to marble and shows increases in absolute REE concentrations from limestone to marble, suggesting that REE were added and not subtracted from the carbonate rocks. This suggests that the carbonate rocks were not a likely source of the REE.

The shales are a possible source, however, metasomatism has caused no significant changes or only minor increases in the REE concentrations of the shales. This suggests that the shales did not donate REE and if anything, REE were added.

The REE concentrations of an aqueous fluid derived during the late stages of a crystallizing magma are not known. Balashov and others (1969) discussed general trends of increase in REE concentration and relative lREE enrichment with increasing alkalinity of the magma. Nagasawa and Schnetzler (1971) point out that sometimes the final products of fractional crystallization of magmas have lower REE concentrations and less lREE enrichment than intermediate products of magma differentiation. Condie and Lo (1971) found similar trends in a differentiated granitic body in Wyoming. Cullers and others (1976) conclude that the residue of fractional crystallization is more SiO2-rich, has higher REE concentrations and is more depleted in Eu.

The Hanover-Fierro intrusive is the most likely source of the REE. The Hanover-Fierro stock is the only example in which the REE concentrations decreased from the unaltered to the altered sample which may suggest that the stock lost REE. However, little changes in the lREE concentrations are observed.

The REE concentrations and fractionation of the altered sediments may not characterize the REE concentrations and fractionation patterns of the source(s).

Suggested Genetic Model

The skarn deposit at the Continental mine has been genetically related to the intrusion of the Hanover-Fierro stock, primarily because of the spatial zonation of skarn assemblages around the intrusive. However, the introduction of meteoric and/or connate water derived from the sedimentary rocks may have had an important effect on the formation of skarn.

The most probable source of the REE is the Hanover-Fierro stock. The REE may have been introduced into the sediments as an aqueous fluid phase that evolved during the late stages of crystallization of the intrusive. This fluid was probably rich in volatile compounds such as water, halides, carbonates, and alkalies that tend to accumulate as residual fluids as these magmas crystallize. The REE concentration of this residue is unknown and depends upon the composition and origin of the intrusive. REE present in this residue could be transported as F, CO_3, and SO_4 complexes (Beus, 1958; Kosterin, 1959; Bandurkin, 1961; Mineyev, 1963; and Choppin and others, 1963).

It cannot be conclusively determined when the REE were introduced into the skarn. The REE may have been introduced during the replacement of the sedimentary rocks by skarn minerals, or, later during ore mineralization, or, during hydrothermal alteration or during all of these processes. REE are greatly concentrated in the garnets and are only slightly concentrated in the magnetite. However, this may

be more related to the partitioning of the REE into the minerals than to the availability of the REE.

During the late stages of crystallization, Fe and Si derived from the intrusive were introduced into the lower dolomitic formations and massive magnetite and forsterite replaced dolomite. Limestone was replaced by skarn containing garnet, diopside, epidote, wollastonite, and calcite. Garnet formation was accompanied by a fluid with salinities ranging from 4.5 to 19.0 eq. wt.% NaCl and temperatures on the order of 215°C to 435°C and mostly in the range of 245°C to 345°C. A magmatic origin with dilution from meteoric and/or connate water is postulated for the fluids responsible for skarn formation.

Ore mineralization followed skarn formation. Magnetite replaced garnet and/or filled open spaces. Later, pyrite and chalcopyrite cemented brecciated garnet, replaced magnetite and garnet and filled open spaces. During ore mineralization the fluids were boiling with salinities ranging from 2.0 to 47.0 eq. wt.% NaCl and temperatures ranging from 220°C to <600°C. CO_2-rich fluid inclusions associated with later ore mineralization suggest the presence of high CO_2 during ore mineralization. A magmatic origin is postulated for the fluids responsible for ore mineralization. Skarn formation and ore mineralization occurred at pressures on the order of 315 to 320 bars.

The fluids responsible for skarn formation differ in

origin from the fluids responsible for later ore mineralization. A mechanism is required to explain the increase in temperature from earlier skarn formation to later, higher temperature ore mineralization. The most likely explanation is that the fluids responsible for skarn formation were derived from the earlier equigranular portion of the Hanover-Fierro intrusive (Fig. 55). The equigranular facies intruded south of the Continental deposit and the fluids from this intrusive probably would have time to cool and mix with meteoric and/or connate water. The later higher temperature, higher salinity, fluid inclusions associated with ore mineralization originated later from the closer intrusion of the porphyritic facies (Fig. 55). The high temperatures and salinities and the occurrence of magnetite in the fluid inclusions agrees with a suggested magmatic source for the ore mineralizing fluids. Some of the lower temperature and lower salinity fluid inclusions associated with mineralization may have formed very late during ore mineralization and the fluids may have cooled by conduction or by mixing with meteoric or magmatic waters.

Secondary planes that occur in the garnet are evidence of repeated fracturing and brecciation. Some of the secondary planes are filled with high temperature fluid inclusions that may have originated during later higher temperature ore mineralization.

The outward movement of the magmatic fluids containing Fe, Si, Mg, Cu, S, (Zn),(Al) and REE and the inward movement

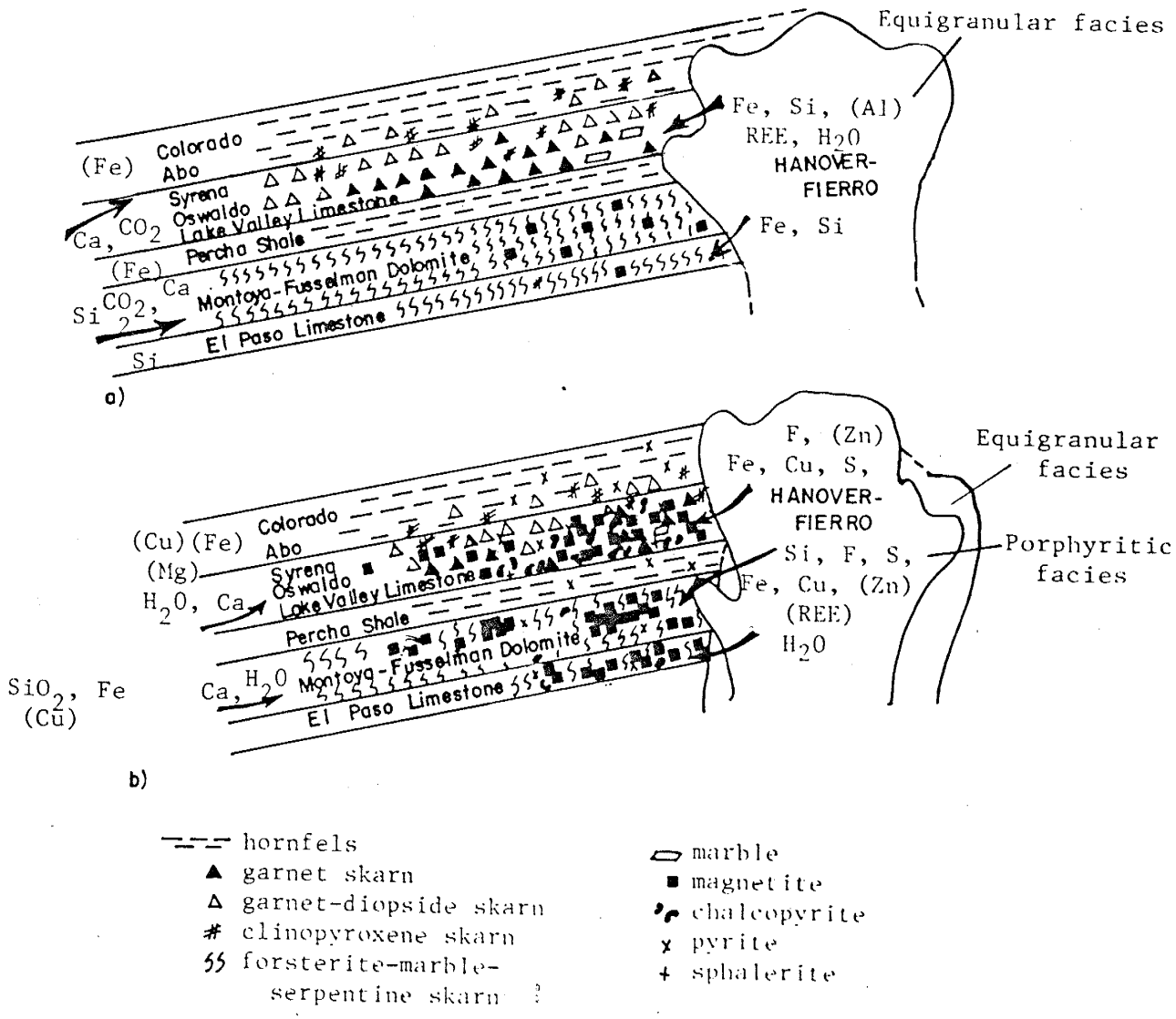

Figure 55. Suggested origin of the fluids responsible for skarn formation a) and ore mineralization b). Elements in parantheses are in lesser quantities. Arrows toward the intrusive indicate the direction of meteoric and/or connate fluids and arrows away from the intrusive indicate the direction of magmatic fluids.

of evolved waters (meteoric and/or connate) containing Ca, (Cu), (Fe), (S), and (REE?) occurred along faults, fractures, bedding planes, and other permeable horizons (Fig. 55). The movement of skarn-forming fluids occurred along the interconnected highly permeable areas. The fact that the shales are relatively impermeable as compared to the limestones suggests that the solutions probably did not affect these more impermeable formations and that these units may have essentially been barriers directing the fluids to more permeable horizons. The lack of change in the REE concentrations of the shales during metasomatism supports this idea. The permeability in the skarn was probably produced by faulting, fracturing and by chemical processes such as decarbonization reactions. The CO_2 produced by decarbonization reactions during skarn formation may have greatly affected the REE concentrations of the mineral assemblages that replaced the sediments and/or altered the REE concentrations at a later time. With cooling of the intrusive, meteoric and or connate water may have become a more important source. Meteoric and/or connate fluids may have changed the REE pattern of the mineral assemblages that replaced the sediments by remobilizing the REE.

Summary and Conclusions

Metasomatism has affected the different sedimentary ormations differently. Dolomites are replaced by magnesian karn comprised of forsterite, serpentine, magnetite and esser amounts of phlogopite and tremolite. Shales are eplaced by hornfels comprised of quartz, feldspar, biotite, nd clinopyroxene. Shaly limestones have been replaced by iopside, quartz, feldspar, epidote, and lesser amounts of arnet. Limestones are replaced by garnet skarn and garnet-linopyroxene skarn.

Ore mineralization follow skarn formation and includes leposition of magnetite followed by deposition of pyrite, halcopyrite and lesser amounts of sphalerite, bornite, halcocite and pyrrhotite. Massive magnetite occurs in orsterite-serpentine skarn and in garnet skarn. In garnet karn, magnetite replaces garnet and/or fills open spaces. ulfides cement brecciated garnet, replace magnetite and arnet, and fill open spaces.

Fluid inclusion studies from garnets indicate skarn ormation mostly in the range of 245°C to 345°C but extending from 215°C to 435°C by fluids with 4.5 to 19.0 eq. t.% NaCl. An origin by mixing of magmatic and meteoric or onnate waters is suggested for these fluids.

Later quartz-bearing veins associated with ore ineralization indicate deposition at 200°C to >600°C by luids with 2.0 to 47.0 eq. wt.% NaCl. The presence of both iquid-rich and vapor-rich fluid inclusions suggest that

these fluids were boiling. Pressure is estimated to be on the order of 315 to 325 bars. A magmatic source is postulated for these fluids with possible late contributions from a meteoric or connate source.

Primary fluid inclusions in garnets and from later quartz-bearing veins are filled with fluids that differ in composition, temperature, and salinity. This suggests that different fluids were responsible for earlier skarn formation and later ore mineralization.

REE were added to the recrystallized and metasomatically altered limestones, limy shales, and quartzites. The REE concentrations of the unaltered, recrystallized, and metasomatically altered dolomites and shales are all similar suggesting that REE were not added. The shales are relatively impermeable and mineralogical evidence and REE analyses indicate that these formations were not greatly affected by metasomatism. Therefore the REE concentrations of the shales were not altered significantly. The magnesian skarn that replaced the dolomites is characterized by minerals that have a small partition coefficient such as magnetite, forsterite, and carbonate. This may explain the low and similar REE concentrations of the unaltered, the recrystallized, and the metasomatically altered dolomites.

The carbonate sediments have absolute REE concentrations that are very low and suggests that they are not the source of the REE. The shales have sufficient REE concentrations but metasomatism has not greatly affected the

REE concentrations of these rocks suggesting that they are not the source. The most likely source of the REE is a late stage fluid derived from the Hanover-Fierro intrusive. The REE concentrations and fractionation patterns of the altered sediments may reflect the REE composition of the fluid derived from the intrusive. However, the REE concentrations of the altered sediments probably also were governed by a) the original composition of the sedimentary rocks, b) the mineral assemblages that replaced the sediments and their partion coefficients for the REE, and, c) by the effects of CO2 and later processes that probably remobilized the REE.

REE are not very effective for determining the source of the mineralizing fluid(s) in this study. The metasomatically altered sediments have a complex origin making it difficult to interpret their REE patterns. The lack of data on the partion coefficients between aqueous fluid/mineral does not allow any modeling studies. Remobilization of the REE probably occurred making it even more difficult to interpret the REE patterns of the altered sediments. However, the REE can place certain constraints on possible sources of the mineralizing fluids. This study shows that REE can be mobile under conditions of metasomatism and to a lesser extent recrystallization. The effects of recrystallization and metasomatism on the REE concentrations of carbonates, shales, and quartzites has been monitored.

REFERENCES

Ahmad,, S.N., and Rose, A.W., (1980) Fluid Inclusions in Porphyry and Skarn Ore at Santa Rita, New Mexico; Econ. Geol. v. 75, pp. 229-250.

Aleksandrov, W.M., Vernadskiy, V.I., (1975) The Geochemistry of Formation of Skarns and Ores in the Crushed Zones of Carbonate Rocks; Geochemistry International, no. 9, pp. 2-18.

Aleksiyev, E. I., (1970) Genetic Significance of the Rare-Earth Elements of Northern Nigeria and the Cameroons; Geochm. Int. 7, 127-132.

Ballmer, G.J., (1949) Geology of the Santa Rita Area: West Texas Geological Society Guidebook Field Trip 3, p.26.

------ (1953) Geology of the Santa Rita Area: New Mexico Geological Socity Guidebook, Fourth Field Conference.

Balashov, Yu. A., Kekilya, M. A., and Nadareyshvili, D.G., (1969) Effect of Alkali Content on Fractionation of the Rare Earths in Rocks of Gabbroid Intrusive, Geochem. Int, no. 6, pp. 476-486.

Balashov, Yu. A., Frenkel, M. Ya., and Yaroschevskiy, A.A. (1970) Effect of the crystallization factor on fractionation of the Rare Earth Elements during Crystallization differentiation of silicates; Geochemistry International, no. 7, pp. 611-614.

Bandurkin, G. A., (1961) Behavior of the Rare Earth in Fluorine-Bearing Media; Geochemistry International, no. 2, pp. 159-167.

Barnes, H.L. and Czamanske, G.K., (1967) Solubilities and transport of ore minerals; in Geochemistry of Hydrothermal Ore Deposits; Barnes, H.L., ed. New York, Holt, Rinehard, and Winston, Inc., pps. 334-381.

Beus, A.A., (1958) The Role of Complexes in Transfers and Accumulations of Rare Elements in Endogenic Solutions; Geochemistry International, no. 4, pp. 388-397.

Buseck, P.R., (1966) Contact Metasomatism and Ore Deposition: Concepcion Del Oro, Mexico; Econ. Geol. v. 61, pp. 97-136.

----- (1967) Contact Metasomatism and ore deposition: Tem Puite, Nevada; Econ. Geol., v. 62, pp. 331-353.

Catheles, L.M., (1977) An Analysis of the Cooling of Intrusives by Ground-Water Convection which Includes Boiling; Econ. Geol., v. 72, pp. 804-826.

Choppin, G.R., and Unrein, P.J., (1963) Halide Complexes of the Lanthanide Elements; J. Inorg. Nucl. Chem., v. 25, pp. 387-393.

Collins, P.L.F., (1979) Gas Hydrates in CO2-Bearing Fluid Inclusions and the Use of Freezing Data for Estimation of Salinity; Econ. Geol., v. 74, pp. 1435-1444.

Condie, K.C., and Lo, H.H., (1971) Trace Element Geochemistry of Louis Lake batholith of early PreCambrian age, Wyoming; Geochim. and Cosmochim. Acta 35, pp. 1099-1119.

Cooper, J.R., (1957) Metamorphism and volume loss in carbonate rocks near Johnson Camp, Cochise County, Arizona; Geol. Soc. Amer. Bull. 68, pp. 577-610.

Cullers, R.L., Medaris, L.G., and Haskin L.A., (1973) Experimental studies of the distribution of Rare Earths as trace elements among silicate minerals and liquids and water; Geochimica et Cosmochimica Acta, 37, pp. 1499-1512.

Cullers, R.L., Chaudhuri, S., Arnold, B., Lee, M., and Wolf, C.W., (1975) Rare earth distributions in clay minerals and in the clay-sized fraction of the Lower Permian Havensville and Eskridge shales of Kansas and Oklahoma; Geochimica et Cosmochimica Acta, vol. 39, pp. 1691-1703.

De Groot-Pommart, C., (1975) A study of iron-bearing and associated mineralizations in the skarns of Seriphos (Cyclades Archipelago, Greece); (abst. by J. Touret) in Fluid Inclusion Research, proceeding of COFFI, editor: Edwin Roedder, vol. 8, p. 47.

Erwood, R.J., Kesler, S.E., and Cloke, P.L., (1979) Compositionally Distinct, Saline Hydrothermal Solutions, Naica Mine, Chihuahua, Mexico; Econ. Geol., v. 74, pp. 95-108.

Felsche, J., and Herrmann, A.G., (1970) Yttrium and Lanthanides 39,57-71; in Handbook of Geochemistry 11-5; editor: K.H. Wedepohl, Springer-Verlag, pp. 39,57-71-A-1 to 39,57-71-O-9.

Flower, R.H., (1953) Paleozoic sedimentary rocks of southern New Mexico; Geol. Soc. Guidebook Field Conf., Southwestern New Mexico, pp. 106-121.

Floyd, P.A. and Winchester, J.S., (1975) Magma type and tectonic setting discrimination using immobile elements; Earth Planet Sci. Letters 27 pp. 211-218.

Floyd, P.A. and Winchester, J.S., (1978) Identification and discrimination of altered and metamorphosed volcanic rocks using immobile elements; Chemical Geol, 21, pp. 291-306.

Forrester, J.D., (1972)..... PhD dissertation
Unpub. M.S. thesis, Cornell Univ.

Ganzeyev, A.A., and Sotskov, Yu.P., (1976) Rare Earth Elements in Fluorites of Different Origin; Geochemistry International, no. 3, pp. 51-56.

Grabezhev, A.I. (1977) On conditions of formation of rare-metal and gold ore hydrothermal deposits (abst.) in Fluid Inclusion Research, Proceeding of COFFI, editor: Edwin Roedder, vol. 10, p. 95.

Graf, J.L., (1977) Rare Earth Elements as Hydrothermal Tracers During the Formation of Massive Sulfide Deposits in Volcanic Rocks; Econ. Geol., v. 72, pp. 527-548.

Haas, J.L.Jr., (1971) The Effects of Salinity on the Maximum Thermal Gradient of a Hydrothermal System at Hydrostatic Pressure; Econ. Geol., v.66, pp. 940-946.

Haskin, L.A., Frey, F.A., and Smith, R.H., (1966) Meteoric, solar and terrestrial Rare Earth Element distributions; Physics and Chemistry of the Earth, no. 7, pp. 167-221.

Haskin, L.A., and Gehl,M.A., (1962) Rare-Earth distribution in sediments; Jour. Geophys. Res. 67, pp. 2537-2541.

Haskin, L.A., and Paster, T.P., (1979) Geochemistry and Mineralogy of the Rare Earths; in Handbook on the Physics and Chemistry of the Rare Earths, editors: K.A. Gschneider, Jr., and L. Eyring, North-Holland Pub. Co., pp. 1-80.

Helgeson, H. C. (1970a) A chemical and thermodynamic model of ore deposition in hydrothermal systems; Min. Soc. Amer. Spec. Papers, pp. 155-186.

Henley, R.W., (1973) Some Fluid dynamics and ore genesis; Trans. Instn Min. Metall., B1-B7.

Hernon, R.M., (1949) Geology and ore deposits of Silver City region, New Mexico; West Texas Geol. Soc. Guidebook, Field trip 3.

Hernon, R.M., Jones, W.R., and Moore, S.L., (1953) Some geological features of the Santa Rita Quadrange, New Mexico Geol. Soc. Guidebook, Fourth Field Conf., Southwestern New Mexico, pp.117-130.

Hernon, R.M., and Jones, W.R., (1967) Ore Deposits in the Central Mining District, Grant County, New Mexico, in Ore Deposits of the United States, Gratton Sales vol. 2, editor: John Ridge, AIME, oo. 1211-1237.

Huang, C.-I, Rose, A.W., and Deines, P., (1975) Isotopic and petrologic studies of contact metasomatic ores at Ely, Nevada; (abst.) in Fluid Inclusion Research, proceedings of COFFI, editor: Edwin Roedder, vol. 8, p.75.

Hynes, A., (1980) Carbonization and Mobility of Ti, Y, and Zr in Ascot Formation Metabasalts, SE Quebec; Contrib. Mineral Petrol. 75, pp. 79-87.

Jones, W.R., (1956) The Central Mining District, Grant County, New Mexico; U.S. Geol. Survey Open File Report.

Jones, W.R., Hernon, R.M., and Pratt, W.P., (1961) Geologic events culminating in primary metallization in the Central Mining district, Grant County, New Mexico, in short papers in the geologic and hydrologic sciences; U.S. Geol. Survey Prof. Paper 424-C, pp. C11-C16.

Jones, W.R., Hernon, R.M., and Moore, S.L., (1967) General Geology of Santa Rita quadrange, Grant County, New Mexico; U.S. Geol. Survey Prof. Paper 555, 144p.

Keevil, N.B., (1942) Vapor pressures of aqueous solutions at high temperatures; Amer. Chem. Soc. Jour., v. 64, p.841-850.

Kesler, S.E., (1968) Contact-localized ore formation at the Meme mine, Haiti; Econ. Geology, v. 63, pp.541-552.

Kosterin, A.V., (1959) The Possible Modes of Transport of the Rare Earths by Hydrothermal Solutions; Geochemistry International, no. 4, pp. 381-387.

Kovalenko, A.S., Snamenskaya, V.P., Afonin, V.P., Pavlinskiy, G.V., and Malov, V.M. Makov, (1966) Behavior of Rare-Earths and Yttrium in metasomatically altered alkalic granites of the Ognitsk Complex (East Sayan): Geochemisty International, no. 5, pp. 406-418.

Kniffen, L.M., (1930) Mining and engineering methods and costs of the Hanover-Bessemer Iron and Copper Co., Fierro, New Mexico: U. S. Bur. Mines Inf. Circ. 6361, 20p.

Kwak, T.A.P., and Tan, T.H., (1981) The Geochemistry of Zoning in Skarn Minerals at the King Island (Dolphin) Mine; Econ. Geol. V. 76, pp. 468-497.

Landon, R.E., (1929) Metamorphism and ore deposition in the Santa Rita-Hanover Fierro area, New Mexico-a study of igneous metamorphism: Chicago Univ., Unpub. PhD. thesis.

Lasky, S.G., (1930) Geology and ore deposits of the Bayard area Central Mining district, New Mexico: U. S. Geol. Survey Bull. 870, 144p.

Mitchell, R.H., and Brunfelt, A.O. (1975) Rare earth element geochemistry of the Fen Alkaline Complex, Norway, Contr. Mineral. Petrol. 52, pp. 247-259

Martin, R.F., Whitley, J.E., and Wooley, A.R., (1978) An Investigation of Rare-Earth Mobility: Fenitized Quartzites, Borralan Complex, N.W. Scotland; Contrib. Mineral Petrol. 66, pp. 69-73.

Mineyev, D.A., (1963) Geochemical Differention of the Rare Earths: Geochemistry International, no. 12, pp. 1129-1149.

Mineyev, D.A., Makarochkin, B.A., and Shabin, A.G., (1962) On the behavior of Lanthanides during alteration of Rare Earth Minerals: Geochemistry International, no. 7, pp. 684-693.

Moller, P., Morteani, G., Hoefs, J., and Parekh, P.P, (1979) The Origins of the Ore-Bearing Solutions in the Pb-Zn Veins of the Western Harz, Germany, as deduced from Rare-Earth Element and Isotope Distributions in Calcites; Chemical Geology, 26, pp. 197-215.

Moller, P., Dulski, P., Schley, F., Luck, J., and Szacki, W., (1981) A New Way of Interpreting Trace Element Concentrations with respect to Modes of Mineral Formation; Jour. of Geochemical Exploration, 15, pp. 271-284.

Ohmoto, H., Rye. R.O., and Holland,, H.D., (1968) Lead-zinc Ore Deposition in the Bluebell Mine, British Columbia, Canada, in Fluid Inclusion Research, proceeding of COFFI, editor: Edwin Roedder, vol. 1, p.7.

Paige, S., (1909) The Hanover iron-ore deposits, New Mexico: U.S. Geol. Survey Bull. 380-E, pp. 199-214.

Pearce, J.A., and Cann, (1973) Tectonic setting of basic volcanic rocks determined using trace element analyses; Earth Planet Sci Letter 19, pp. 290-300.

Pearce, J.A., and Norry, M.J., (1979) Petrogenetic implications of Ti, Sr, Y, and Nb variations in volcanic rocks; Contrib. Mineral Petrol. 69, pp. 33-47.

Perstev, N.N., (1973) Skarns as magmatic and postmagmatic formations; Internat. Geology Rev., v. 16, no. 5, pp. 572-582.

Potter II, R.W., Clynne, M.A., and Brown, D.L., (1978) Freezing point depression of aqueous sodium chloride solutions; Econ. Geol., v. 73, no. 2, pp. 284-285.

Roedder, E.W., (1971) Fluid Inclusion Studies on Porphyry-Type Ore Deposits at Bingham, Utah, Butte, Montana, and Climax, Colorado; Econ. Geol., V. 66, pp. 98-120.

----- (1971) Fluid-inclusion Evidence on the Enviroment of Formation of Mineral Deposits of the Southern Appalachian Valley; Econ. Geol., v.66, pp.777-791.

----- (1972) Composition of fluid inclusions: Geological Survey Prof. Paper 440JJ

-----(1977) Fluid Inclusions as Tools in Mineral Exploration; Econ. Geol., v. 72, pp. 503-525.

Ronov, A.B., Balashov, Yu.A., Girin, Yu.P., Bratishko, R.Kh., and Kazakov, G.A., (1972) Trends in Rare-Earth Distribution in the Sedimentary Shell and in the Earth's Crust; Geochemistry International, no. 12, pp. 987-1016.

Ronov, A.B., Balashov, Yu.A., Girin, Yu.P., Bratishko, R.Kh., and Kazakov, G.A., (1974) Regularities of rare-earth element distributions in the sedimentary shell in the crust of the earth; Sedimentology 21, pp. 171-193.

Schmitt, H.A. (1933b) The Central Mining District, New Mexico: Amer. Inst. Mining Metall. Engineers Contr., no. 39, 22p; 1935b, Trans., v. 115, p.187-208.

----- (1939) The Pewabic Mine, New Mexico: Geol. Soc. Amer. Bull., v.50, no.5, pp. 777-818.

----- (1948) The contact pyrometasomatic aureoles: Amer. Inst. Mining Metall. Engineers Tech. Pub. 2357, v. 12, no. 3, 9 p.

Schimuzu, N. and Kushiro, I., (1975) The partioning of rare earth elements between garnet and liquid at high pressures: Preliminary experiments: Geophysical Research Letters, 2, pp. 413-416.

Shoji, T., (1975) Role of temperature and CO2 pressure in the formation of skarn and its bearing on mineralization: Econ. Geol., v.70, pp.739-749.

Sigurdson, D.R., and Lawrence, E.F., (1976) Mineral paragenesis and fluid inclusion thermometry at four tungsten deposits in the western USA: (abst.) in Fluid Inclusion Research, proceeding from COFFI, editor: Edwin Roedder, vol. 8, p. 169.

Sourijan, S., and Kennedy, G.C., (1962) The System H2O-NaCl at Elevated Temperatures and Pressures; Amer. Jour. of Science, Vol. 260, pp. 115-141.

Spencer, A.C. and Paige, S., (1935) Geology of the Santa Rita Mining District, New Mexico: U.S. Geol. Survey Bull. 859, 78 p.

Stuckless, J.S., and Miesch, A.T., (1981) Petrogenetic Modeling of a Potential Uranium Source Rock, Granite Mountains, Wyoming; Geol. Survey Prof. Paper 1225, 34p.

Tan, T.H., and Kwak, T.A.P., (1979) The measurement of the thermal history around the Grassy Granodiorite, King Island, Tasmania, by use of fluid inclusion data; Jour. Geol., v.87, pp.43-54.

Taylor, H.P., Jr. (1974) The application of oxygen and hydrogen isotope studies to problems of hydrothermal alteration and ore deposition: Econ. Geol., 69, 843-883.

Towell, D.G., R. Volfovsky, and Winchester, J.W. (1965) Rare Earth Element abundances in the standard granite G-1 and standard diabase W-1 Geochim. Cosmochim. Acta 29, pp. 569-572.

Turner, F.J., (1968) Metamorphic Petrology Mineralogical and Field Aspects; McGraw-Hill, 413 p.

Touret, J., (1977) The Significance of Fluid Inclusions in Metamorphic Rocks; in Thermodynamic in Geology, editor; D.G. Fraser, D. Reidel Pub. Co., pp. 203-227.

Wendlandt, F.R., and Harrison, W.J. (1979) Rare Earth Partioning Between Immiscible Carbonate and Silicate Liquids and CO2 Vapor: Results and Implications for the Formation of Light Rare Earth-Enriched Rocks: Contrib. Mineral. Petrol. 69, pp. 409-419.

White, D.E., Hem. J.D., and Waning, G.A., (1974) Diverse origins of hydrothermal ore fluids; Econ. Geol., v. 69, pp. 954-973.

Winchell, H., (1958) The composition and physcial properties of garnet: Amer. Mineralogist, v. 43, p. 595.

Winkler, H.G.F., (1979) Petrogenesis of Metamorphic Rocks Fifth Edition, Springer-Verlag 348 p.

Yousefpour, M.V., (1977) Geology and Contact Pyrometasomatic ore deposits at the Continental mine, Fierro, New Mexico; Unpub. M.S. thesis, Colo. School Mines.

-----(1979) Genesis of skarn polymetallic deposits in the Hanover-Fierro area, New Mexico; Unpub. Phd thesis, Colo. School Mines.

Zharikov, V.A. (1970) Skarns: International Geol. Rev. 12, pp. 541-559; 619-647; 760-775.

Zielinski, R.A. and Frey, F.A., (1974) An experimental study of the partioning of rare earth element (Gd) in the system diopside-aqueous vapor; Geochimica et Cosmochimica Acta, vol. 38, pp. 545-565

CBQ1	BLISS QUARTZITE Quartz-epidote-hornblende-actinolite hornfels; locally schistose. Quartz, epidote, poikiolitic hornblende, being replaced by biotite, magnetite, epidote, quartz, and apatite. Magnetite is ubiquitous. Quartz:60% epidote, hornblende, actinolite:30% magnetite:15% other:5% Veins: magnetite+actinolite+quartz+hornblende+biotite+sphene actinolite+hornblende+biotite+magnetite
CG2	HANOVER-FIERRO GRANODIORITE Altered granodiorite; phenocrysts: plagioclase, hornblende, minor feldspar and biotite. groundmass: quartz, feldspar, hornblende, plagioclase, Hornblende phenocrysts altering to biotite, magnetite; biotite phenocrysts altering to chlorite, magnetite, sphene; Plagioclase phenocrysts altering to sericite, muscovite, biotite, chlorite. Accessory magnetite and sphene.
CEP3	EL PASO LIMESTONE Forsterite-diopside hornfels predominately massive, granular forsterite that has been replaced by serpentine, humite group minerals and possibly phlogopite:50% Clinopyroxene occurs in isolated patches:15% Tremolite, actinolite, chlorite, biotite, phlogopite:10-15%. Numerous veins, clays and magnetite:10% Magnetite veining and replacing forsterite. Veins: magnetite+biotite+serpentine+clays magnetite+clays+biotite+serpentine
CM4	MONTOYA DOLOMITE Forsterite-marble hornfels marble/brucite marble:95% altering forsterite:5% Predominately marble brucite/marble with isolated occurrences of altering forsterite. Secondary magnetite and serpentine are associated with the forsterite.
CMA5	ALEMAN CHERT-MONTOYA DOLOMITE Alternating layers of marble and altered forsterite grains associated with serpentine. Marble comprises the majority of the slide. Forsterite is altering to large masses of serpentine, clays, humite group minerals?, chlorite and magnetite. Veins: pyrite veins magnetite veins
CMAL5	ALEMAN CHERT-MONTOYA DOLOMITE Banded serpentine associated with altering olivine, coarse and fine-grained calcite, serpentine, serpentine+calcite, and boudin-shaped chalcedony: all occurring in alternating bands. Accessory minerals include apatite, euhedral magnetite, and clays.
CGD6	ALTERED GRANODIORITE DIKE IN THE MONTOYA DOLOMITE Primarily massive, anisotropic garnet, that is irregularly zoned. Garnets are surrounded by carbonate, altered plagioclase, chlorite, clays, quartz(?), granular epidote. Accessory apatite and zircon. Veins: Irregular blebs and veins:calcite+clay+granular epidote.

CC7	CHERT HORIZON ADJACENT TO ALTERED GRANODIORITE DIKE MONTOYA DOLOMITE Predominately chert matrix; epidote and kaolinite form irregular blebs and rings in the chert Veins: Chalcedony+zoned calcite Quartz+calcite veinlets
CBR8	BRECCIA IN MONTOYA DOLOMITE Extremely complex and altered rock with inclusions of chert, granodiorite dike, and altered Montoya Dolomite. Recognizable minerals include: diopside, forsterite, epidote, phlogopite, anisotropic garnet, actinolite, hornblende, iron oxides and clay.
CGD9	ALTERED GRANODIORITE DIKE IN THE MONTOYA DOLOMITE Primarily massive, anistropic, irregularly zoned, fractured garnet, surrounded by a matrix of primarily calcite, and lesser amounts of clay, altered feldspars and quartz. Large plagioclase phenocrysts are being replaced by garnet. Other minerals in the altering groundmass include epidote, muscovite, sphene and iron oxides.
CD10	CUTLER DOLOMITE MONTOYA DOLOMITE Forsterite-marble hornfels; for- brucite/marble :95% altering forsterite 5% Predominately marble or brucite marble with patches of iron oxides and altering forsterite ? The altering patches are comprised of actinolite, chlorite, serpentine(?) clays, biotite, and granular calcite.
CD11	CUTLER DOLOMITE MONTOYA DOLOMITE Forsterite-(diop) hornfels complicated mixture of altering forsterite 5% phlogopite:10% actinolite-tremolite:15% magnetite-pyrite-chalcopyrite:15% carbonate and clays:25% diopside:5% also epidote, chlorite, muscovite, biotite, green spinel, talc. Veins: chlorite+serpentine veins
CLH12	HANOVER LIMESTONE Magnetite skarn; massive magnetite:60% with irregular blebs and stringers of altering diopside, garnet carbonate, euhedral magnetite, quartz and secondary actinolite-tremolite, epidote, chlorite. Pyrite and chlacopyrite:5%. Diopside replacing carbonate(?) Garnet replacing diopside(?) Veins: calcite+quartz+amphibole+epidote+magnetite calcite+epidote+quartz+actinolite+chlorite
COSH13	FELSITE DIKE IN THE OSWALDO FORMATION Altered dike; granular quartz, altered feldspar, altered hornblende assoc with actinolite, apatite, clays and epidote comprise the majority of the slide. In the fine grained groundmass just described, are brown, clay(?) which have replaced large grains, most likely plagioclase phenocrysts remanent of the original igneous rock. Veins: Very large vein of epidote+actinolite+magnetite+coarse-grained quartz+chlorite Granular quartz+actinolite+epidote

COSH14	PARTING SHALE BASE OF THE OSWALDO FORMATION Biotite-epidote hornfels; granular quartz, feldspar:75% epidote, biotite, chlorite, clay and carbonates, and accessory sphene and zircon. Fairly large masses of epidote surround the larger iron oxide grains. Smaller iron oxide grains occur in the groundmass. Veins: Calcite+magnetite+chlorite quartz+calcite+epidote+sericite-muscovite
COSGT15 (COS15)	OSWALDO FORMATION Garnet skarn; anisotropic, zoned, fractured garnets:80% Magnetite is replacing garnets and filling open spaces:15% chalcedony and calcite occur as irregular blebs and fill open spaces:5% Disseminated sulfides:pyrite and chalcopyrite Accessory apatite
COSGT215 (COS15)	OSWALDO FORMATION Altered garnet skarn; massive, highly anisotropic, fractured garnet:85% occurring in a matrix of carbonate:5% and chalcedony filling open spaces:5% Magnetite, pyrite, and chalcopyrite. Garnet is replacing the carbonate. Garnets show isotropic centers, and anisotropic margins. Magnetite replacing garnet and filling open spaces. Sulfides replacing the magnetite. Numerous veins: quartz+calcite calcite+pyrite+chalcopyrite quartz+magnetite+inclusion free garnet calcite+garnet+quartz+magnetite
CPSAG16 (PSAG16)	AUGER MEMBER OF THE PERCHA SHALE Garnet-diopside hornfels; predominately highly anisotropic, zoned garnets that have replaced carbonate and diopside(?) being replaced by carbonate at a later time. Calcite assumes shape of garnet and exhibits characteristic zoning of the remanent garnet therefore garnet, calcite diopside, and minor epidote:75% calcite and quartz fill open spaces:10% Numerous other minerals occur and include:epidote, tremolite(?), wollastonite(?), chlorite, actinolite, and accessory sphene and apatite. Magnetite:7% replaces garnet locally. Veins: Calcite+quartz Calcite+quartz+garnet+chlorite Quartz veinlets Garnet+calcite+apatite Garnet+quartz+magnetite
CLVLB17 (CLVL17)	LOWER BLUE LAKE VALLEY LIMESTONE Garnet skarn; massive, highly anisotropic, highly fractured garnet with abundant inclusions is the predominant mineral and is associated with irregular blebs of carbonate and lesser amounts of quartz. Garnets are replacing carbonate. Some areas of calcite and carbonate may be associated with diopside. Magnetite grains and veinlets are common and replace the garnet. Nontronite(?) and epidote assoc. with garnet. Other minerals present include: chlorite, actinolite, and epidote. Veins: Quartz+inclusion free garnet+magnetite (garnet appears to be floating in the quartz) Quartz veinlets Calcite+inclusion free garnet+magnetite+clays

CLVLB217 (CLV127)	LOWER BLUE LAKE VALLEY LIMESTONE Altered garnet skarn; irregular, highly fractured, granular garnet is the predominate mineral These garnets have less inclusions than the previously described section and may indicate more complete replacement. In some areas garnet appears extremely brecciated and veined and occurs in a groundmass of carbonate and epidote and clay. Garnets are surrounded by irregular blebs and veinlets of predominately calcite and lesser amounts of quartz, clay, and tremolite. Garnet is replacing carbonate and magnetite is replacing and veining garnet. Magnetite and clay veins cut the entire rock. Numerous veins: calcite calcite+quartz calcite+quartz+epidote+magnetite+clay quartz+magnetite calcite+quartz+garnet+magnetite
CPS18	PERCHA SHALE Biotite (chlorite) hornfels; very fine grained hornfels comprised of quartz, feldspar, biotite, chlorite, and actinolite that make up the majority of the groundmass. Other minerals include: iron oxides, dlays, minor plagioclase, and apatite. Numerous veins: calcite+clay predominately quartz+magnetite+biotite+rare plagioclase quartz quartz+coarse-grained biotite quartz+pyrite+magnetite
COS19	OSWALDO FORMATION Garnet skarn; massive,zoned garnets comprise approximately:80% quartz:8% calcite5% magnetite:8% The quartz, calcite, and magnetite commonly form in the open spaces surrounding garnet. Garnets have anisotropic margins with more isotropic centers. Garnets contain abundant inclusions of predominately calcite Magnetite is replacing garnet Sulfides replacing magnetite Other minerals include actinolite, chlorite, epidote, nontronite, and hematite. Veins: calcite quartz
CBTQ20	BEARTOOTH QUARTZITE Orthoquartzite; predominately recrystallized quartz, chacterized by numerous triple point junctions approximately:95% sparsely occurring areas of muscovite-sericite, chlorite-clay. Accessory minerals include zircon which is quite prevalent in one area and rare apatite grains. Quartz grains are commonly surrounded by granular quartz and clays and less commonly muscovite and sericite and chlorite.

CABO21	(Clinopyroxene(?)) hornfels; predominately fine grained quartz. fairly large grains and being associated with actinolite, clays, and carbonate. Epidote and actinolite are possibly after clinopyroxene(?) Other minerals include: zircon, apatite, and fluorite which occurs in veins. Veins: Coarse-grained clinozoisite+chlorite Quartz+minor epidote+fluorite+opaques Epidote+chlorite+opaques+rare orthoclase Calcite+quartz
CCF22	COLORADO FORMATION Biotite hornfels; very fine-grained somewhat indistinguishable groundmass of predominately quartz, and feldspar. Biotite, muscovite, chlorite, sericite also occur in the groundmass in lesser quantities. Original sedimentary layering is still present and is recognizable by differences in the amount of iron oxides, and mafic minerals present in specific layers. Quartz and orthoclase grains are extremely irregular, the orthoclase being replaced by chlorite and sericite and granular quartz(?) and the quartz grains being surrounded by granular quartz, muscovite, sericite and chlorite. Veins: quartz+chlorite+opaques
CAMP24	AMPHIBOLITE DIKE COLORADO FORMATION Extremely altered amphibolite dike; Large, altering phenocrysts of hornblende predominate in a green-yello groundmass of actinolite, chlorite, epidote, clays and other unidentifiable minerals. Veins: chlorite+magnetite+pyrite+chalcopyrite
CDS25	SILLCOLORADO FORMATION Altered granodiorite dike; phenocrysts of extremely altered plagioclase and hornblende and orthoclase(?) Plagioclase phenocrysts altering to chlorite, epidote, and clays. Hornblende phenocrysts altering to chloritized actinolite with numerous inclusions of apatite, magnetite, and sphene. Groundmass is essentially unresolvable with the exception of identifiable plagioclase microlites, other grains are possibly feldspar and quartz. Epidote Veins: quartz+sulfides+magnetite
CDS26	SILLCOLORADO FORMATION Extremely altered granodiorite(?) dike; phenocrysts of altering plagioclase, feldspar, and hornblende. Plagioclase phenocrysts altering to dark brown clay, epidote, and sphene Hornblende phenocrysts altering to chlorite, actinolite, sphene and minor biotite and epidote. A few areas of fairly large fractured quartz grains associated with actinolite needles (relict quartz phenocrysts(?) Groundmass is comprised of orthoclase, quartz,actinolite, clays, sphene and rare plagioclase. Altering phenocrysts resemble groundmass when the alteration becomes extensive.

CSY127	SYRENA FORMATION Diopside-garnet-hornfels; small, irregular, light brown garnets that are in a groundmass of extremely altered diopside grains and wollastonite, quartz, feldspar, carbonates and clay. Garnets are clearly associated with the granular diopside. Large plagioclase grains occur and contain numerous inclusions of diopside and apatite. Irregular garnet is replacing the diopside. Veins: Inclusion free garnet+actinolite needles+minor calcite+clay Chalcedony+diopside+carbonate+inclusion free garnet+opaques Magnetite on margins+diopside+chalcedony
CSY227	SYRENA FORMATION Diopside-garnet hornfels; Large, euhedral diopside grains altering to granular diopside and chloritized actinolite. Light brown irregular blebs of garnet are forming by replacement of diopside. These diopside grains and associated minerals occur is a groundmass of quartz and feldspar. Large grains of plagioclase are dotted with numerous inclusions of diopside associated with garnet and apatite. The large commonly euhedral originally diopside grains and associated altering and replacing minerals are very distinct within the very fine-grained groundmass of feldspars and quartz. Veins: Diopside+plagioclase+quartz+microcline+garnet(?)+sphene+apatite Quartz+(garnet)+orthoclase+secondary serpentine Quartz+garnet Garnet+chlorite+diopside
CSYGTB28 (C28)	SYRENA GARNET BANDS Garnet skarn; massive garnet predominates:85% and is surrounded by irregular blebs of predominately diopside:10%and carbonate:approximately 5%.Diopside is replacing carbonate and garnet is replacing the diopside. Commonly, the garnets and diopside appear brecciated and are surrounded by carbonate. Much of the garnet is isotropic and lacks zoning. Veins: calcite+garnet+diopside quartz+calcite+sulfides
CSYGTB228 (C28)	ALTERED SYRENA GARNET BANDS Altered garnet skarn; massive garnet predominates:80% and is surrounded by irregular masses of diopside, carbonate and quartz. This sample contains less diopside than the previous sample, approximately: 5% and carbonate and minor amphibole 15%. Garnet contains numerous inclusions of carbonate and diopside. Garnet replacing diopside and diopside replacing carbonate. Accessory apatite Veins: Predominately calcite+quartz+minor chlorite Calcite+quartz+garnet+minor chlorite+magnetite-hematite Calcite veinlets

	and lesser amounts of biotite, and orthoclase Hornblende phenocrysts contain inclusions of euhedral sphen, quartz, epidote, orthoclase, chlorite, magnetite, and rare grains of zircon. Biotite phenocrysts associated with sphene orthoclase, and magnetite; quartz and apatite inclusion less commonly. Orthoclase phenocrysts have clay alteration associated with particular growth zones. Groundmass: the groundmass is very fine-grained and is comprised of quartz, orthoclase, hornblende, sphene, magnetite, and minor plagioclase. Porphyritic texture and glomerophyric texture associated with plagioclase phenocrysts.
PAG30	AUGEN MEMBER OF THE PERCHA SHALE Recrystallized carbonate/marble and shale; This rock is fairly complicated and is comprised primarily of carbonate with compositional layering related to the amount of clay, Fe-oxides, and mafic minerals associated with the carbonate. In areas of fine-grained carbonate and clays; there appear to be unidentifiable blebs and nodules of carbonate, Fe-oxides, and unidentifiable birefringent mineral. Other areas are comprised of predominately calcareous shaly material and have irregular blebs and stringers of more carbonate-rich material. Identifiable minerals include granular epidote, chlorite, actinolite, carbonate, Fe oxides tremolite. Veins: Predominately calcite+epidote Calcite+chlorite+epidote
LB31	LOWER BLUE LAKE VALLEY LIMESTONE Marble(?); predominately carbonate and unidentifiable clays that exhibit a wide variety of grain sizes:85-90%. Euhedral to subhedral tremolite occurs sparsely throughout the rock. Large grains of carbonate that are much smaller than the groundmass in which it occurs commonly occurs in areas throughout the rock. Some of these larger carbonate grains are altering around the margins to a fine-grain carbonate more characteristic of the groundmass. Fe-oxides occur spotted throughout the rock. Veins: calcite
H32	HANOVER LIMESTONE LAKE VALLEY LIMESTONE Marble; predominately very coarse grained carbonate grains up to 5-10 mm. in size, that form interlocking euhedral to subhedral grains. Minor Fe-oxides occur; otherwise extremely pure marble.
PS33	PARTING SHALE BASE OF THE OSWALDO FORMATION Chlorite hornfels; Irregular and granular chalcedony, feldspar biotite, chlorite, and Fe-oxides comprise the majority of the slide. All grains are extremely irregular and granular. Quartz grains are always anhedral and show a wide variation in size Accessory apatite. Veins: Two parallel veins of sulfides+quartz+chlorite+abundant apatite needles+biotite+chalcedony+ Fe-oxides and hematite.

P34	Biotite hornfel; Extremely fine-grained quartz/chalcedony, carbonate, aligned biotite altering to chlorite, Fe-oxides, actinolite and clays comprise the majority of the rock. Orientated grains reflect the orignal bedding. Disseminated sulfides. Veins: Wollastonite+quartz+chlorite+diopside Calcite+wollastonite+quartz Quartz+chlorite Quartz Wollastonite+minor chlorite
C35	COLORADO FORMATION Biotite hornfels; extremely fine-grained comprised essentially of quartz, feldspar, biotite chlorite, and Fe-oxides. May be rare grains of birefringent diopside(?) Original sedimentary layering is preserved and individual layers are distinguishable by the presence of aligned micas and concentrations of Fe-oxides. Accessory apatite. Vein: Chlorite+sulfides
PS36	PERCHA SHALE slate; Primarily very fine-grained carbonate and chert groundmass with circular nodules or blebs that contain cherty and indistinguishable grains. Most all grains are not distinguishable due to the very small size.
PD37	FUSSELMAN DOLOMITE Marble; Fine-grained, anhedral, turbid marble :95% Small, isolated occurrences of chert. Fibrousy clay grains(?) Rare tremolite grains. Veins: Euhedral dolomite+Fe-oxides Calcite+Fe-oxides
PSA38 (PS38)	AUGEN MEMBER OF THE PERCHA SHALE Extremely fine-grained carbonate, quartz, aligned micas and amphibole, altered diopside(?), Fe oxides and clay. Larger grains of Diopside are close to veins. In areas of complex veining the garnet and diopside spread outward from teh veins and begin to form irregular blebs and areas in the rock. Numerous veinlets: Wollastonite+garnet(margin)+carbonate(interior) Chlorite+minor quartz Extensive, very irregular veins and veinlets of garnet and lesser amounts of diopside(interior)+carbonate(interior) Pyrite+garnet+quartz+clays Vesuvianite grains(?)+calcite Wollastonite+garnet+quartz Flourite+minor carbonate and vesuvianite(?) Irregular predominately garnet veins with minor diopside in the center

	stems. The carbonate grains are dusted with very small inclusions. Fe-oxides occur between carbonate grains. Carbonate grains comprise approximately:98% and are extremely variable in size.
LVLM40	LOWER BLUE LAKE VALLEY LIMESTONE Fossiliferous limestone; Medium-coarse grained carbonate grains with NUMEROUS fossil fragments. Original layering is preserved showing areas of more micritic carbonate and areas of more coarser-grained sparry calcite. Fossils include: Pelecypods, numerous kinds of foraminifera, brachiopods, spicules and many other unidentifiable fossil fragments.
PSA41	AUGEN OF THE PERCHA SHALE Fossiliferous limestone; Entire groundmass is comprised of micritic or fine-grained turbid carbonate with rare patches of cherty quartz and a few rare patches of sparry calcite. Fe-oxides occur. Fossils are common but not as abundant as in the previous sample. Fossils include: crinoid stems, echinoderm fragments, foraminifera, and gastropods.
PS42	PERCHA SHALE Shale; Rock is comprised of extremely fine-grained quartz, feldspar, and dark brown biotite. Fe-oxides are locally concentrated. Some original sedimentary structures are present marked by the accumulation of biotite and Fe-oxides. Veins: quartz+biotite+magnetite+Fe-staining
B43	BLISS QUARTZITE Hematitic quartzite; predominately quartz, chlorite, and Fe-oxides in approximately equal amounts comprise the majority of the rock. Minor muscovite and biotite(?) Irregular blebs of carbonate occur. Quartz grains have indistinguishable boundaries and resemble chert. Fe-oxides form spider web matrix and veins the entire rocks and surrounds the original quartz grains.
BQ45	BLISS QUARTZITE Quartzite; anhedral quartz grains comprise the majority of the rock with anhedral carbonate grains filling open spaces between the quartz. Also, rare fragments of chert. Calcite often forms locally large areas which entirely surround a group of quartz grains. Fe-oxides surround open spaces between all the quartz grains. Unidentifiable, fibrousy yellow-green in plane polarized light and Black-grey X-nicols perhaps some clay(?)
EPL46	EL PASO LIMESTONE Dolomite/calcite; Carbonate, euhedral, zoned dolomite and quartz and Fe-oxides comprise the majority of the rock. Zoned, euhedral, dolomite has Fe-oxide alteration occurring along specific growth zones. Areas of large, anhedral carbonate grains occur. Other areas are comprised of a more micritic carbonate and Fe-oxides and quartz.

M47	UPHAM MEMBER MONTOYA DOLOMITE Dolomite; Essentially anhedral to subhedral, very turbid dolomite of medium grain size. Some dolomite shows rhombohedral cleavage and form. Minor bleb of quartz.
GT1-1	MASSIVE GARNETS OSWALDO FORMATION Very large garnets, highly fractured, commonly zoned. Garnets contain inclusion primarily of carbonate and diopside grains. Carbonate, diopside, clay in fractures that cut brecciated garnet. Magnetite and sulfides fill open spaces between garnet grains. Other minerals include: chlorite, actinolite and epidote.
GT-2	MASSIVE GARNET Massive garnets, extremely brecciated with fractures being filled with carbonate, clay, chlorite and secondary actinolite. Pyrite veinlets cut between garnets filling open spaces.
GT-3	MASSIVE GARNET Extremely zoned, extremely brecciated garnets; fractures filled with carbonate, diopside and clays. Calcite+pyrite veinlets cut the garnet. The veins that cut the garnet appear to be altering the garnet. Diopside comprises a large proportion of the slide and are being extensively altered to clay. Epidote occurs and may be related to the alteration of garnet.
GT-4	MASSIVE GARNET Zoned garnets, with numerous inclusions of altering diopside and lesser inclusion of carbonate. Garnet is replacing diopside. Diopside inclusions in the garnet are altered to chlorite. Garnets in groundmass of diopside, carbonate, quartz, and chalcedony. The quartz, carbonate, and diopside occur in relatively equal amounts and some of this groundmass entirely surrounds garnet grains.

APPENDIX II

Samples For Fluid Inclusion Study

Samples used for fluid inclusion study came from the Continental open pit and the #3 shaft. Samples in which the inclusions were too small or optically too poor for effective study are not included in this list. Samples GT1-1 and GT-4 were collected from underground workings by staff geologists. Stratigraphic formations, locations, and mine coordinates were obtained from mine geologists.

GT-1 Garnet-magnetite-pyrite-chalcopyrite skarn. Both red and green garnets occur and commonly garnets exhibit a green interior which is highly fractured and a red-orange exterior which is extremely zoned. Euhedral-subhedral garnets range in size form 2-6 mm. Predominately magnetite and to a lesser extent pyrite and chalcopyrite replace garnet and fill interstices. Secondary calcite also fills open spaces between garnets.

GT1-1 Garnet-magnetite-pyrite-chalcopyrite skarn. Both red and green garnets occur together in approximately equal amounts. The garnets are extremely zoned on the outer edges but are massive towards the interior where they are extremely fractured. Garnets range in size from 8-10 mm. Magnetite and to a lesser extent pyrite, and chalcopyrite locally replace garnets and fill interstices.

GT-4 Garnet-magnetite-pyrite-chalcopyrite skarn. Red and green garnets occur together, commonly exhibiting green fractured massive interiors with red-orange extremely zoned exterior. The massive interiors of most of these garnets contain abundant diopside and some chlorite and calcite inclusions. Garnets range from 8-10 mm. in size. Magnetite and to a lesser extent pyrite and chalcopyrite replace garnets and fill interstices between garnets. Secondary calcite coats and fills spaces between garnets.

GT-5 Garnet skarn. Large, generally euhedral green garnets between 5-30 mm. in size occur with minor magnetite and secondary calcite that commonly coats the garnet crystals. The garnets exhibit a massive, highly fractured interior with an extremely zoned exterior.

CLV-H-48 Ore zone, Hanover Formation-Quartz+pyrite+chalcopyrite+magnetite vein approximately 1.5-2.0 mm. wide that irregularly cuts the massive magnetite-pyrite-chalcopyrite+limestone skarn.

CLV-H-48D Ore zone, Hanover Formation-Quartz+pyrite+chalcopyrite+ magnetite occur together in a vein approximately 2.5 2.5mm. wide. The vein forms an extremely irregular contact and cuts the massive magnetite-pyrite-chalcopyrite+limestone skarn.

C-28 Garnet skarn Syrena Formation- Quartz vein with magnetite concentrated toward the margins of the vein and sparsely occurring within the vein is approximately 1.0 mm. wide and cuts massive red-garnet skarn in the Syrena Formation.

CCF-22 Extremely granular and sheared quartz+pyrite+chalcopyrite+magnetite vein and veinlets cut the hornfels Colorado Formation. These irregular veins range in size from 1.0-3.0 mm. in size.

APPENDIX III

INDIVIDUAL FLUID INCLUSION MEASUREMENT
GT-1

Sample	Homo. Temp.	Eq. wt. % NaCl	Incl. type	Sample	Homo. Temp.	Eq. wt. % NaCl	Incl. type
GT-1a	228	18.36	S	GT-1d	154	17.74	S is
GT-1a	229	---	S	GT-1d	160	16.81	S is
GT-1a	247	---	S	GT-1d	217	---	P is
GT-1a	225	---	S	GT-1d	150	17.83	S is
GT-1a	179	---	S is	GT-1d	175	16.43	S is
GT-1a	256	---	S	GT-1d	190	---	S is
GT-1a	283	12.30	P gp	GT-1d	198	---	P
GT-1a	261	11.11	P is	GT-1d	242	10.24	P
GT-1a	249	13.44	P gp	GT-1d	256	---	P
GT-1a	260	11.47	P gp	GT-1d	201	---	?
GT-1a	236	---	P is	GT-1d	260	---	P is
GT-1a	289	---	P is	GT-1d	372	---	P
GT-1a	288	---	P is	GT-1d	167	---	S is
GT-1a	292	---	P is	GT-1e	220	10.99	P (?)
GT-1a	266	12.30	P is	GT-1e	224	10.49	P (?)
GT-1a	205	17.46	P(?)is	GT-1e	232	10.49	P (?)
GT-1a	208	18.36	P(?)is	GT-1e	220	10.49	P (?)
GT-1a	220	18.79	P(?)is	GT-1e	242	9.47	P (?)
GT-1a	215	18.79	P(?)is	GT-1e	194	---	P (?)
GT-1a	223	17.92	P(?)is	GT-1e	221	11.83	P (?)
GT-1a	235	16.04	P(?)is	GT-1e	224	11.71	P (?)
GT-1a	239	17.00	P	GT-1e	224	11.95	P (?)
GT-1a	234	16.04	P	GT-1e	221	11.59	P (?)
GT-1a	241	---	P	GT-1e	214	11.95	P (?)
GT-1a	233	17.00	P	GT-1e	224	---	P (?)
GT-1a	222	---	S	GT-1e	208	---	P (?)
GT-1a	233	---	S	GT-1e	204	---	S (?)
GT-1a	236	---	S	GT-1e	208	---	P (?)
GT-1a	258	---	S	GT-1e	219	---	P (?)
GT-1a	245	---	P	GT-1e	222	---	P (?)
GT-1a	221	---	P gp	GT-1e	189	---	S is
GT-1c	271	9.86	P gp	GT-1e	214	---	S is
GT-1c	265	14.52	P gp	GT-1e	233	---	S pl
GT-1c	289	---	P gp	GT-1e	205	---	S pl
GT-1c	243	---	P gp	GT-1e	244	---	S pl
GT-1c	251	---	P gp	GT-1e	247	---	S pl
GT-1c	234	14.52	P gp	GT-1e	193	---	S pl
GT-1c	207	---	S	GT-1e	199	---	S pl
GT-1c	255	---	S	GT-1e	215	---	P is
GT-1c	250	---	S	GT-1e	167	---	S is
GT-1c	243	---	S	GT-1f	397	---	P gp
GT-1c	247	---	S	GT-1f	255	---	P gp
GT-1d	238	---	P	GT-1f	292	---	P gp
GT-1d	230	---	P	GT-1f	330	---	P gp
GT-1d	258	---	P is	GT-1f	256	---	P gp
GT-1d	248	8.94	P is	GT-1f	299	---	P gp
GT-1d	248	9.47	P is	GT-1f	335	---	P gp
GT-1d	248	10.24	P is	GT-1f	196	---	P gp
GT-1d	251	---	P is	GT-1f	201	---	P gp

GT-1f	196	---	P gp	GT-1h	283	---	P gp
GT-1f	210	---	P gp	GT-1h	315	---	P gp
GT-1f	223	14.52	P is	GT-1h	322	---	P gp
GT-1f	205	15.55	P is	GT-1h	270	---	P gp
GT-1f	218	17.46	P is	GT-1h	316	---	P gp
GT-1f	196	17.46	P is	GT-1h	238	---	P gp
GT-1f	173	---	S is	GT-1	257	---	P gp
GT-1f	184	---	S is	GT-1h	254	---	P gp
GT-1f	214	17.92	P is	GT-1h	261	---	P gp
GT-1f	209	16.04	P is	GT-1h	280	---	P gp
GT-1f	212	---	P is	GT-1h	277	---	P gp
GT-1g	210	---	P is	GT-1h	324	---	P gp
GT-1g	206	---	P is	GT-1i	167	---	S is
GT-1g	260	---	P is	GT-1i	170	---	S is
GT-1g	173	---	S is	GT-1i	174	---	S is
GT-1g	274	---	P gp	GT-1i	178	---	S is
GT-1g	357	---	P gp	GT-1i	209	---	P gp
GT-1g	326	---	P gp	GT-1i	209	---	P gp
GT-1g	230	---	P gp	GT-1i	170	---	P gp(?)
GT-1g	212	---	P is	GT-1i	223	---	P is
GT-1g	212	---	P is	GT-1i	201	---	P is
GT-1g	344	---	P is	GT-1i	214	---	P is
GT-1g	226	---	P is	GT-1i	221	---	P gp
GT-1g	287	---	P is	GT-1i	223	---	P is
GT-1g	223	---	P gp	GT-1i	195	---	S is
GT-1g	242	---	P gp	GT-1i	246	---	P is
GT-1g	203	---	P gp	GT-1i	292	---	P is
GT-1g	226	---	P gp	GT-1i	230	---	P
GT-1g	261	---	P gp	GT-1i	230	---	P
GT-1g	213	---	P gp	GT-1i	258	---	P
GT-1g	208	---	S is	GT-1i	251	---	P
GT-1g	201	---	S is	GT-1i	272	---	P
GT-1g	214	---	S is	GT-1i	206	---	P is
GT-1g	209	---	P gp	GT-1i	206	---	P is
GT-1h	210	---	P gp	GT-1a	200	---	S is
GT-1h	215	---	P gp	GT-1c	202	---	S is
GT-1h	232	---	P gp	GT-1d	291	---	P is
GT-1h	246	---	P gp	GT-1i	212	---	S (?)
GT-1h	255	---	P is	GT-1c	212	---	S (?)
GT-1h	324	---	P is	GT-1b	195	---	S (?)
GT-1h	335	---	P is	GT-1e	249	---	P is
GT-1h	254	---	P is	GT-1c	253	---	P is
GT-1h	337	---	P is	GT-1c	232	---	P is
GT-1h	262	---	P is	GT-1a	212	---	P is
GT-1h	295	---	P is	GT-1a	212	---	P is
GT-1h	260	---	P is	GT-1a	266	---	P is
GT-1h	201	---	P is	GT-1a	236	---	P is
GT-1h	272	---	P is	GT-1c	185	18.36	(?)
GT-1h	225	---	P is	GT-1a	185	---	P gp
GT-1h	218	---	P is	GT-1a	188	---	S pl
GT-1h	277	---	P is	GT-1b	178	---	S pl
GT-1h	240	---	P is	GT-1b	253	---	P is
GT-1h	257	---	P is	GT-1b	178	---	is

GT-1c	258	10.24	P is	GT-1c	238	---	S
GT-1c	261	---	S(?)	GT-1c	331	10.24	P
GT-1c	265	---	S(?)	GT-1c	253	10.24	P
GT-1c	264	---	S(?)	GT-1c	258	10.24	P
GT-1c	239	---	S(?)				

INDIVIDUAL FLUID INCLUSION MEASUREMENT
GT-4

Sample	Homo. Temp.	Eq. wt. % NaCl	Incl. type	Sample	Homo. Temp.	Eq. wt. % NaCl	Incl. type
GT-4a	199	---	S pl	GT-4b	251	7.58	P is
GT-4a	265	---	P is	GT-4b	257	---	P is
GT-4a	250	---	P is	GT-4b	259	6.72	P is
GT-4a	208	---	P is	GT-4b	247	---	P is d
GT-4a	327	13.77	P is	GT-4b	254	---	P is
GT-4a	299	---	P is	GT-4b	251	---	P is
GT-4a	256	---	P is	GT-4b	205	---	P is
GT-4a	253	---	P is	GT-4b	220	---	P is
GT-4a	240	---	P is	GT-4c	326	---	S pl
GT-4a	222	7.85	P is	GT-4c	317	15.04	P pl
GT-4b	267	---	P is	GT-4c	328	---	P pl ds
GT-4b	307	---	P is	GT-4c	211	---	P pl
GT-4b	266	---	P is	GT-4c	317	---	P pl
GT-4b	248	---	P is	GT-4c	333	---	P pl
GT-4b	266	---	P is	GT-4c	337	---	S pl
GT-4b	258	6.43	P is	GT-4c	337	---	S pl
GT-4b	255	7.85	P is	GT-4c	337	---	S pl
GT-4b	261	7.85	P is	GT-4e	272	---	P pl
GT-4b	253	---	P is	GT-4e	295	---	P pl
GT-4b	259	---	P is	GT-4e	305	---	P pl
GT-4b	250	8.13	P is	GT-4e	250	---	P pl
GT-4b	255	7.85	P is	GT-4e	264	---	P pl
GT-4b	260	7.58	P is	GT-4e	254	6.43	P pl
GT-4b	259	7.58	P is	GT-4a	245	---	P
GT-4a	452	9.07	V ??	GT-4a	286	---	P
GT-4a	410	7.58	V ??	GT-4a	255	8.67	P
GT-4a	272	---	L				
GT-4a	254	4.51	L				

INDIVIDUAL FLUID INCLUSION MEASUREMENT
GT1-1

Sample	Homo. Temp.	Eq. wt. % NaCl	Incl. type	Sample	Homo. Temp.	Eq. wt. % NaCl	Incl. type
GT1-1a	156	19.13	S	GT1-1c	243	---	P is
GT1-1a	147	17.92	S	GT1-1c	235	10.62	P is
GT1-1a	263	---	P is	GT1-1c	244	---	P is
GT1-1a	274	---	P is	GT1-1c	252	---	P is
GT1-1a	300	---	P is	GT1-1c	235	10.37	P is
GT1-1a	305	---	P is	GT1-1c	245	10.24	P is
GT1-1a	309	12.65	P is	GT1-1c	258	---	P is
GT1-1a	264	---	P is	GT1-1c	243	10.86	P is
GT1-1a	366	---	P (?)	GT1-1c	249	11.83	P is
GT1-1a	281	12.65	P is	GT1-1c	253	11.11	P is
GT1-1a	282	---	P is	GT1-1c	244	---	P is
GT1-1b	363	7.85	S pl	GT1-1c	249	---	P is
GT1-1b	207	11.83	P (?)	GT1-1c	247	---	P is
GT1-1b	157	11.71	P (?)	GT1-1c	255	---	P is
GT1-1b	215	12.07	P (?)	GT1-1c	256	9.60	P is
GT1-1b	306	4.63	P is	GT1-1c	238	---	P is
GT1-1b	194	13.99	P (?)	GT1-1d	274	9.98	P is d
GT1-1b	204	14.62	P (?)	GT1-1d	208	15.95	P is
GT1-1b	189	12.99	P (?)	GT1-1d	217	16.91	P is d
GT1-1b	210	13.10	P (?)	GT1-1d	325	---	P(?) S
GT1-1b	204	13.10	P (?)	GT1-1d	435	---	P(?) S
GT1-1b	259	9.60	P is	GT1-1d	435	---	P(?)S(
GT1-1b	239	14.20	P is	GT1-1d	220	---	P is
GT1-1b	203	12.88	S pl(?)	GT1-1d	266	---	P gp
GT1-1b	214	12.88	S pl(?)	GT1-1d	307	---	P is
GT1-1c	359	---	S pl(?)	GT1-1d	384	---	P gp(?
GT1-1c	354	---	S pl(?)	GT1-1d	367	---	P is
GT1-1c	400	---	(?)	GT1-1d	242	---	P is
GT1-1c	262	---	P is	GT1-1d	274	---	P is
GT1-1c	251	16.24	P is	GT1-1d	317	---	P is
GT1-1c	268	---	P is	GT1-1d	243	---	P is d
GT1-1c	272	---	P is	GT1-1d	266	---	P is
GT1-1c	235	---	P is	GT1-1d	357	---	P is
GT1-1c	236	10.11	P is	GT1-1d	345	---	P is
GT1-1c	245	10.11	P is	GT1-1d	323	---	P is
GT1-1c	245	10.11	P is	GT1-1d	275	---	P gp
GT1-1c	246	---	P is	GT1-1d	255	10.99	P gp
GT1-1c	246	---	P is	GT1-1d	274	---	P gp
GT1-1c	251	---	P is	GT1-1d	247	10.99	P gp
GT1-1c	250	9.98	P is	GT1-1e	276	---	P is
GT1-1c	244	9.98	P is	GT1-1e	291	---	P is
GT1-1c	242	10.11	P is	GT1-1e	263	---	P is
GT1-1c	233	9.98	P is	GT1-1e	191	---	P(?)
GT1-1c	235	---	P is	GT1-1e	221	---	P(?)
GT1-1c	233	9.98	P is	GT1-1e	212	13.22	P(?)
GT1-1c	259	---	P is	GT1-1e	192	---	P(?)
GT1-1c	244	---	P is	GT1-1e	215	13.10	P(?)

GT1-1e	295	---	P is	GT1-1e	361	---	P is
GT1-1e	291	---	P is	GT1-1e	331	---	P is
GT1-1e	286	---	P is				

INDIVIDUAL FLUID INCLUSION MEASUREMENT
GT-5

Sample	Homo. Temp.	Eq. wt. % Nacl	Incl. type	Sample	Homo. Temp.	Eq. Wt. % Nacl	Incl. type
GT-5a	242	---	P gp	GT-5b	244	9.21	P gp
GT-5a	331	---	P is	GT-5b	241	9.34	P gp
GT-5a	327	---	P is	GT-5b	247	9.21	P gp
GT-5a	352	---	P is	GT-5b	263	---	P gp
GT-5a	256	10.86	P is	GT-5b	253	16.24	P gp
GT-5a	252	---	P is	GT-5b	250	16.24	P gp
GT-5a	251	9.98	P is	GT-5b	256	---	P gp
GT-5a	243	9.98	P is	GT-5b	262	14.41	P gp
GT-5a	251	---	P is	GT-5b	245	10.24	P gp
GT-5a	242	9.21	P is	GT-5b	250	---	P gp
GT-5a	245	9.07	P is	GT-5b	234	10.24	P gp
GT-5a	252	8.67	P is	GT-5b	247	10.24	P gp
GT-5a	266	8.81	P is	GT-5b	252	---	P gp
GT-5a	263	8.67	P is	GT-5b	252	10.24	P gp
GT-5a	252	8.67	P is	GT-5b	242	9.86	P gp
GT-5a	255	---	P is	GT-5b	253	8.54	P gp
GT-5b	311	11.95	P is	GT-5b	241	10.24	P gp
GT-5b	237	10.49	P is	GT-5b	242	10.24	P gp
GT-5b	311	---	P is	GT-5b	235	8.81	P gp
GT-5b	257	11.47	P is	GT-5b	246	8.81	P gp
GT-5b	258	15.65	P is	GT-5c	251	---	P is
GT-5b	276	---	P is	GT-5c	263	---	P is
GT-5b	312	---	P is	GT-5c	267	---	P is
GT-5b	272	12.30	P is	GT-5c	246	---	P is
GT-5b	289	12.19	P is	GT-5c	232	9.34	P is
GT-5b	266	11.59	P is	GT-5c	335	11.59	S pl
GT-5b	232	---	P is	GT-5c	206	9.73	S pl
GT-5b	259	13.99	P is	GT-5c	248	10.24	S pl(?)
GT-5b	157	---	S is	GT-5c	256	8.67	S pl(?)
GT-5b	161	12.88	S pl	GT-5c	263	---	P is
GT-5b	189	13.66	S pl	GT-5c	243	---	P is
GT-5b	184	12.65	S	GT-5c	267	---	P is
GT-5b	163	12.88	S	GT-5c	255	10.62	P is
GT-5b	267	---	P is	GT-5c	242	11.47	P is
GT-5b	265	---	P is	GT-5c	226	11.41	P is
GT-5b	260	---	P is	GT-5c	269	---	P is
GT-5b	221	11.95	P is	GT-5c	270	9.73	P is
GT-5b	222	11.83	P is	GT-5c	255	---	P is
GT-5b	234	10.62	P is	GT-5c	234	9.34	P is
GT-5b	230	10.62	P is	GT-5c	255	9.73	P is
GT-5b	233	10.62	P is	GT-5c	248	9.34	P is
GT-5b	252	---	P is	GT-5d	327	---	P is

GT-5b	253	---	P is	GT-5d	426	16.43	P is
GT-5b	236	---	P is	GT-5d	296	---	P is
GT-5b	249	6.87	P gp	GT-5d	291	15.45	P is
GT-5b	249	9.73	P gp	GT-5d	305	16.53	P is
GT-5b	255	---	P gp	GT-5d	304	14.09	P is
GT-5d	267	---	P gp	GT-5d	318	---	P gp
GT-5d	424	---	P gp	GT-5d	314	---	P gp
GT-5d	412	---	P gp				

INDIVIDUAL FLUID INCLUSION MEASUREMENT
CLV-H-48D

Sample	Homo. Temp.	Eq. wt. % NaCl	Incl. type	Sample	Homo. Temp.	Eq. wt. % NaCl	Incl. type
CLV-H-48D	409	---	V S	CLV-H-48D	349	5.40	L
CLV-H-48D	465	9.47	V S	CLV-H-48D	361	---	L
CLV-H-48D	312	35.50	L ST	CLV-H-48D	384	8.13	L
CLV-H-48D	375	16.91	L	CLV-H-48D	392	---	V
CLV-H-48D	245	8.13	L	CLV-H-48D	347	24.31	L
CLV-H-48D	354	---	V	CLV-H-48D	353	---	L
CLV-H-48D	298	23.15	L	CLV-H-48D	449	---	V
CLV-H-48D	406	2.06	L	CLV-H-48D	193	+0.7	L CO2
CLV-H-48D	489	---	L	CLV-H-48D	361	+0.9	L CO2
CLV-H-48D	504	---	V S cpb	CLV-H-48D	213	+1.1	L CO2
CLV-H-48D	424	---	L S	CLV-H-48D	218	+1.0	V CO2
CLV-H-48D	459	9.47	V S cpb	CLV-H-48D	309	37.00	L ST
CLV-H-48D	464	---	V S cpb	CLV-H-48D	428	23.22	L
CLV-H-48D	254	---	L	CLV-H-48D	398	8.13	V
CLV-H-48D	353	---	L	CLV-H-48D	443	23.15	L
CLV-H-48D	349	---	L	CLV-H-48D	388	---	V
CLV-H-48D	464	---	L	CLV-H-48D	384	---	V
CLV-H-48D	472	---	L cpb	CLV-H-48D	203	2.72	L
CLV-H-48D	403	9.47	V cpb	CLV-H-48D	235	+1.1	L CO2
CLV-H-48D	401	---	V cpb	CLV-H-48D	305	+1.4	L CO2
CLV-H-48D	429	---	V cpb	CLV-H-48D	313	+0.5	L CO2
CLV-H-48D	432	---	V cpb	CLV-H-48D	385	+1.1	L CO2
CLV-H-48D	394	---	V cpb	CLV-H-48D	251	+0.9	L CO2
CLV-H-48D	398	---	V cpb	CLV-H-48D	118	+4.1	V CO2
CLV-H-48D	422	5.40	V	CLV-H-48D	119	+0.9	V CO2
CLV-H-48D	189	19.21	L	CLV-H-48D	253	+0.3	L CO2
CLV-H-48D	334	---	L	CLV-H-48D	264	---	L
CLV-H-48D	181	+7.1	L CO2	CLV-H-48D	237	0.18	L
CLV-H-48D	183	+.8	L CO2	CLV-H-48D	266	0.18	L
CLV-H-48D	180	+.9	L CO2	CLV-H-48D	331	19.13	L
CLV-H-48D	362	---	L	CLV-H-48D	241	---	V
CLV-H-48D	368	---	L	CLV-H-48D	336	+1.0	V CO2
CLV-H-48D	246	---	L	CLV-H-48D	340	---	L
CLV-H-48D	361	---	L	CLV-H-48D	208	+1.5	L CO2
CLV-H-48D	350	---	L	CLV-H-48D	116	+1.0	V CO2
CLV-H-48D	362	---	L				
CLV-H-48D	350	---	L				

INDIVIDUAL FLUID INCLUSION MEASUREMENT
C-28

Sample	Homo. Temp.	Eq. wt. % NaCl	Incl. type	Sample	Homo. Temp.	Eq. wt. % NaCl	Incl. type
C-28	449	10.49	V	C-28	289	17.65	L
C-28	442	10.49	V	C-28	292	18.79	L
C-28	452	12.88	V	C-28	223	---	L
C-28	255	1.56	L	C-28	428	---	V
C-28	267	40.00	L ST m	C-28	424	---	V
C-28	314	46.00*	L ST m	C-28	600	---	?
C-28	431	---	V	C-28	278	23.56	L
C-28	312	46.00*	L ST m	C-28	298	28.10	L
C-28	428	---	V	C-28	294	9.47	L
C-28	423	---	V	C-28	224	2.56	L
C-28	279	43.50*	L ST m	C-28	423	---	V
C-28	315	47.00*	L ST m	C-28	425	---	V
C-28	317	47.00*	L ST m	C-28	382	---	V
C-28	414	---	V	C-28	256	---	L
C-28	422	---	V	C-28	374	---	V
C-28	432	---	V	C-28	370	---	L
C-28	432	---	V	C-28	447	33.00	L ST
C-28	454	5.85	V	C-28	430	32.50	L ST
C-28	475	9.98	V	C-28	336	16.41	L
C-28	384	38.00	L ST m	C-28	314	17.00	L
C-28	423	33.00	L ST m	C-28	425	32.50	L ST
C-28	424	34.50	L ST m	C-28	512	32.50	L ST
C-28	426	34.50	L ST m	C-28	360	---	L
C-28	399	38.00	L ST m	C-28	400	40.00	L ST
C-28	600	23.77	?	C-28	389	38.00	L ST
C-28	294	20.51	L	C-28	568	---	L dp
C-28	238	19.54	L	C-28	590	---	L dp
				C-28	590	---	L dp

INDIVIDUAL FLUID INCLUSION MEASUREMENT
CLV-H-48

Sample	Homo. Temp.	Eq. wt. % NaCl	Incl. type	Sample	Homo. Temp.	Eq. wt. % NaCl	Incl. type
CLV-H-48a	357	---	L	CLV-H-48b	491	---	L
CLV-H-48a	559	---	V	CLV-H-48b	487	---	V
CLV-H-48a	477	---	L	CLV-H-48b	435	---	L
CLV-H-48a	534	---	V	CLV-H-48b	420	---	V
CLV-H-48a	312	---	L	CLV-H-48b	419	---	V
CLV-H-48a	423	---	V	CLV-H-48b	475	---	V
CLV-H-48a	408	---	V	CLV-H-48b	434	---	V
CLV-H-48a	393	---	V	CLV-H-48b	235	---	L
CLV-H-48a	416	---	V	CLV-H-48b	451	---	L
CLV-H-48a	403	---	V	CLV-H-48b	457	---	V
CLV-H-48a	267	---	L	CLV-H-48b	473	---	L
CLV-H-48a	509	---	V	CLV-H-48b	497	---	V
CLV-H-48a	262	---	L	CLV-H-48b	436	---	V
CLV-H-48a	323	---	L	CLV-H-48b	371	---	L
CLV-H-48a	530	---	V	CLV-H-48b	365	---	L
CLV-H-48a	531	---	V	CLV-H-48b	422	---	V
CLV-H-48a	395	---	V	CLV-H-48b	340	---	L
CLV-H-48a	434	---	V	CLV-H-48b	318	---	L
CLV-H-48a	288	---	L	CLV-H-48b	344	---	L
CLV-H-48a	416	---	V	CLV-H-48b	451	---	V
CLV-H-48a	403	---	V	CLV-H-48b	487	---	V
CLV-H-48a	389	---	L	CLV-H-48b	432	---	V
CLV-H-48a	517	---	V	CLV-H-48b	424	---	V
CLV-H-48a	359	---	L	CLV-H-48b	412	---	V
CLV-H-48a	353	33.50	L ST	CLV-H-48b	264	---	V
CLV-H-48a	476	---	V	CLV-H-48b	215	---	L
CLV-H-48a	495	---	V	CLV-H-48b	264	---	V
CLV-H-48a	534	---	V	CLV-H-48b	240	---	L S
CLV-H-48a	483	---	V	CLV-H-48b	240	---	L S
CLV-H-48b	329	---	L	CLV-H-48b	241	---	L S
CLV-H-48b	472	---	V	CLV-H-48b	239	---	L S
CLV-H-48b	435	---	L	CLV-H-48b	252	---	L S
CLV-H-48b	416	---	V	CLV-H-48b	378	---	V
CLV-H-48b	463	---	V	CLV-H-48b	462	---	L
CLV-H-48b	482	---	V	CLV-H-48b	374	---	V
CLV-H-48b	454	---	L	CLV-H-48b	448	---	V
CLV-H-48b	456	---	V	CLV-H-48b	418	---	L
CLV-H-48b	390	36.50	L ST	CLV-H-48b	418	---	V
CLV-H-48b	413	---	V	CLV-H-48b	423	---	V
CLV-H-48b	438	---	V	CLV-H-48c	422	---	V
CLV-H-48b	418	---	L	CLV-H-48c	352	---	V
CLV-H-48b	411	---	V	CLV-H-48c	414	---	V
CLV-H-48	295	---	L	CLV-H-48c	428	---	L
CLV-H-48	487	---	V	CLV-H-48c	408	---	L
CLV-H-48	403	---	V	CLV-H-48c	374	---	V

CLV-H-48c	341	---	L	CLV-H-48a	352	+2.1	L CO2
CLV-H-48c	331	---	L	CLV-H-48a	364	---	L
CLV-H-48c	428	---	V	CLV-H-48a	327	---	L
CLV-H-48c	266	---	L	CLV-H-48a	440	---	L
CLV-H-48c	249	---	L	CLV-H-48a	262	---	L
CLV-H-48a	292	7.8	L	CLV-H-48c	204	---	L
CLV-H-48a	432	---	L	CLV-H-48c	325	---	L
CLV-H-48a	332	---	L	CLV-H-48c	486	---	V
CLV-H-48b	472	---	L	CLV-H-48c	424	---	V
CLV-H-48b	385	---	V	CLV-H-48c	261	---	L S
CLV-H-48b	428	---	V	CLV-H-48c	513	---	L
CLV-H-48b	260	0.0	L CO2	CLV-H-48c	269	---	L
CLV-H-48b	258	---	L				
CLV-H-48b	257	---	L				
CLV-H-48a	322	+1.4	L CO2				
CLV-H-48a	235	0.0	L				

INDIVIDUAL FLUID INCLUSION MEASUREMENT
CCF-22

Sample	Homo. Temp.	Eq. wt. % NaCl	Incl. type	Sample	Homo. Temp.	Eq. wt. % NaCl	Incl. type
CCF-22a	269	---	L	CCF-22i	387	---	L S
CCF-22a	302	---	L	CCF-22h	351	38.00	L ST
CCF-22c	325	---	L	CCF-22h	224	37.50	L ST
CCF-22c	242	32.50	L ST	CCF-22h	426	---	L
CCF-22c	265	32.50	L ST	CCF-22h	401	---	L d
CCF-22c	248	---	L	CCF-22h	440	---	L
CCF-22c	311	47.00*	L ST S	CCF-22h	439	---	L
CCF-22d	315	47.00*	L ST S	CCF-22h	333	36.00	L ST
CCF-22d	303	45.00*	L ST	CCF-22h	550	---	?
CCF-22d	550	---	?	CCF-22h	550	---	?
CCF-22d	194	---	L	CCF-22h	373	---	L
CCF-22d	418	19.21	L	CCF-22h	195	---	L
CCF-22d	234	33.00	L ST d	CCF-22h	372	---	L
CCF-22d	231	40.00/340	L ST d	CCF-22h	248	---	L
CCF-22d	229	40.00/341	L ST d	CCF-22h	550	---	?
CCF-22i	225	37.50	L ST	CCF-22d	400	44.00	L ST
				CCF-22d	403	43.50	L ST

Abbreviations

P	primary fluid inclusion
S	secondary fluid inclusion
L	a fluid inclusion that homogenizes into a liquid phase
V	a fluid inclusion that homogenizes into a vapor phase
CO2	the fluid inclusion contains a CO2 phase
is	an isolated fluid inclusion that does not occur associated or near to other similar inclusions
gp	a fluid inclusion that occurs on a growth plane in a garnet mineral and therefore is assumed to be of primary origin.
ST	a fluid inclusion containing a daughter salt in which the salt is NaCl
d	daughter mineral present in the fluid inclusion not including NaCl or magnetite daughter minerals
ds	several daughter minerals present in the fluid inclusion not including NaCl or magnetite daughter minerals
m	daughter mineral present in the inclusion is identified as magnetite
h	daughter mineral present in the inclusion is identified as hematite
?	the fluid inclusion did not homogenize before 550 or 600 degrees (C) and therefore the homogeniztion phase is not known
550	the fluid inclusion did not homogenize by 550 degrees
600	the fluid inclusion did not homogenize by 600 degrees
cpb	the fluid inclusion exhibits critical point behavior
+	refers to the last melting temperature which is above zero and therefore the equivalent wt.% NaCl is not determinable, usually refers to CO2 inclusions.
*	refers to high salinity inclusions in which the NaCl crystal remained after the homogenization of the vapor bubble.
/#	a number after a slash mark refers to the temperature at which a daughter mineral disappeared, probably this is KCl.

Salinity determinations for fluid inclusions based on the disappearance of NaCl crystal are approximated using using the wt.% NaCl curve by Keevil, (1942) and salinity determinations from freezing point depression was taken from Potter and others, (1978)

APPENDIX IV

REE Concentrations (ppm) and REE Concentrations Chondrite Normalized For Individual Samples.

	CG2		CBQ1		CEP3		CM4	
	Conc.	Norm.	Conc.	Norm.	Conc.	Norm.	Conc.	Norm.
La	30.17	91.40	44.89	142.2	167.8	487.1	3.24	8.39
Ce	58.06	65.97	98.38	111.8	282.5	321.0	5.46	6.20
Nd	n.d.	n.d.	40.83	68.00	88.66	144.8	n.d	n.d.
Sm	4.63	25.58	9.46	52.24	16.40	90.60	1.07	5.91
Eu	1.32	19.13	1.81	26.23	4.45	64.99	.718	10.41
Tb	.866	18.44	.608	12.94	2.96	63.00*	<.210	<4.47
Yb	1.21	6.07	4.41	22.04	5.26	26.30	.426	2.13
Lu	.361	10.62	.690	20.30	.707	20.81	.097	2.85
REE	96.62	237.2	201.7	455.7	568.8	1218	11.22	40.36
Eu/Eu*		.835		n.d.		.812		1.93
La/Yb		15.08		6.45		18.52		3.94
La/Sm		3.57		2.72		5.38		1.42
Tb/Yb		3.04		.587		2.40		2.10

	CMA5		CGD6		CGD9		CD10	
	Conc.	Norm.	Conc.	Norm	Conc.	Norm	Conc.	Norm.
La	6.56	20.05	16.98	52.36	26.84	82.86	1.59	5.35
Ce	5.12	5.82	38.92	44.23	61.14	69.48	<5.67	6.44
Nd	n.d.	n.d.	n.d.	n.d.	36.92	61.53	n.d.	n.d.
Sm	1.16	6.41	6.01	33.20	10.15	56.07	.296	1.64
Eu	.703	14.49	3.68	53.32	3.59	73.91	.606	8.78
Tb	<.335	<7.13	<.697	<14.82	.751	15.98	.199	4.24
Yb	<.618	<3.09	1.41	7.07	3.27	16.33	<.327	1.64
Lu	<.216	<6.37	.301	8.88	.539	15.87	.041	1.19
REE	14.71	63.36	68.00	213.88	143.2	392.03	9.88	29.28
Eu/Eu*		1.93		2.32		2.46		4.18
La/Yb		6.49		7.41		5.07		3.26
La/Sm		3.13		1.58		1.48		3.26
Tb/Yb		2.31		2.10		.979		2.59

	CDM11		CLH12		COSD13		COSH14	
	Conc.	Norm.	Conc.	Norm.	Conc.	Norm.	Conc.	Norm.
La	1.96	5.71	13.80	41.80	22.16	67.15	19.85	60.17
Ce	<9.22	10.47	16.04	18.23	54.08	61.45	31.03	35.26
Nd	n.d.	n.d.	n.d.	n.d.	n.d.	n.d.	n.d.	n.d.
Sm	.122	.673	3.54	19.56	6.64	36.66	5.22	28.81
Eu	.593	8.59	1.58	22.90	3.34	48.40	1.35	19.56
Tb	<.307	6.53	.694	14.77	1.05	22.41	1.22	26.00*
Yb	<.889	4.44	1.09	5.44	2.92	14.60	4.44	22.18
Lu	.106	3.12	.198	5.81	.506	14.90	<.544	16.29
REE	13.20	39.55	36.94	128.51	90.70	265.57	68.65	207.7
Eu/Eu*		3.94		1.31		1.56		.738
La/Yb		1.29		7.68		4.60		2.99
La/Sm		8.48		2.14		1.83		2.30
Tb/Yb		1.47		2.72		1.53		1.55

	COS15		PAG16		CLV117		CLV217	
	Conc.	Norm.	Conc.	Norm.	Conc.	Norm.	Conc.	Norm
La	34.64	105.0	32.60	98.78	14.17	42.92	18.53	56.17
Ce	51.92	59.00	57.08	64.84	44.00	50.00	57.06	64.84
Nd	20.18	33.64	23.79	39.66	n.d.	n.d.	n.d.	n.d.
Sm	2.80	15.81	5.73	31.68	1.28	7.09	3.16	17.45
Eu	.644	9.33	2.00	28.99	1.06	15.33	1.89	27.39
Tb	<.385	8.19	.865	18.40	<.254	5.40	<.279	4.85
Yb	<.944	4.72	1.19	5.93	<.838	4.19	.464	2.32
Lu	.164	4.81	.277	6.69	.153	4.50	<.075	2.20*
REE	111.7	241.1	123.5	294.9	62.13	130.0	81.45	305.3
Eu/Eu*		.811		1.12		2.32		2.61
La/Yb		22.24		16.66		10.24		24.21
La/Sm		6.64		3.12		6.05		3.22
Tb/Yb		1.74		3.10		1.29		2.09

	CPS18		COS19		CBTQ20		CABO21	
	Conc.	Norm.	Conc.	Norm.	Conc.	Norm.	Conc.	Norm.
La	49.52	150.4	27.88	84.48	4.34	13.15	68.21	208.81
Ce	79.47	90.31	48.64	55.27	<7.15	8.13	132.4	150.18
Nd	n.d.	n.d.	n.d.	n.d.	n.d.	n.d.	n.d.	n.d.
Sm	6.26	34.61	2.62	14.48	.518	2.86	8.64	47.79
Eu	1.30	18.84	.664	9.63	.465	6.74	1.75	25.36
Tb	.955	20.31	<.423	9.00	<.111	2.36	.907	19.30
Yb	2.76	13.78	<1.03	5.16	.455	2.28	2.65	13.23
Lu	.460	13.54	.197	5.80	.095	2.81	.510	14.99
REE	140.7	341.83	81.45	183.8	13.13	38.33	215.1	479.7
Eu/Eu*		.711		.860		2.81		.746
La/Yb		10.91		16.37		5.77		15.78
La/Sm		4.35		5.83		4.60		4.37
Tb/Yb		1.47		1.74		1.04		1.46

	GTH		GT11		GT1		GT2	
	Conc.	Norm.	Conc.	Norm.	Conc.	Norm.	Conc.	Norm.
La	35.87	108.70	28.09	85.11	37.77	113.90	17.70	55.87
Ce	54.27	61.67	61.17	70.65	63.78	72.41	57.87	65.79
Nd	n.d.	n.d.	n.d.	n.d.	n.d.	n.d.	18.96	31.60
Sm	5.38	29.75	2.07	11.42	4.60	25.42	2.13	11.77
Eu	2.11	30.57	1.67	24.16	1.86	27.01	1.83	26.52
Tb	<.517	11.00*	<.401	8.53	<.408	8.68	<.459	9.76
Yb	2.74	13.70	<.808	4.01	.647	3.24	<.819	4.09
Lu	.497	14.97*	<.175	5.14	.129	3.80*	.184	5.40*
REE	101.4	269.9	94.38	209.0	108.7	254.5	99.95	210.8
Eu/Eu*		1.46		2.46		1.64		2.21
La/Yb		7.93		21.22		35.15		13.66
La/Sm		3.65		7.45		4.48		4.75
Tb/Yb		.802		2.13		2.65		2.39

	GT3	
	Conc.	Norm
La	38.21	117.03
Ce	154.0	175.00
Nd	47.97	79.87
Sm	5.18	28.64
Eu	3.18	46.08
Tb	<.405	8.62
Yb	<.735	3.68
Lu	.146	4.30*
REE	249.8	463.2
Eu/Eu*		2.88
La/Yb		31.80
La/Sm		4.09
Tb/Yb		2.34

	GT4	
	Conc.	Norm.
	20.58	77.22
	81.02	92.07
	45.17	75.28
	5.69	31.45
	2.10	30.43
	<.558	11.88
	<.759	3.80
	.150	4.40*
	156.1	326.5
		1.44
		20.32
		2.46
		3.13

	CCF22	
	Conc.	Norm.
	35.06	106.8
	61.57	69.97
	24.32	40.54
	6.03	33.32
	2.17	31.45
	1.15	24.47
	2.00	9.98
	.413	12.14
	132.7	328.1

		10.65
		3.19
		2.45

	CCV23	
	Conc.	Nor
	18.70	59.
	16.99	19.
	n.d.	n.d
	2.58	14.
	.989	14.
	.523	11.
	1.95	6.5
	.218	6.4
	41.95	131
		1.0
		9.0
		4.1
		1.6

	CDS25	
	Conc.	Norm.
La	36.56	110.77
Ce	59.14	67.21
Nd	n.d.	n.d.
Sm	7.57	41.81
Eu	4.07	58.99
Tb	<.748	15.90
Yb	3.34	16.70
Lu	.538	15.82
REE	111.9	259.9
Eu/Eu*		2.36
La/Yb		6.63
La/Sm		2.65
Tb/Yb		.952

	CSY127	
	Conc.	Norm.
	37.71	114.27
	68.21	77.51
	n.d.	n.d.
	5.72	31.62
	.655	9.49
	.978	20.80
	1.47	7.35
	.252	7.41
	114.9	268.4
		.351
		15.54
		3.61
		2.83

	CSY227	
	Conc.	Norm.
	646.3	1958
	845.3	960.5
	254.6	424.2
	12.37	68.34
	1.73	25.07
	1.10	23.38
	1.46	7.30
	.245	7.20
	1763	3474
		.748
		268.2
		28.65
		3.12

	C28	
	Conc.	Nor
	17.74	53.
	40.17	45.
	n.d.	n.d
	3.92	21.
	1.53	22.
	.642	16.
	<.644	3.2
	.114	3.3
	64.71	163
		1.2
		16.
		2.4
		4.2

	G29	
	Conc.	Norm.
La	36.01	109.1
Ce	60.71	68.99
Nd	n.d.	n.d.
Sm	5.71	31.53
Eu	1.65	23.91
Tb	1.13	24.04
Yb	2.99	14.93
Lu	.464	13.65
REE	108.7	286.2
Eu/Eu*		.956
La/Yb		7.31
La/Sm		3.46
Tb/Yb		1.61

	PAG30	
	Conc.	Norm.
	32.83	99.49
	42.43	48.22
	24.23	40.39
	3.95	21.82
	.749	10.86
	.637	13.55
	1.46	7.30
	.262	7.71
	106.6	249.3
		.621
		13.63
		4.56
		1.86

	H32	
	Conc.	Norm.
	9.97	30.21
	8.00	9.09
	n.d.	n.d.
	2.54	14.06
	.703	10.19
	.599	12.74
	1.12	5.60
	.115	3.38
	23.1	85.3
		.772
		5.39
		2.15
		2.28

	P34	
	Conc.	Nor
	15.46	46.
	32.03	36.
	n.d.	n.d
	4.23	23.
	.767	11.
	<.785	16.
	2.55	12.
	.331	9.7
	56.13	156
		.55
		3.6
		2.0
		1.3

	PS36	
	Conc.	Norm.
La	31.20	94.53
Ce	65.45	74.38
Nd	n.d.	n.d.
Sm	4.47	24.71
Eu	.728	10.55
Tb	.569	12.10*
Yb	1.18	5.90
Lu	.277	6.69
REE	103.8	228.9
Eu/Eu*		.555
La/Yb		16.02
La/Sm		3.83
Tb/Yb		1.81

	FD37	
	Conc.	Norm.
	1.74	5.37
	<.593	6.74
	n.d.	n.d.
	.0526	.291
	.556	8.06
	<.232	1.94
	<.349	1.75
	.102	3.02
	8.99	30.17
		3.35
		3.06
		18.45
		1.11

	PS38	
	Conc.	Norm.
	26.92	81.56
	56.68	64.41
	21.36	35.60
	4.21	23.25
	1.17	16.96
	<4.94	7.68
	1.40	7.00
	.211	6.20
	116.9	242.7
		.808
		11.65
		3.51
		1.10

	LVLH39	
	Conc.	Norm.
	5.50	16.66
	<.621	7.06
	n.d.	n.d.
	.650	3.59
	.608	8.81
	<.226	4.80*
	.735.	3.68
	.039	1.15
	13.97	45.75
		2.04
		4.52
		4.64
		1.30

	LVLM40	
	Conc.	Norm.
La	4.63	14.04
Ce	6.99	7.95
Nd	n.d.	n.d.
Sm	1.14	6.32
Eu	<.510	7.39
Tb	1.45	3.09
Yb	<.467	2.33
Lu	<.074	2.19*
REE	15.25	43.32
Eu/Eu*		1.68
La/Yb		6.00
La/Sm		2.22
Tb/Yb		1.32

	PSA41	
	Conc.	Norm.
	8.11	24.59
	13.11	14.91
	n.d.	n.d.
	1.51	8.34
	1.17	16.96
	<.248	5.29
	<.467	2.33
	.069	2.02
	24.68	74.44
		2.23
		3.58
		2.95
		2.27

	PS42	
	Conc.	Norm.
	42.92	130.4
	86.22	98.05
	n.d.	n.d.
	5.61	30.94
	1.53	22.17
	<3.12	6.14
	1.26	6.30
	.221	6.52
	140.9	300.5
		.821
		20.64
		4.21
		1.02

	B43	
	Conc.	Norm.
	9.82	29.75
	25.07	28.49
	n.d.	n.d.
	2.54	14.06
	<.752	10.90
	4.51	9.60*
	1.89	9.45
	.272	8.00
	40.79	110.3

		3.15
		2.12
		1.02

	BQ45	
	Conc.	Norm.
La	14.40	43.63
Ce	36.00	41.02*
Nd	n.d.	n.d.
Sm	5.60	30.92
Eu	2.10	30.43
Tb	<5.51	11.72
Yb	2.30	11.50
Lu	.304	8.94
REE	66.36	178.2
Eu/Eu*		1.52
La/Yb		3.79
La/Sm		1.41
Tb/Yb		1.02

	EPL46	
	Conc.	Norm.
	11.47	34.76
	39.70	45.11
	n.d.	n.d.
	3.16	17.45
	1.50	21.74
	.587	12.50
	2.27	11.37
	.244	7.17
	58.92	149.8
		1.50
		5.05
		1.99
		1.10

	M47	
	Conc.	Norm.
	2.56	7.76
	<6.09	6.92
	n.d.	n.d.
	.400	2.21
	.489	7.09
	<.283	6.02
	<.390	1.95
	0.43	1.26
	10.64	33.22
		2.14
		3.97
		3.51
		3.09

	OS50	
	Conc.	Norm.
	1.68	5.09
	<4.42	5.02
	n.d.	n.d.
	.382	2.11
	.720	10.43
	.142	3.02
	.684	3.42
	.068	1.99
	8.10	31.08
		4.17
		1.49
		2.41
		.883

APPENDIX V
Concentrations Of Selected Trace Elements For Individual Samples

	CG1	CBQ1	CEP3	CM4	CMA5	CGD6	CGD9	CD10	CDM11
Rb	104.7	83.4	n.d.	<16.1	n.d.	n.d.	n.d.	n.d.	n.d.
Cs	<.339	n.d.	n.d.	<.475	<.428	<.822	n.d.	n.d.	n.d.
Ba	921.1	475.9	n.d.	n.d.	n.d.	n.d.	n.d.	<31.0	<95.8
Sc	6.42	12.62	4.60	.478	.539	8.88	7.78	n.d.	n.d.
Zr	n.d.	<279	<334	n.d.	n.d.	n.d.	n.d.	n.d.	n.d.
Hf	4.08	6.43	3.29	n.d.	n.d.	4.90	5.08	n.d.	n.d.
Ta	.343	1.01	<.101	n.d.	n.d.	<.210	<.096	n.d.	n.d.
Zn	n.d.	n.d.	1.62	12.52	<1.55	n.d.	n.d.	1.22	11.02
Cr	104.2	265.5	86.45	15.43	n.d.	162.0	165.9	14.70	66.15
Co	6.48	10.03	29.02	6.05	4.16	n.d.	101.5	n.d.	101.5
Ni	<161.5	n.d.	n.d.	<162.2	n.d.	n.d.	<164.4	n.d.	n.d.
Pa	6.87	5.74	4.15	.311	3.24	6.76	8.66	4.05	<.317
Np	1.78	2.69	21.28	5.40	4.40	5.26	10.14	1.29	1.10

	CLH12	COSD13	COSH14	COS15	PSAG16	CLV117	CLV217	CPS18	COS19
Rb	n.d.	<20.8	58.73	n.d.	42.91	<46.3	n.d.	273.0	<46.2
Cs	n.d.	n.d.	.995	n.d.	<.678	n.d.	.978	10.98	n.d.
Ba	n.d.	<44.6	326.6	n.d.	611.7	n.d.	n.d.	154.3	n.d.
Sc	<.422	8.66	12.76	2.09	10.44	.687	1.15	26.15	1.78
Zr	n.d.	<214	361.5	n.d.	402.0	n.d.	<289.5	n.d.	n.d.
Hf	n.d.	6.58	15.97	n.d.	5.29	n.d.	n.d.	6.40	n.d.
Ta	n.d.	0.38	0.76	0.73	0.28	0.39	0.31	0.73	0.30
Zn	1.53	n.d.	n.d.	1.18	n.d.	3.16	n.d.	n.d.	739.4
Cr	85.75	451.6	611.8	658.7	408.9	510.9	482.6	458.3	739.4
Co	104.43	11.99	7.70	42.53	18.07	83.43	9.73	24.50	211.74
Ni	314.3	954.0	11124	1227	860.4	947.4	878.6	690.0	1235
Pa	.624	6.94	13.06	1.16	7.18	.494	1.18	12.73	.816
Np	1.82	3.38	5.52	18.99	2.46	7.35	14.29	3.59	18.56

	CBTQ20	CABO21	GTH	GT11	GT1	GT2	GT3	GT4	CCF22
Rb	n.d.	n.d.	n.d.	n.d.	n.d.	n.d.	n.d.	n.d.	158.9
Cs	n.d.	<.884	1.06	n.d.	n.d.	<1.09	.387	.933	2.24
Ba	62.45	2880	<84.9	<95.	<99.	<99.4	<1.03	<84.35	740.8
Sc	1.34	26.02	.626	n.d.	.787	<.297	n.d.	6.81	15.46
Zr	n.d.	n.d.	<318.7	n.d.	n.d.	<291.0	n.d.	n.d.	n.d.
Hf	3.15	8.84	n.d.	<1.36	n.d.	<1.77	n.d.	<1.38	n.d.
Ta	0.20	0.64	n.d.	n.d.	n.d.	n.d.	n.d.	n.d.	0.50
Zn	n.d.	n.d.	1.94	n.d.	n.d.	n.d.	n.d.	n.d.	n.d.
Cr	1591	1111	23.31	22.44	20.74	28.00	19.71	99.92	258.2
Co	12.72	11.45	24.75	1.74	2.72	n.d.	2.53	2.81	51.19
Ni	3084	1525	n.d.	<191.5	n.d.	n.d.	n.d.	n.d.	499.1
Pa	2.10	15.90	.783	<.394	<1.07	.578	2.36	3.79	10.27
Np	.781	5.59	27.31	14.61	32.13	10.14	21.09	18.59	4.43

(Vb)

	CCV23	CDS25	CSY127	CSY227	C28	G29	PAG30	H32	P34
Rb	n.d.	49.95	n.d.	<36.81	n.d.	126.1	<8.88	<17.23	148.1
Cs	2.27	n.d.	n.d.	n.d.	<.943	<.567	n.d.	n.d.	1.63
Ba	n.d.	75.66	n.d.	n.d.	n.d.	537.3	n.d.	n.d.	639.9
Sc	3.93	15.75	16.05	16.74	3.87	9.10	9.23	.843	18.80
Zr	n.d.	<240.1	n.d.	n.d.	<287.6	n.d.	n.d.	n.d.	<417.9
Hf	n.d.	6.23	5.03	3.80	2.47	5.25	4.34	n.d.	6.01
Ta	n.d.	n.d.	0.46	0.60	<0.19	0.20	0.36	<.328	.917
Zn	n.d.	n.d.	n.d.	n.d.	1.21	n.d.	n.d.	---	---
Cr	141.0	56.65	158.4	174.4	199.3	102.4	97.06	<9.70	148.9
Co	892.4	7.67	36.27	51.94	15.42	9.82	1.93	<1.49	6.12
Ni	634.27	n.d.	120.21	238.6	n.d.	16.46	134.1	n.d.	n.d.
Pa	6.88	2.50	9.97	33.40	1.97	9.25	6.93	<.179	11.34
Np	2.69	1.73	6.16	6.46	5.99	2.39	3.09	.208	3.54

	PS36	FD37	PS38	LVLH39	LVLM40	PSA41	PS42	B43	BQ45
Rb	242:5	n.d.	<26.42	<15.29	n.d.	23.89	286.4	106.8	<30.05
Cs	13.71	<.446	n.d.	<.420	<.316	1.41	18.34	n.d.	n.d.
Ba	446.9	n.d.	444.9	<36.55	n.d.	42.37	140.6	<97.24	n.d.
Sc	21.96	.300	16.47	.701	.148	2.42	23.03	40.51	4.84
Zr	n.d.	n.d.	540.0	n.d.	n.d.	n.d.	403.4	n.d.	n.d.
Hf	3.83	<.465	4.99	n.d.	n.d.	.933	4.80	n.d.	n.d.
Ta	.851	n.d.	.840	n.d.	n.d.	n.d.	0.61	<.644	---
Zn	---	---	---	---	0.26	n.d.	n.d.	---	---
Cr	122.2	n.d.	125.6	<12.46	<14.64	16.46	122.2	n.d.	116.5
Co	9.94	<.936	7.79	n.d.	n.d.	n.d.	15.28	61.57	---
Ni	57.34	n.d.	n.d.	n.d.	83.76	n.d.	87.05	n.d.	37.88
Pa	12.66	n.d.	10.77	.709	.309	1.64	11.53	1.31	3.06
Np	6.23	.693	2.45	.595	8.53	.812	5.56	1.01	1.74

	EPL46	M47	OS50
Rb	20.91	n.d.	---
Cs	.394	<.464	<.286
Ba	173.28	n.d.	---
Sc	2.56	.692	.292
Zr	<156.5	n.d.	n.d.
Hf	3.34	<.641	---
Ta	0.14	n.d.	n.d.
Zn	n.d.	---	n.d.
Cr	26.98	<1.08	24.60
Co	7.02	<.906	1.56
Ni	n.d.	n.d.	18.43
Pa	2.95	.327	n.d.
Np	2.19	.724	2.73

APPENDIX VI

History Of The Central Mining District

Copper production in the Central Mining District began in 1804 and continued until the end of the 19th century, with intermittent production due to numerous attacks by the Apache Indians. The Central mining district, often referred to as the Hanover district, was probably first organized in 1860 (Spencer and Paige, 1935). The Hanover mine located in the hanging wall of the Barringer fault just southeast of the present day Continental mine, was producing copper as early as 1858, with a production of nearly 500 tons of copper reported between 1858-1861 (Spencer and Paige, 1935). The iron ore deposits in the vicinity of Fierro were first mined in 1891. The Hanover-Bessermer Iron Association and its successor the Hanover-Bessermer Iron and Copper company were the greatest producers of copper, lead and zinc ore (Spencer and Paige, 1935) in the Hanover district between 1896 and 1931. The Hanover-Bessemer Iron and Copper Company was later taken over by its parent company, the United States Smelting, Refining, and Mining Company, and then taken over by a subsidary, U.V. industries in the 1930's.

In 1962, an extensive drilling program in the area was begun and economic tonnage was discovered. This drilling program resulted in the development of the present day Continental underground mine and open pit. In 1979, the

Continental mine was taken over by the Sharon Steel Company. Presently, the mine is producing 750,000 tons per year of copper and iron from underground workings and 1,700,000 ton per year from the open pit (Worthington, pers. commun.)

APPENDIX VII

The Sm values for samples M47, FD37, CD11, and CD10 of the Montoya-Fusselman Dolomites are interpreted as analytical error (Fig. VII a) and therefore these data points were eliminated and the Sm values were extrapolated (Fig. 43). At very low REE concentrations, there is an increased chance of analytical error. Also, there were some problems with obtaining accurate Sm values from the INAA equipment.

Sm and Tb for sample CBQ1 and Tb for sample BQ45 of the Bliss Quartzite are interpreted as analytical error (Fig. VII b) and therefore their REE concentrations were eliminated and their values were extrapolated (Fig. 49).

If there is no data point for a REE listed (Figs. 38-52) this means that the value was extrapolated.

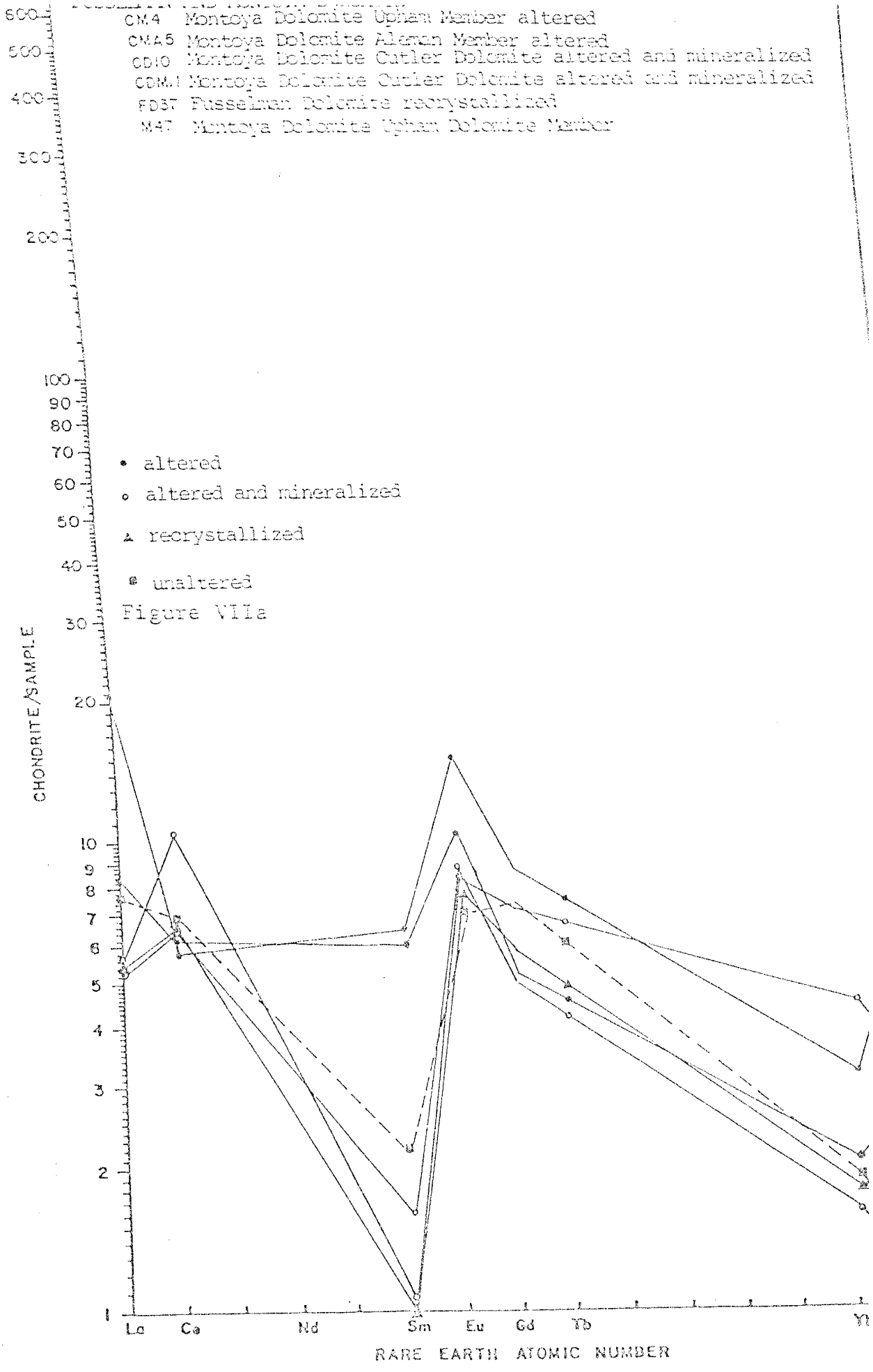
CM4 Montoya Dolomite Upham Member altered
CMA5 Montoya Dolomite Aleman Member altered
CD10 Montoya Dolomite Cutler Dolomite altered and mineralized
CDM1 Montoya Dolomite Cutler Dolomite altered and mineralized
FD37 Fusselman Dolomite recrystallized
M47 Montoya Dolomite Upham Dolomite Member
• altered
o altered and mineralized
▲ recrystallized
unaltered
CHONDRITE/SAMPLE
RARE EARTH ATOMIC NUMBER
La
Ce
Nd
Sm
Eu
Gd
Tb
Yt

Figure VIIa

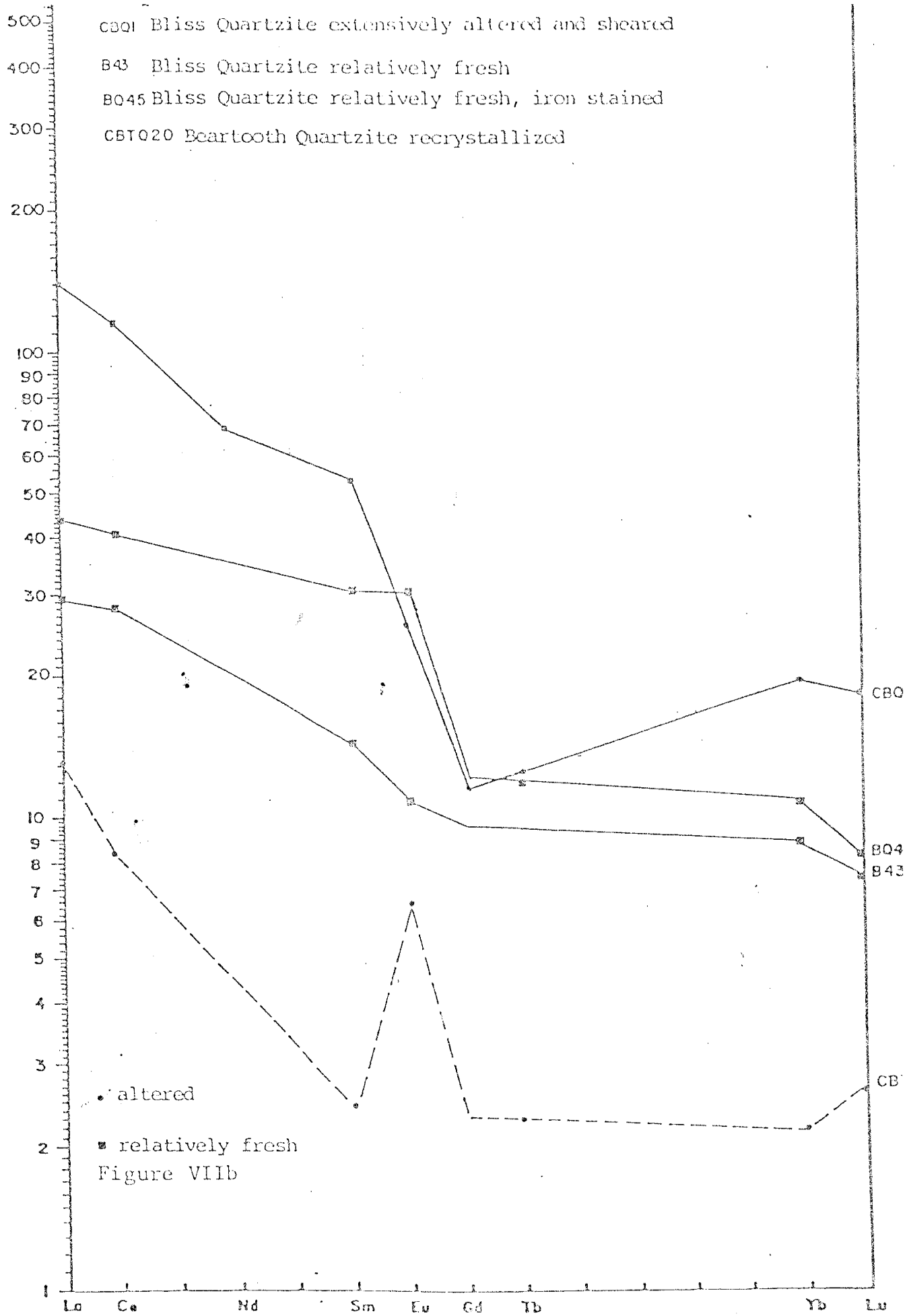
CBQ1 Bliss Quartzite extensively altered and sheared
B43 Bliss Quartzite relatively fresh
BQ45 Bliss Quartzite relatively fresh, iron stained
CBTQ20 Beartooth Quartzite recrystallized
500
400
300
200
100
90
80
70
60
50
40
30
20
10
9
8
7
6
5
4
3
2
1
CBQ
BQ4
B43
CB
altered
relatively fresh
La
Ce
Nd
Sm
Eu
Gd
Tb
Yb
Lu
Figure VIIb

APPENDIX VIII
MASS-VOLUME CALCULATION

Assuming that the intrusive is approximately 3.0 kms
Skarn extends outward approximately 0.8 kms

Volume of skarn = $4/3 \ (R^3-R^3)/2$ (divided by 2 because only using the upper half of the intrusive)
$4/3 \ (3.8^3-3^3)/2$
$= 11.39 \text{ km}^3$ skarn

Volume of the intrusive = $4/3 \ (R^3)$
$= 4/3 \ (3^3)$
$= 38 \text{ km}^3$

If skarn formation required the addition of approximately 25% by weight SiO_2, according to Barnes (1974) .09 wt. % SiO_2 can be carried in water at 340 C and 300 bars and at 240 C (a drop of 100 C) .05 wt. % SiO_2 can be carried in water. Therefore, assume water deposited .04 eq.wt% SiO.

Therefore added SiO_2 to skarn is:
$11.4 \text{ kms}^3 * .25 * 2.6*10^{15} \text{ gms/km}^3$
$= 7.41*10^{15}$

Water needed
$7.41*^{15}/.0004 = 1.852*10^{19}$ gms H_2O neccessary to deposit SiO_2 observed

Assume that the magma gave off ~ 4% H_2O
$38 \text{ kms}_3 * 2.6*10^{15} \text{ gms/km}^3 * .04 =$
$=3.95$ gms H_2O

This very approximate calculation indicates that there was not enough water supplied from the magma to carry the silica required to produce the amount of skarn present surrounding the Hanover-Fierro intrusive.

This thesis is accepted on behalf of the faculty of the Institute by the following committee:

David L. Norman
Adviser

Dec 21, 1981
Date